



Transport coefficients of magnetized neutron star cores

Peter Shternin^a, Dmitry Ofengeim

Ioffe Institute, Politekhnicheskaya 26, St. Petersburg 194021, Russia

Received: 4 November 2021 / Accepted: 11 February 2022 / Published online: 4 March 2022

© The Author(s), under exclusive licence to Società Italiana di Fisica and Springer-Verlag GmbH Germany, part of Springer Nature 2022
Communicated by Laura Tolos

Abstract We review the calculations of the kinetic coefficients (thermal conductivity, shear viscosity, momentum transfer rates) of the neutron star core matter within the framework of the Landau Fermi-liquid theory. We restrict ourselves to the case of normal (i.e. non-superfluid) matter. As an example we consider simplest $npe\mu$ composition of neutron star core matter. Utilizing the CompOSE database of dense matter equations of state and several microscopic interactions we analyze the uncertainties in calculations of the kinetic coefficients that result from the insufficient knowledge of the properties of the dense nuclear matter and suggest possible approximate treatment. In our study we also take into account non-quantizing magnetic field. The presence of magnetic field makes transport anisotropic leading to the tensor structure of kinetic coefficients. We find that the moderate ($B \lesssim 10^{12}$ G) magnetic field do not affect considerably thermal conductivity of neutron star core matter, since the latter is mainly governed by the electrically neutral neutrons. In contrast, shear viscosity is affected even by the moderate $B \sim 10^8\text{--}10^{10}$ G. Based on the in-vacuum nucleon interactions we provide practical expressions for calculation of transport coefficients for any equation of state of dense matter.

1 Introduction

Neutron stars (NSs) are the most compact astrophysical objects known that are still stable against the gravitational collapse. This is possible because NSs are largely composed of strongly interacting degenerate baryons (although quark cores, other hadronic, or mixed models are also discussed), which pressure is strong enough to counterbalance the gravity forces. This is strongly supported by the inferences on the masses ($\sim 1\text{--}2 M_\odot$) and radii ($R \sim 10\text{--}20$ km) obtained for

these objects by astrophysical methods, which correspond to the mean densities few $\times \rho_0$ with $\rho_0 = 2.8 \times 10^{14}$ g cm⁻³ being the nuclear saturation density.

Understanding properties of matter under such extreme conditions is a subject of fundamental importance for modern physics. Such studies allow one to test the predictions of the nuclear matter theories for the conditions unreachable in the terrestrial settings over the astrophysical observations.

Various physical input is required to model processes and dynamical phenomena that can occur during the NS life. Among it there are the transport properties of the NS matter, see, e.g. [1] for review.

In the present study we revisit the calculation of the transport coefficients of NS core matter based on the Landau Fermi-liquid theory. We give relatively detailed description of the technique used to calculate these coefficients and to identify how they enter the evolution equations that are then used in the modelling of various physical processes. It is not possible to give a detailed account of many aspects of neutron star transport theory in one article, so we restrict ourselves here to the transport coefficients mediated by collisions between the particles composing baryonic NS cores. We left aside more exotic compositions such as meson condensates, or quark cores. We ignore processes related to the reactions. In this sense we do not consider the bulk viscosity, since the bulk viscosity mediated by collisions is negligible. It should be calculated using a different technique in comparison to other transport coefficients (see., e.g., [1]). We also do not consider the possibility of nucleon pairing which can result in the superfluidity/superconductivity phenomena in NS cores. The transport coefficients of the superfluid/superconducting NS cores are much less explored and the consistent picture is not drawn yet.

We, however, include the magnetic field effects into consideration. Magnetic field plays an important role in NS physics. Indeed, the most common astrophysical manifestation of the NSs are the radio pulsars the operation of which is

^ae-mail: pshternin@gmail.com (corresponding author)

driven by the magnetic field. The studies of magnetars show that the surface field can reach values up to 10^{14} – 10^{15} G [2]. It is natural to assume that the NS core matter can be under the influence of a strong magnetic field. The effect of the magnetic field on the transport properties of the NS crust is studied in great detail, see, e.g. [3–7], however the transport coefficients of the magnetized NS cores received less attention.

Magnetic field makes the motion of charged particles curvilinear, this affects their response to the external perturbations. Neutral particles feel the effects of magnetic field indirectly, through the interaction with charged species (the neutral particles can also have the magnetic momenta). The influence of the magnetic field on the charge particles in degenerate matter can be described by the cyclotron frequency on the Fermi surface of particle species a

$$\omega_{\text{BF}a} = \frac{q_a B}{m_a^*}, \quad (1)$$

where q_a is the electric charge of the particle species a and m_a^* is its effective mass at the Fermi surface. In this paper we assume that the magnetic field is non-quantizing, i.e. $\omega_{\text{BF}a} \lesssim T$. For typical NS core conditions, this inequality is most easily violated for lightest particles, i.e., electrons at $B \gtrsim 10^{14} T / (10^8 \text{ K}) \text{ G}$ [8,9]. When $T \ll \omega_{\text{BF}a}$, but $\omega_{\text{BF}a} \ll T_{\text{Fa}}$, where T_{Fa} is the degeneracy temperature of particle species a , the field is weakly quantizing. In this case particles populate many Landau levels. Transport coefficients in this case demonstrate oscillating behavior around the classical (i.e. non-quantizing) values, and are well-described by the expressions which neglect quantization after the oscillations are smeared out. Therefore the results discussed here will be relevant for a moderately weak quantizing field as well.

At very large fields, known as the strongly quantizing regime, $\omega_{\text{BF}a} \gtrsim T_{\text{Fa}}$, particles populate mainly the lowest Landau levels. For electrons, this corresponds to unrealistically large $B \gtrsim 10^{18} \text{ G}$ [9] and can barely happen in NS cores (but not in the crust e.g., [3]).

The calculations of the transport coefficients of NS core matter are hampered by the poorly known properties of the baryon interactions at supranuclear densities. The equation of state (EOS) of such matter is not known and many models are available on the market. Recent progress in theory and observations shrinks the range of available models, but the robust picture is yet to be established.

From the practical point of view it is desirable to have the publically available repository containing relevant properties of dense matter for variety of proposed models in coherent manner, so they can be readily used for astrophysical implications. For the EOSs, this route is taken, e.g., by the Com-

pOSE database.¹ It contains a data on a large number of EOSs relevant for a NS and supernovae simulations.

In principle, it would be convenient for such database to contain as well the set of the transport coefficients relevant for each EOS. However, no simple solution for this task is seen. Transport coefficients are not universal and for each EOS should be calculated under the same underlying microscopic model. At the moment this does not look feasible.

In the present study we identify what information is needed from the microscopic theory for calculating transport coefficients of magnetized NS cores. Specifically, here we consider the beta-stable nucleonic matter with baryon number density $\lesssim 1 \text{ fm}^{-3}$, temperature $T \leq 10^{10} \text{ K}$ and magnetic field $\lesssim 10^{14} \text{ G}$. Utilizing a range of the nucleonic EOSs from the ComPOSE database and a few microscopic interactions we illustrate the potential scatter that can emerge in calculations. We then elaborate on the ‘poor man’ solution for nucleonic NS cores based on the in-vacuum nucleon interaction. This approach allows one to calculate transport coefficients for any EOS and we provide practical approximate expressions allowing to do this.

The paper is organized as follows. In Sect. 2 we review the first-order relativistic hydrodynamics equations in order to identify the occurrence of the transport coefficients studied here. We do not consider effects of the General Relativity since we deal with the microscopic calculations of the transport coefficients which are performed in the local Lorentz frame. The typical mean free path scale is much smaller than the macroscopic scale where the curvature of space-time manifests itself. In Sect. 3 we consider the transport theory of Fermi liquids. In particular, in Sect. 3.3 we briefly introduce the irreducible spherical tensor formalism convenient for studying the problem in magnetic field. In Sect. 3.6 we outline the general expressions for calculation of transport coefficients at lowest variational order. In Sect. 4 the quasi-particle collisions governed by electromagnetic (Sect. 4.1) and strong (Sect. 4.2) interactions are considered. In Sect. 5 we apply the described formalism to the transport coefficients in nucleonic NS cores. In Sect. 5.1 we consider effective scattering cross-sections. In Sect. 5.2 we describe partial contributions to transport coefficients in non-magnetized matter and Sect. 5.3 we discuss transport coefficients in presence of the magnetic field. We conclude in Sect. 6.

We give the practical expressions for the calculation of transport coefficients for nucleonic NS core matter in Appendix B.

Throughout the paper we set $\hbar = c = k_B = 1$. The metric tensor convention is $g_{\mu\nu} = \text{diag}(1, -1, -1, -1)$, and the Greek indices are used for the components of four-vectors while the Roman ones for components of three-vectors. Bold font is used for three-vectors. The Levi-Civita antisymmetric

¹ <https://www.compose.obspm.fr/>.

tensor $\epsilon^{\mu\nu\alpha\beta}$ is normalized as $\epsilon^{0123} = 1$. Dirac matrices obey $\gamma^5 = -i\gamma^0\gamma^1\gamma^2\gamma^3$.

2 Hydrodynamic equations

Let us start from formulating the relativistic hydrodynamic equations, e.g. [10, 11], for the normal (i.e. non-superfluid) NS core matter which is a mixture of r species (e.g. neutrons, protons, electrons, etc.). We assume that collision timescales between the various species are compatible with the equilibration timescale for the single species. Therefore it is appropriate to describe the NS core mixture as a single fluid. If this condition is not met (as can generally happen in terrestrial or astrophysical plasmas) or if the superfluidity is taken into account, then more complicated multifluid hydrodynamics should be constructed, see, e.g., [12–15].

Hydrodynamic equations consist of the conservation equation for the energy–momentum tensor $\mathcal{T}^{\mu\nu}$ and the conservation equations for the particle currents $j_{(a)}^\mu$, $a = 1, \dots, r$. The latter equations read

$$\partial_\mu j_{(a)}^\mu = 0. \tag{2}$$

In principle, the particle currents are not conserved since the weak reactions can operate in the NS core. In this case the right-hand side of Eq. (2) should contain reaction terms. In case of reaction mixtures it is, in principle, more natural to consider the exactly conserved currents (i.e. baryon number current) instead of particle currents. However, the timescales of the weak reactions in the NS cores are much larger than the collision timescales we will deal below. Therefore we omit these terms for brevity.²

We assume that the large-scale electromagnetic field can be present in the system. The equation for the energy–momentum tensor of the fluid is then

$$\partial_\mu \mathcal{T}^{\mu\nu} = F^{\nu\lambda} J_\lambda, \tag{3}$$

where $F^{\mu\nu}$ is the electromagnetic field tensor and J^μ is the electromagnetic current

$$J^\mu = \sum_{a=1}^r q_a j_{(a)}^\mu. \tag{4}$$

We assume for simplicity that the magnetic fields are not overwhelmingly large so that the matter is unpolarized and the magnetic pressure can be neglected. More general discussion can be found in [16–18].

One defines the so-called local rest frame (LRF) of the fluid which for the ideal fluid is defined as a frame where the

energy flow \mathcal{T}^{0i} , momentum components densities \mathcal{T}^{i0} , and particle flows $j_{(a)}^i$, $i = 1, 2, 3$, vanish. For the fluids outside equilibrium, the definition of the LRF becomes ambiguous [10, 19]. In any case, the rest frame of the fluid is described by the hydrodynamic four-velocity U^μ normalized as $U^\mu U_\mu = 1$. In the LRF, $U^\mu = (1, 0, 0, 0)$, and in the laboratory frame $U^\mu = \gamma(1, \mathbf{V})$ where \mathbf{V} is three-velocity and $\gamma = (1 - V^2)^{-1/2}$ is the corresponding Lorentz factor. We define the orthogonal projector

$$\Delta^{\mu\nu} = g^{\mu\nu} - U^\mu U^\nu \tag{5}$$

and decompose the four-gradient operator as

$$\partial^\mu = U^\mu U^\nu \partial_\nu + \Delta^{\mu\nu} \partial_\nu \equiv U^\mu D + \nabla^\mu. \tag{6}$$

In the LRF, $D \rightarrow \partial_t$ and $\nabla^\mu \rightarrow (0, -\nabla)$, where $\nabla = \partial_r$ is the spatial gradient operator.

Using the hydrodynamic velocity, the particle currents can be written as

$$j_{(a)}^\mu = n_a U^\mu + \Delta j_{(a)}^\mu, \tag{7}$$

where $\Delta j_{(a)}^\mu$ is the dissipative correction, which vanishes in equilibrium, and n_a is the number density of particle species a . Total particle number density is

$$n = \sum_{a=1}^r n_a \tag{8}$$

and the decomposition of the total particle current j^μ is

$$j^\mu \equiv \sum_{a=1}^r j_{(a)}^\mu \equiv n U^\mu + \Delta j^\mu, \tag{9}$$

where Δj^μ is the total dissipative particle flux. Similarly, the decomposition of the energy–momentum tensor into the ideal and non-ideal part is

$$\mathcal{T}^{\mu\nu} = (\mathcal{E} + P)U^\mu U^\nu - P g^{\mu\nu} + \Delta \mathcal{T}^{\mu\nu}, \tag{10}$$

where \mathcal{E} is the internal energy density of the fluid, P is the thermodynamic pressure, and $\Delta \mathcal{T}^{\mu\nu}$ is the dissipative correction. Local equilibrium thermodynamic quantities n_a , \mathcal{E} , and P are assumed to be related by the thermodynamic laws to the local temperature $T(x)$ and chemical potentials $\mu_a(x)$ via the standard relations provided the equation of state (e.g., in the form $P = P(\{\mu_a\}, T)$) is given. The thermodynamic laws are

$$d\mathcal{E} = T dS + \sum_a \mu_a dn_a, \tag{11a}$$

$$H \equiv \mathcal{E} + P = T S + \sum_a \mu_a n_a, \tag{11b}$$

$$dP = S dT + \sum_a n_a d\mu_a, \tag{11c}$$

where H is the total enthalpy density and S is the equilibrium entropy density.

² For the hyperonic cores there can exist also strong inelastic processes of a form $A + B \leftrightarrow C + D$. For simplicity, we assume the equilibrium state with respect to such reactions, so the particle currents are still conserved.

The decompositions (7)–(10) describe fluids close to the local equilibrium state so that the dissipative corrections are small and can be systematically expanded in derivatives of the thermodynamic field variables (e.g., [20])

$$\Delta T^{\mu\nu} = \mathcal{O}(\partial) + \mathcal{O}(\partial^2) + \dots, \tag{12}$$

$$\Delta j^\mu = \mathcal{O}(\partial) + \mathcal{O}(\partial^2) + \dots. \tag{13}$$

Truncating these expansions leads subsequently to the first-order hydrodynamics, second-order hydrodynamics, etc.

There is a principle ambiguity in how to define the fields $T(x)$, $\{\mu_a(x)\}$, and $U^\mu(x)$ in order to write the decompositions (7)–(10) in non-equilibrium case. The different possibilities are commonly referred as a ‘choice of the frame’ (e.g., [20]).

The standard choice assumes that the dissipative corrections are transverse to U^μ :

$$U_\mu \Delta j_{(a)}^\mu = 0, \tag{14a}$$

$$U_\mu U_\nu \Delta T^{\mu\nu} = 0, \tag{14b}$$

and additional condition is required to fix U^μ . Two traditional options are due to Eckart [21] and Landau and Lifshitz [19]

$$\Delta j^\mu = 0, \quad \text{Eckart}, \tag{15a}$$

$$U_\mu \Delta T^{\mu\nu} = 0, \quad \text{Landau–Lifshitz}. \tag{15b}$$

It is well-known, however, that the first-order hydrodynamics equations in these frames suffer from acausal and unstable behavior [22], see detailed discussion in, e.g., [10, 11, 14]. In principle, that these theories allow for unstable modes and acausal heat propagation does not mean that the actual studies will necessarily encounter these problems. In most of studies concerned with the NS core transport, up to our knowledge, the first-order theory was enough. This is not the case for the heavy ion collisions and may change with the progress of the simulations of NS mergers.

The solutions to these problems were proposed, for instance, on the basis of second-order theories of extended irreversible thermodynamics [23–25] or Carter’s variational formalism (e.g. [14]), see [26] for a recent review. Alternatively it was recently proposed that the first-order hydrodynamics equations can be made stable if the frames beyond traditional Eckart or Landau–Lifshitz one are considered [20, 27–37]. The latter formalism was recently explored numerically [38] and equations were extended to the second order in general frame [39]. Notice that in fact the certain frames can be preferred over others on the physical basis (i.e. the so-called thermodynamics frame [29, 40], see also [41]).

The discussion of the validity and sufficiency of the first order or second order description is beyond the scope of the present paper [14, 26, 36, 42]. We restrict ourselves to much less ambitious task. We are interested in the microscopic calculations of the transport coefficients (thermal conductivity, shear viscosity, diffusion coefficients) appearing already

in the first-order theory. These coefficients are governed by quasiparticle collisions and are invariant in the first order under the choice of the frame [20, 33, 43].

In order to identify these coefficients let us formulate the entropy production law. The expression for the canonical entropy current is based on the first law of thermodynamics [10]

$$T S^\mu = P U^\mu + U_\nu T^{\mu\nu} - \sum_a \mu_a j_{(a)}^\mu \tag{16a}$$

$$= T S U^\mu + U_\nu \Delta T^{\mu\nu} - \sum_a \mu_a \Delta j_{(a)}^\mu. \tag{16b}$$

In principle, in a non-equilibrium state the true entropy current, which strictly obeys the second law of thermodynamics $\partial_\mu S^\mu \geq 0$, is not necessarily given by Eq. (16a), but it can also contain correction terms [44–47]. However, in the domain of validity of the first-order theory, one can remain with Eq. (16a). Then the inequality $\partial_\mu S^\mu \geq 0$, in principle, becomes approximate [20, 36, 42].

Using Eqs. (2), (3), (7), (10), and (11), the divergence of the canonical entropy current can be written as

$$\zeta \equiv \partial_\mu S^\mu = \Delta T^{\mu\nu} \partial_\mu \frac{U_\nu}{T} - \sum_a \Delta j_{(a)}^\mu \partial_\mu \frac{\mu_a}{T} - \frac{1}{T} E^\lambda J_\lambda, \tag{17}$$

which is valid in any frame [36]. Taking into account the discussion above, we further assume that the matching conditions (14) hold, but do not yet fix U^μ .

The term $E^\lambda \equiv U_\nu F^{\lambda\nu}$ in Eq. (17) is the electric field four-vector resulting from the decomposition of the electromagnetic field tensor

$$F^{\mu\nu} = E^\mu U^\nu - E^\nu U^\mu + \epsilon^{\mu\nu\alpha\beta} U_\alpha B_\beta, \tag{18}$$

where $B^\mu \equiv \frac{1}{2} \epsilon^{\mu\nu\alpha\beta} U_\nu F_{\alpha\beta}$ is the magnetic field four-vector. We assume that the magnetic field is large, i.e. $B = \mathcal{O}(1)$, while the electric field is induced by the dissipative processes, so $E = \mathcal{O}(\partial)$.

The equations of motion are obtained by employing Eqs. (6) and (7) in Eq. (2) and by contracting Eq. (3) with U_ν and Δ_ν^λ [10]. One obtains

$$D n_a + n_a \nabla_\mu U^\mu = -\partial_\mu \Delta j_{(a)}^\mu, \tag{19a}$$

$$D \mathcal{E} + H \nabla_\mu U^\mu = -U_\nu \partial_\mu \Delta T^{\mu\nu} + E^\sigma J_\sigma, \tag{19b}$$

$$H D U^\lambda - \nabla^\lambda P - \Delta_\nu^\lambda F^{\nu\sigma} J_\sigma = -\Delta_\nu^\lambda \partial_\mu \Delta T^{\mu\nu}. \tag{19c}$$

At the first order in gradients, right-hand sides of Eq. (19) vanish.

To proceed further, let us define particle fractions as $y_a \equiv n_a/n$ and introduce diffusion currents $i_{(a)}^\mu$ via

$$j_{(a)}^\mu = y_a j^\mu + (\Delta j_{(a)}^\mu - y_a \Delta j^\mu) \equiv y_a j^\mu + i_{(a)}^\mu. \tag{20}$$

Notice that at first order $i_{(a)}^\mu$ are independent of the choice of U^μ (and of the frame selection in general). The diffusion

currents sum to zero:

$$\sum_{a=1}^r i_{(a)}^\mu = 0. \tag{21}$$

We also assume that the system is electrically neutral in the LRF, $\sum_a q_a n_a = 0$. The electromagnetic current is then

$$J^\mu = \sum_a q_a \Delta j_{(a)}^\mu = \sum_a q_a i_{(a)}^\mu. \tag{22}$$

Due to charge neutrality, the electromagnetic current is orthogonal to the fluid velocity, i.e. $U_\mu J^\mu = 0$. This retains only the magnetic part of the Lorentz force, $\Delta_\nu^\lambda F^{\nu\sigma} J_\sigma = U_\alpha \epsilon^{\alpha\lambda\mu\nu} J_\mu B_\nu$, in the left-hand side of Eq. (19c). Notice that in multifluid hydrodynamics, different ‘fluids’ might have different LRFs, and the definition of local charge neutrality becomes more subtle, see, e.g., [48].

The dissipative correction to the energy–momentum tensor $\Delta T^{\mu\nu}$ can be further decomposed as

$$\Delta T^{\mu\nu} = U^\mu Q^\nu + U^\nu Q^\mu + \Pi^{\mu\nu}, \tag{23}$$

where Q^μ is the dissipative part of the energy flux

$$Q^\mu = U_\nu \Delta T^{\nu\lambda} \Delta_\lambda^\mu \equiv I_{(q)}^\mu + h \Delta j^\mu = J_{(q)}^\mu + \sum_a h_a \Delta j_{(a)}^\mu, \tag{24}$$

$I_{(q)}^\mu$ is the heat flux (which is frame-independent in first order), $h \equiv H/n$ is the specific enthalpy per particle, $J_{(q)}^\mu$ is the reduced heat flux, $J_{(q)}^\mu = I_{(q)}^\mu - \sum_a h_a i_{(a)}^\mu$, and h_a is the specific enthalpy of the particle species a , so that $h = \sum_a y_a h_a$. Notice that the specific enthalpies cannot be defined in the phenomenological single-fluid theory. They, however, will arise naturally from the Fermi-liquid kinetic theory (discussed below).

The term $\Pi^{\mu\nu}$ in Eq. (23) is the non-equilibrium part of the stress tensor which in view of Eq. (14) is

$$\Pi^{\mu\nu} = \Delta_\lambda^\mu T^{\lambda\delta} \Delta_\delta^\nu + P \Delta^{\mu\nu} = \Delta_\lambda^\mu \Delta T^{\lambda\delta} \Delta_\delta^\nu. \tag{25}$$

Using the decompositions (23)–(24), the entropy current in (16b) can be rewritten in the following forms

$$S^\mu = \frac{S}{n} j^\mu + \frac{1}{T} \left(I_{(q)}^\mu - \sum_a \mu_a i_{(a)}^\mu \right) \tag{26a}$$

$$= \sum_a s_a j_{(a)}^\mu + \frac{J_{(q)}^\mu}{T} \tag{26b}$$

which do not depend on U^μ [43]. The quantities s_a in Eq. (26) are partial specific entropies to which all said above about h_a applies as well.

Let us now rewrite the entropy production rate (17) with the help of Eqs. (23), (24), (19c), and (11) in several equivalent forms [49]

lent forms [49]

$$T\zeta = \Pi^{\mu\nu} \nabla_\mu U_\nu - I_{(q)}^\mu \left(\frac{\nabla_\mu T}{T} - D U_\mu \right) - T \sum_a i_{(a)}^\mu \nabla_\mu \frac{\mu_a}{T} + \frac{1}{n} j_\mu F^{\mu\lambda} J_\lambda \tag{27a}$$

$$= \Pi^{\mu\nu} \nabla_\mu U_\nu - J_{(q)}^\mu \left(\frac{\nabla_\mu T}{T} - D U_\mu \right) - \sum_a i_{(a)}^\mu \left(d_{(a)\mu}^E - \frac{h_a}{hn} \Delta_{\mu\nu} F^{\nu\lambda} J_\lambda \right) \tag{27b}$$

$$= \Pi^{\mu\nu} \nabla_\mu U_\nu - J_{(q)}^\mu \left(\frac{\nabla_\mu T}{T} - D U_\mu \right) - \sum_a \Delta j_{(a)}^\mu \left(d_{(a)\mu} - \frac{h_a}{hn} \Delta_{\mu\nu} F^{\nu\lambda} J_\lambda \right). \tag{27c}$$

In order to derive these equations, we expressed the acceleration $D U_\mu$ from (19c) taken at $\mathcal{O}(\partial)$ (i.e. neglecting its right-hand side). However, we traditionally kept the acceleration term in the combination $T^{-1} \nabla_\mu T - D U_\mu$ which multiplies the heat fluxes in Eq. (27).

In Eq. (27) we introduced four-vectors

$$d_{(a)}^{E\mu} = \tilde{d}_{(a)}^\mu - \frac{q_a}{n} j_\nu F^{\nu\mu}, \tag{28a}$$

$$d_{(a)}^\mu = \tilde{d}_{(a)}^\mu + q_a E^\mu, \tag{28b}$$

where

$$\tilde{d}_{(a)}^\mu = T \nabla^\mu \frac{\mu_a}{T} - T \frac{h_a}{h} \sum_b y_b \nabla^\mu \frac{\mu_b}{T}. \tag{29}$$

All these vectors are linearly dependent since

$$\sum_{a=1}^r y_a \tilde{d}_{(a)}^\mu = 0, \tag{30}$$

and, owing to charge neutrality,

$$\sum_{a=1}^r y_a d_{(a)}^{E\mu} = \sum_{a=1}^r y_a d_{(a)}^\mu = 0. \tag{31}$$

The first Eq. (27a) is manifestly frame independent, since it contains frame-independent fluxes. The second Eq. (27b) is rewritten using the reduced heat flux, since it naturally emerges from the kinetic theory and is also frame-independent.

Notice that the thermodynamic forces coupled to the diffusion currents contain [the last term of Eq. (27b)] the electric field in the specific frame [namely, particle, or the Eckart one, cf. Eqs. (28a) and (28b)]. Notice also that the $\Delta_{\mu\nu}$ projector in the magnetic term can be dropped since $i_{(a)}^\mu$ is orthogonal to U^μ .

Consider, finally, the third form of the entropy production equation (27c). Here dissipative particle current and the vector $d_{(a)}^\mu$ depend on the choice of frame (but not the entropy production itself). However, Eq. (27c) has the structure that

is readily obtained from the kinetic theory by integrating the corresponding single-particle transport equations, see below. In the Eckart frame [Eq. (15a)] Eqs. (27b) and (27c) coincide. This suggest that it is convenient to work in the Eckart frame for the calculation of the transport coefficients.

Equation (27b) has a form of bilinear combinations of thermodynamic forces and fluxes

$$T\zeta = - \sum_{k=\zeta,\eta,q, Da} \mathcal{Y}_k \cdot \mathcal{X}_k, \tag{32}$$

where \mathcal{X}_k are thermodynamic forces, corresponding to different transport phenomena. Namely,

$$\mathcal{X}_\zeta = \nabla^\mu U_\mu \tag{33a}$$

corresponds to the bulk viscosity ($k = \zeta$),

$$\mathcal{X}_\eta^{\mu\nu} = \frac{1}{2} \left(\Delta_\sigma^\mu \Delta_\tau^\nu + \Delta_\sigma^\nu \Delta_\tau^\mu - \frac{2}{3} \Delta^{\mu\nu} \Delta_{\sigma\tau} \right) \nabla^\sigma U^\tau \tag{33b}$$

corresponds to the shear viscosity ($k = \eta$),

$$\mathcal{X}_q^\mu = \frac{\nabla^\mu T}{T} - DU^\mu \tag{33c}$$

corresponds to thermal conductivity ($k = \kappa$), and r thermodynamic forces ($k = Da$ with $a = 1 \dots r$)

$$\mathcal{X}_{Da}^\mu = d_{(a)}^{E\mu} - \frac{\hbar_a}{\hbar n} \Delta^{\mu\nu} F_{\nu\lambda} J^\lambda \tag{33d}$$

drive the diffusion processes. In Eq. (32), \mathcal{Y}_k are the corresponding thermodynamic fluxes

$$\mathcal{Y}_\zeta = -\frac{1}{3} \Delta_{\mu\nu} \Pi^{\mu\nu} \equiv \Pi, \tag{34a}$$

$$\mathcal{Y}_\eta^{\mu\nu} = - \left(\Delta_\sigma^\mu \Delta_\tau^\nu - \frac{1}{3} \Delta^{\mu\nu} \Delta_{\sigma\tau} \right) \Pi^{\sigma\tau} \equiv -\Pi^{(\mu\nu)}, \tag{34b}$$

$$\mathcal{Y}_q^\mu = J_{(q)}^\mu, \tag{34c}$$

$$\mathcal{Y}_{Da}^\mu = i_{(a)}^\mu. \tag{34d}$$

In Eqs. (34a), (34b) we decomposed the stress tensor in the isotropic part (described by the viscous pressure Π) and the traceless symmetric part (shear stress tensor), for which we use the short-hand notation $\Pi^{(\mu\nu)}$.

The irreversible thermodynamics states that the fluxes are the linear combinations of forces (and vice versa), namely

$$\mathcal{Y}_k = - \sum_{k'} \hat{L}_{kk'} \mathcal{X}_{k'}, \tag{35}$$

where $\hat{L}_{kk'}$ is the matrix of the transport coefficients. Here and up to the end of this section we omit the tensor component indices for brevity, and use hats to stress tensor character of corresponding quantities (in order to eliminate the explication of tensor component indices). Entropy production now is given by the quadratic form on the thermodynamic forces \mathcal{X}_k . The transport coefficients matrix $\hat{L}_{kk'}$ needs to be semi-positive definite for the second law of thermodynamics to be

valid. In addition, the matrix $\hat{L}_{kk'}$ obeys Onsager reciprocal relations [50]

$$\hat{L}_{kk'}(\mathbf{B}) = \pm \hat{L}_{k'k}^T(-\mathbf{B}), \tag{36}$$

where the superscript T means transposition with respect to the tensor multiindex, and one needs to use the plus sign if the thermodynamic forces k and k' have the same time-reversal symmetry, and minus in other case (i.e. for the cross-coefficients between viscosity and diffusion; however these coefficients are zero due to inversion symmetry).

The Curie principle states that in the isotropic media the thermodynamic fluxes and forces of different tensor dimensions do not mix [51]. In the presence of the magnetic field, the system possesses lower-degree axial symmetry and one can write

$$\mathcal{Y}_\zeta = -\zeta \mathcal{X}_\zeta - \hat{\zeta}_1 \hat{\mathcal{X}}_\eta, \tag{37}$$

$$\hat{\mathcal{Y}}_\eta = 2\hat{\eta} \hat{\mathcal{X}}_\eta - \hat{\zeta}_1 \mathcal{X}_\zeta, \tag{38}$$

where ζ is the bulk viscosity coefficient, $\hat{\eta}$ is the shear viscosity which, in general, is a four-rank tensor, and $\hat{\zeta}_1$ is the cross-term viscosity coefficient which is a traceless symmetric second-rank tensor. Due to inversion symmetry there are no cross terms between the vector fluxes and the viscous forces and vice versa. Below (Sect. 3.3) we will see that for a wide class of systems including NS cores one may consider $\hat{\zeta}_1 = 0$ due to a particular form of the Lorentz force [52]. If more general interaction with magnetic field is considered (e.g. the particles' magnetic moments are taken into account), one may have $\hat{\zeta}_1 \neq 0$.

For the vector fluxes the general situation is more cumbersome. One can expand Eq. (35) in the explicit form

$$J_q = -\hat{L}_{qq} \mathcal{X}_q - \sum_a \hat{L}_{qa} \mathcal{X}_{Da}, \tag{39a}$$

$$i_{(a)} = -\hat{L}_{aq} \mathcal{X}_q - \sum_b \hat{L}_{ab} \mathcal{X}_{Db}, \tag{39b}$$

which contains thermal conductivity, diffusion, and thermodiffusion processes. At the level of first-order irreversible thermodynamics there is a freedom to choose the thermodynamic forces and fluxes in various ways by changing a basis of the expansion of the entropy production as a quadratic form. For instance, it is possible to use thermodynamic fluxes \mathcal{Y}_k in place of forces, and take thermodynamic forces \mathcal{X}_k as the fluxes. Notice that the thermodynamic force \mathcal{X}_{Da} as defined in Eq. (33d) contains the term proportional to J , which in turn is the linear combination of the diffusion currents, i.e. \mathcal{Y}_{Da} . This means that Eq. (39b) can be viewed as a system of linear equations for $i_{(a)}$. Solving this system, one expresses the diffusion currents $i_{(a)}$ via the linear combination of the thermal force \mathcal{X}_q and the true diffusion forces $\tilde{\mathcal{X}}_{Da}$, which do not contain the magnetic field term, i.e.

$$\tilde{\mathcal{X}}_{Da} = d_{(a)}^E. \tag{40}$$

The entropy production is still given by the quadratic form with some different transport coefficient matrix related to the $\hat{L}_{kk'}$. We do not write the explicit transformation between these formulations here. Instead we rewrite the diffusion law in the so-called Stephan–Maxwell form. To do this we first rewrite the linear transport laws in the form where the set of thermodynamic forces contains \mathcal{X}_q and the diffusion currents $i_{(a)}$, while the thermodynamic fluxes are \mathcal{X}_{Da} and still J_q :

$$J_q = -T\hat{\kappa}\mathcal{X}_q - \sum_a \hat{R}_{qa}i_{(a)}, \tag{41a}$$

$$\mathcal{X}_{Da} = -\hat{R}_{aq}\mathcal{X}_q - \sum_b \hat{R}_{abi(b)}, \tag{41b}$$

where the thermal conductivity tensor $\hat{\kappa}$ is introduced, $\hat{R}_{qa}(\mathbf{B}) = \hat{R}_{aq}^T(-\mathbf{B})$, and $\hat{R}_{ab}(\mathbf{B}) = \hat{R}_{ba}^T(-\mathbf{B})$ is the conjugate set of the tensor transport coefficients. Multiplying Eq. (41b) by n_a , summing over a , and employing Eqs. (21–22) and Eq. (30), one observes

$$\sum_b q_b \hat{\Delta} \hat{F} i_{(b)} = \sum_a \hat{R}_{aq} \mathcal{X}_q + \sum_{ab} n_a \hat{R}_{abi(b)}. \tag{42}$$

Since this equality should be valid for any \mathcal{X}_q and any $i_{(b)}$ satisfying Eq. (21), the coefficients \hat{R}_{ab} , \hat{R}_{aq} should satisfy [53]

$$\sum_a n_a \hat{R}_{aq} = 0, \tag{43a}$$

$$\sum_a n_a \hat{R}_{ab} - q_b \hat{\Delta} \hat{F} = n \hat{R}, \tag{43b}$$

where the tensor \hat{R} does not depend on b . Now Eq. (41b) can be rewritten in the Stephan–Maxwell form

$$n_a \mathcal{X}_{Da} = -n_a \hat{R}_{aq} \mathcal{X}_q + \sum_b \hat{J}_{ab} \left(\frac{i_{(b)}}{n_b} - \frac{i_{(a)}}{n_a} \right) - q_a \hat{\Delta} \hat{F} i_{(a)}, \tag{44}$$

where

$$\hat{J}_{ab} = -n_a n_b (\hat{R}_{ab} - \hat{R}) \tag{45}$$

is the set of the $r(r - 1)/2$ independent friction tensor coefficients also known as the momentum transfer rates. Since according to Eq. (43a) there is $r - 1$ independent thermal diffusion coefficient \hat{R}_{aq} , there are $r(r + 1)/2$ tensors in total which describe the heat and particle diffusion. Notice that the magnetic term in the second line in Eq. (44) does not contribute to the entropy production rate. Indeed, according to Eq. (27b) entropy production contains the product $i_{(a)} \mathcal{X}_{Da}$. The magnetic term contribution from (44) is then $q_a i_{(a)} \hat{\Delta} \hat{F} i_{(a)} = q_a i_{(a)} \hat{F} i_{(a)}$ which vanishes due to asymmetry of the electromagnetic field tensor.

In the isotropic case (in our context – in the absence of magnetic field) all transport coefficients described above are

scalars. In presence of the magnetic field, they become tensors with a certain symmetry with respect to the magnetic field direction. We discuss this structure in detail in Sect. 3.3 based on the irreducible spherical tensor formalism.

In the terrestrial settings transports coefficients defined in the effective hydrodynamics theories can be (at least in principle) obtained from experiment. In the astrophysical settings this is more complicated. Therefore the reliable values for transport coefficients should be derived on the basis of some microscopic theory.

Within the linear response regime, the expressions for the transport coefficients can be given by the Kubo-type formulae (e.g., [54]). Appropriate expressions for the relativistic hydrodynamics (including magnetized case) can be found, e.g., in [16–18, 55] and references therein. The practical analytical calculations of the transport coefficients in this approach can be complicated since they require resummation of infinite number of diagrams.

Another alternative that works in the weak-coupling limit is the kinetic theory framework. Here we assume that the low-temperature conditions in NS cores allow to represent matter as a mixture of weakly interacting quasiparticles and describe it within the Landau Fermi-liquid theory [56]. Then the transport coefficients can be calculated from the kinetic theory for Fermi-liquids, which we describe below.

3 Transport theory of Landau Fermi-liquids

3.1 General setup and definitions

Landau Fermi-liquid theory does not consider the ground state of the system. In contrast it deals with the slightly excited states and assumes that these states of the condensed system are described in terms of weakly interacting quasiparticles which have a one-to-one correspondence to the actual particle states of the system. The Landau Fermi-liquid theory was initially formulated in the non-relativistic setup. The relativistic generalization closely following the original consideration was constructed for the single-component fluid by Baym and Chin [57] (see also the generalization for mixtures [58]). The manifestly covariant generalization exists [59–61] based on the expansion of the pressure variation instead of the energy density variation.

For the purpose of the transport coefficients calculation, it is easiest to work in the rest frame of the fluid. Since the gradients of the hydrodynamic velocity enter the equations for the thermodynamic forces, one also considers the laboratory frames that are close to the LRF, i.e. which have non-relativistic velocities $V \ll 1$. In this case the formulation by Baym and Chin [57] is natural. After necessary velocity gradients are identified in equations, one can set $V = 0$. The resulting equations are similar to their non-relativistic coun-

terparts, having in difference mainly the relativistic quasiparticle dispersion law [57], see also [43].

The quasiparticle states are characterized by the quasi-classical distribution functions $f_a(\mathbf{p}, \mathbf{r}, t)$. Below we will omit the coordinate dependence of the distribution functions for brevity. Distribution functions also depend on the spin quantum numbers (and other quantum numbers, if present). We do not consider here interesting spin-dependent effects, and restrict ourselves to the spin-unpolarized state. Let us abbreviate

$$\int_{\mathbf{p}} \equiv \sum_{\sigma} \int \frac{d^3 \mathbf{p}}{(2\pi)^3}, \tag{46}$$

where σ is a spin state index. Notice that since we work in the LRF, we do not introduce the Lorentz-invariant volume element here. This allows to consider relativistic and non-relativistic cases on the same footing.

The particle densities (zero components of the particle currents) are assumed to be given by the integration of the quasiparticles distribution functions

$$j_{(a)}^0 = \int_{\mathbf{p}} f_a(\mathbf{p}). \tag{47}$$

In principle, one usually defines the family of the space-like hyperplanes orthogonal to some time-like vector π^μ , so that the densities of hydrodynamic variables are defined as, e.g. $\pi_\mu j_{(a)}^\mu$ [41, 62]. We leave this generalization aside and take $\pi^\mu = (1, 0, 0, 0)$.

The momentum density T^{i0} is also defined to be a known functional of $f_a(\mathbf{p})$

$$T^{i0} = \sum_a \int_{\mathbf{p}} p^i f_a(\mathbf{p}). \tag{48}$$

In contrast, the energy density T^{00} is considered as an unknown functional of the set of distribution functions $\{f_a(\mathbf{p})\}$, $a = 1, \dots, r$. However for the small departures from the equilibrium ground state, the variations in energy-momentum density can be written as

$$\delta T^{\mu 0} = \sum_a \delta T_{(a)}^{\mu 0} = \sum_a \int_{\mathbf{p}} p_{(a)}^\mu(\mathbf{p}) \delta f_a(\mathbf{p}), \tag{49}$$

where

$$p_{(a)}^\mu \equiv (\varepsilon_a(\mathbf{p}), \mathbf{p}) \tag{50}$$

and $\varepsilon_a(\mathbf{p})$ is the quasiparticle energy, which itself is the functional of the distribution functions $\varepsilon_a(\mathbf{p}) = \varepsilon_a(\mathbf{p})[\{f_b(\mathbf{p})\}]$. The variational derivative of the quasiparticle energies with respect to the distribution functions

$$\delta \varepsilon_a(\mathbf{p}) = \sum_b \int_{\mathbf{p}'} f_{ab}(\mathbf{p}, \mathbf{p}') \delta f_b(\mathbf{p}') \tag{51}$$

defines the Landau Fermi-liquid interaction $f_{ab}(\mathbf{p}, \mathbf{p}')$.

Entropy density of (quasi)particle species a has a purely combinatorial nature and is given by the same expression as for the non-interacting gas

$$S_a = - \int_{\mathbf{p}} \left[f_a(\mathbf{p}) \log f_a(\mathbf{p}) + (1 - f_a(\mathbf{p})) \log(1 - f_a(\mathbf{p})) \right]. \tag{52}$$

The local equilibrium state described by a set of the local equilibrium distribution functions $\{f_a^{l.e.}\}$ is obtained by maximizing total entropy density subject to constraints $j_{(a)}^0[f^{l.e.}] = j_{(a)}^0$ and $T^{\mu 0}[f^{l.e.}] = T^{\mu 0}$, where j_a^0 and $T^{\mu 0}$ are the actual local values of particle density and energy-momentum density, respectively, which are well-defined as expectation values of the corresponding quantum-mechanical operators for a given state of the system. This conditional extremum problem amounts to maximization of the functional

$$\sum_a \left[S_a[f^{l.e.}] - \alpha_a \left(j_{(a)}^0[f^{l.e.}] - j_{(a)}^0 \right) - \beta_\mu \left(T_{(a)}^{\mu 0}[f^{l.e.}] - T_{(a)}^{\mu 0} \right) \right], \tag{53}$$

where α_a and β^μ are Lagrange multipliers, which are identified as [41]

$$\alpha_a = -\frac{\mu_a}{T}, \quad \beta^\mu = \frac{U^\mu}{T}. \tag{54}$$

Equating to zero the variation of Eq. (53) over distribution functions f_a results in the local equilibrium distribution functions

$$f_a^{l.e.} = f_F \left(\frac{p_{(a),l.e.}^\mu U_\mu(\mathbf{r}, t) - \mu_a(\mathbf{r}, t)}{T(\mathbf{r}, t)} \right), \tag{55}$$

where

$$f_F(x) = [\exp(x) + 1]^{-1} \tag{56}$$

is the Fermi function. Notice that here the local equilibrium dispersion law appears in $p_{(a),l.e.}^\mu = (\varepsilon_a^{l.e.}(\mathbf{p}), \mathbf{p})$, which itself is the functional of Eq. (55).

Using Eq. (54) in variation of Eq. (53) results in the thermodynamic relation

$$U_\mu dT^{\mu 0} = T dS + \sum_a \mu_a dj_{(a)}^0, \tag{57}$$

where $S = \sum_a S_a$, which when written in the LRF reduces to Eq. (11a).

Fermi-liquid theory describes low-temperature systems close to the $T = 0$ ground state. In this case Eq. (55) reduces to the Heaviside step function

$$f_a^{l.e.}(\mathbf{p}) = \Theta(p_{Fa} - p), \tag{58}$$

where

$$p_{Fa} = (3\pi^2 n_a)^{1/3} \tag{59}$$

is the quasiparticle species a Fermi momentum. This means that all states with $p < p_{Fa}$ are occupied and those with $p > p_{Fa}$ are vacant. For small perturbations from equilibrium, the distribution function varies only in the vicinity of the Fermi surface. One defines the quasiparticle Fermi velocity

$$v_{Fa} = \left(\frac{\partial \varepsilon_a^{l.e.}(p)}{\partial p} \right)_{p=p_{Fa}} \tag{60}$$

and (Landau) effective mass on the Fermi surface

$$m_a^* = \frac{p_{Fa}}{v_{Fa}}. \tag{61}$$

The evolution of the distribution function is described by the Landau-Boltzmann transport equation [56,57]

$$\frac{\partial f_a}{\partial t} + \frac{\partial \varepsilon_a}{\partial \mathbf{p}} \nabla f_a - \left(\frac{\partial \varepsilon_a}{\partial \mathbf{r}} - \mathbf{F}_a \right) \nabla_{\mathbf{p}} f_a = I_a[\{f_b\}], \tag{62}$$

where the important difference from the Boltzmann equation for a gas [43,63] is contained in the appearance of the $\partial \varepsilon_a / \partial \mathbf{r}$ term. In Eq. (62), \mathbf{F}_a is the external force (not included in the microscale mean field) which we here take as the Lorentz force

$$\mathbf{F}_a = q_a (\mathbf{E} + [\mathbf{v}_a \times \mathbf{B}]), \tag{63}$$

where $\mathbf{v}_a = \partial \varepsilon_a / \partial \mathbf{p}$. Finally, the term $I_a[\{f_b\}]$ is the collision integral for the quasiparticle species a which describes the change of the distribution function due to collisions and depends, in principle, on the full set of the distribution functions, $b = 1, \dots, r$.

Transport Eq. (62) allows one to derive a general equation of transfer for any state variable ψ . Introducing

$$\langle \psi \rangle = \int_{\mathbf{p}} \psi f_a, \tag{64}$$

and integrating (62) multiplied by ψ one obtains

$$\begin{aligned} \partial_{\mu} \langle v_a^{\mu} \psi \rangle &= \frac{\partial \langle \psi \rangle}{\partial t} + \nabla \cdot \langle \mathbf{v}_a \psi \rangle \\ &= \left\langle \frac{\partial \psi}{\partial t} + \mathbf{v}_a \nabla \psi - (\nabla \varepsilon_a - \mathbf{F}_a) \frac{\partial \psi}{\partial \mathbf{p}} \right\rangle \\ &\quad + \int_{\mathbf{p}} \psi I_a, \end{aligned} \tag{65}$$

where we assumed that $\nabla_{\mathbf{p}} \cdot \mathbf{F}_a = 0$ like in the case of Lorentz force. The term $\langle v_a^{\mu} \psi \rangle$, where

$$v_a^{\mu} = \frac{\partial \varepsilon_a}{\partial p_{(a)}^{\mu}} = (1, \mathbf{v}_a), \tag{66}$$

gives the flux of the variable ψ and the right-hand side of Eq. (65) is the quantity ψ production (or source) term.

Setting $\psi = 1$ in Eq. (65) results in the particle current conservation laws Eqs. (2) with $j_{(a)}^{\mu} = \langle v_a^{\mu} \rangle$. Notice, that in general, $\mathbf{v}_a \neq \mathbf{p}_a / \varepsilon_a$ as holds in the free space. Here it is assumed that the collision integrals conserve particle numbers, i.e. $\int_{\mathbf{p}} I_a = 0$, since we do not consider reactions.

Similarly the transfer equations for four-momenta $\psi = p_{(a)}^{\mu}$ summed over the particle species lead, with the help of Eq. (49), to the energy–momentum tensor conservation law Eq. (3) with the definition [56,57]

$$T_{(a)}^{\mu\nu} = \int_{\mathbf{p}} p^{\mu} v_a^{\nu} f_a(\mathbf{p}) - g^{\mu\nu} \left(\int_{\mathbf{p}} \varepsilon_a(\mathbf{p}) f_a(\mathbf{p}) - T_{(a)}^{00} \right). \tag{67}$$

Notice that for the ideal relativistic gas [43,63] the last term is exactly zero. In deriving Eq. (67), we assumed that the collisions conserve energy and momentum

$$\sum_a p_{(a)}^{\mu} I_a = 0, \tag{68}$$

i.e. there are no external scattering mechanisms and the energy–momentum leakage due to emission processes is neglected. Substituting of the local equilibrium function Eq. (55) into Eq. (52), integrating by parts, summing over particles, and using the definition (49) one obtains in LRF the Eq. (11b) and, hence, the Gibbs-Duhem relation Eq. (11c).

Comparing Eqs. (52) and (64) one observes that the entropy transfer equation can be derived by setting $\psi = \psi_S^{(a)} = -\log f_a + (1 - f_a^{-1}) \log(1 - f_a)$. Current for $\psi_S^{(a)}$ is identified with the partial entropy current of the particle species a and Eq. (65) results in

$$\partial_{\mu} \langle v_a^{\mu} \psi_S^{(a)} \rangle \equiv \zeta_a = \int_{\mathbf{p}} \log \left(\frac{1 - f_a}{f_a} \right) I_a[\{f_b\}]. \tag{69}$$

The right-hand side, summed over particle species, gives the total entropy production, i.e. $\zeta = \sum_a \zeta_a$. It vanishes for the local equilibrium functions Eq. (55) if the collision probabilities which enter the collision integral also correspond to the local equilibrium state.

The collision integral in the right-hand side of Eq. (62) contains contribution from the binary quasiparticle collisions between all species and has the Uehling–Uhlenbeck form

$$I_a[\{f_b\}] = \sum_b I_{ab}, \tag{70}$$

where

$$\begin{aligned} I_{ab}[f] &= -\frac{1}{1 + \delta_{ab}} \int_{\mathbf{p}_1'} \int_{\mathbf{p}_2} \int_{\mathbf{p}_2'} w_{ab}(\mathbf{p}, \mathbf{p}_2; \mathbf{p}_1', \mathbf{p}_2') \\ &\quad \times [f_1 f_2 (1 - f_1')(1 - f_2') \\ &\quad - (1 - f_1)(1 - f_2) f_1' f_2'], \end{aligned} \tag{71}$$

where we abbreviated $f_1 = f_a(\mathbf{p})$, $f_1' = f_a(\mathbf{p}_1')$, $f_2 = f_b(\mathbf{p}_2)$, $f_2' = f_b(\mathbf{p}_2')$, and the kernel $w_{ab}(\mathbf{p}, \mathbf{p}_2; \mathbf{p}_1', \mathbf{p}_2')$

is the differential probability of the quasiparticle collisions.³ It is seen that the collision integral in this form vanishes for the local distribution functions Eq. (55) again if the collision probabilities are calculated for the local equilibrium quasiparticles. However, in general, the local equilibrium functions do not solve the transport Eq. (62), since they do not give zero in the driving term. Both sides of kinetic equation vanish in the global equilibrium state (for the global equilibrium distribution functions). Deviation of the local equilibrium state from the global equilibrium results in the dissipative processes that tend to eliminate these differences.

Unitarity of the scattering matrix for binary collisions, which enters w_{ab} , leads to the Boltzmann H -theorem [43, 63], i.e. to the entropy increase law $\zeta \geq 0$ in Eq. (69) for the collision integral Eq. (71).

The laws of dissipative hydrodynamics are derived from the kinetic theory by considering small deviations around the local equilibrium state. There exist two general methods that perform this expansion. One is the Grad’s moments method [64] and other is the Chapman–Enskog expansion method [65].

The moments method is based on the expansion of the non-equilibrium distribution function in some orthogonal set constructed from p^μ ; the lowest order moments are the physical flows. The expansion is then truncated at a certain finite number of expansion coefficients (moments).

The Chapman–Enskog expansion employs the small parameter, namely the Knudsen number $\text{Kn} = \lambda/L$, where λ is the typical mean free path or the microscopic scale, and L is the typical scale of the state variables gradients, or the macroscopic scale. The distribution functions are then progressively expanded in orders in Kn .

Both methods were derived for non-relativistic systems and are extended to the relativistic sector e.g., [43, 63]. Both approaches suffer from certain limitations, see [66, 67] for a detailed discussion. In the non-relativistic case, lowest order Grad’s method and Chapman–Enskog methods give equivalent formulations, while this is not so in the relativistic case. The relativistic generalization of the Grad’s moments method allowed [25] to construct the casual second-order hydrodynamic equations. On the other hand, the Chapman–Enskog formulation is asymptotically correct (in small Kn limit). There are evidences from the numerical analysis of the solution of the relativistic Boltzmann equations, that the Chapman–Enskog procedure is favored, e.g., [67] and references therein, see, however, [68]. The methods combining advantages of the both procedures are proposed in the non-relativistic (e.g., [53]) and relativistic [66, 69] setup.

³ In case of inelastic collisions (reactions), the final quasiparticle states can correspond to different particle species, i.e. $f_{1'} = f_c(\mathbf{p}_{1'})$ and $f_{2'} = f_d(\mathbf{p}_{2'})$ for a binary reaction $a + b \leftrightarrow c + d$.

Since the Chapman–Enskog method provides asymptotically correct limit for transport equations, the first-order transport coefficients can be reliably calculated in this approach. Below we employ the Chapman–Enskog method at the lowest (linear) order in Kn . To a certain extent, the Chapman–Enskog procedure in a Fermi-liquid turns out to be similar to those for the relativistic gas kinetic theory, described in detail in, e.g., [43, 63, 66].

3.2 Chapman–Enskog procedure

In order to use the Chapman–Enskog procedure one needs to linearize the transport equation (62) around the equilibrium distribution function in terms which are progressively larger in powers of the Knudsen number

$$f_a = f_a^{\text{eq}} + \delta f_a^{(0)} + \delta f_a^{(1)} + \dots \tag{72}$$

where f_a^{eq} is the distribution function in global equilibrium and

$$\delta f_a^{(0)} = f_a^{\text{l.e.}} - f_a^{\text{eq}} \tag{73}$$

is the difference between the local and global equilibrium distribution functions. The quasiparticle energies are functionals of the distribution function and are subject to the similar expansion

$$\varepsilon_a = \varepsilon_a^{\text{eq}} + \delta \varepsilon_a^{(0)} + \delta \varepsilon_a^{(1)} + \dots \tag{74}$$

In the first order one retains zero-order terms in the driving term [left-hand side of Eq. (62)] with the exception of the magnetic part of the Lorentz force and first-order terms in the collision integral. Linearization of the collision integral requires a certain care. Here it is necessary to bear in mind that the conservation laws in the collision probabilities w_{ab} contain true quasiparticle energies. Therefore the collision integral will vanish exactly for any distribution functions of the local equilibrium form if one uses there the true quasiparticle spectrum instead of the local equilibrium one, i.e., if one substitutes $p_{(a),\text{l.e.}}^\mu \rightarrow p_{(a)}^\mu$ in Eq. (55) [52, 56]. It is instructive to introduce the deviation denoted with bar via

$$f_a(\mathbf{p}) = f_a^{\text{l.e.}}(p_{(a),\text{l.e.}}^\mu) + \delta f_a(\mathbf{p}) = f_a^{\text{l.e.}}(p_{(a)}^\mu) + \overline{\delta f_a(\mathbf{p})}. \tag{75}$$

Importantly, the thermodynamic fluxes in the first order are expressed via the functions $\overline{\delta f_a}$ [52]:

$$\Delta \mathbf{j}_{(a)} = \int_{\mathbf{p}} \mathbf{v}_a \overline{\delta f}_a, \tag{76a}$$

$$\mathbf{J}_{(q)} = \sum_a \int_{\mathbf{p}} \mathbf{v}_a (\varepsilon_a - h_a) \overline{\delta f}_a, \tag{76b}$$

$$\Pi^{(ij)} = \sum_a \int_{\mathbf{p}} p^{(i} v_a^{j)} \overline{\delta f}_a. \tag{76c}$$

To obtain Eqs. (76b) and (76c) we used Eq. (67) and the definitions (24) and (25) in the LRF [i.e., in the limit $U^\mu \rightarrow (1, 0, 0, 0)$]. Here and below

$$A^{(ij)} = \frac{1}{2} \left(A^{ij} + A^{ji} - \frac{2}{3} \delta^{ij} A^{kk} \right) \tag{77}$$

is the short-hand notation for the traceless symmetric part of a 3-dimensional tensor A^{ij} .⁴ All variables in Eq. (76), i.e. v_a , ε_a , and h_a , now correspond to the global equilibrium.

The magnetic part of the Lorentz force also vanishes exactly for the distribution function $f_a^{l.e.}(p_{(a)}^\mu)$. We assume that the magnetic field is large, therefore it should be kept in the driving term at the first order. This term thus also contains $\bar{\delta}f_a$ [52].

The linearized transport equation (62) is then given by

$$\begin{aligned} \frac{\partial \delta f_a^{(0)}}{\partial t} + \mathbf{v}_a \nabla \delta f_a^{(0)} - \left(\frac{\partial \delta \varepsilon_a^{(0)}}{\partial \mathbf{r}} - q_a \mathbf{E} \right) \nabla_p f_a^{eq} \\ = -q_a [\mathbf{v}_a \times \mathbf{B}] \nabla_p \bar{\delta} f_a^{(1)} + I_a \left[\left\{ \bar{\delta} f_r^{(1)} \right\} \right], \end{aligned} \tag{78}$$

where v_a , quasiparticle energies and collision probabilities in I_a are calculated for the global equilibrium state. Derivatives in the left-hand side are due to gradients of the macroscopic fields $T(x)$, $\mu_a(x)$, and $\mathbf{V}(x)$.

In order to identify the terms containing velocity gradients, it is necessary to consider the equations in the fixed inertial laboratory frame that moves with the instant velocity $-\mathbf{V}$, $V \ll 1$, relatively to the LRF. Let us indicate state variables in LRF with a bar for a moment, i.e. $\bar{\mathbf{p}}$, $\bar{\varepsilon}_a$, and \bar{f}_a . General principles of Lorentz invariance require that the transformation laws for quasiparticle energy and momentum are the same as for the free particles [57], therefore

$$\bar{\varepsilon}_a^2 - \bar{\mathbf{p}}^2 = \varepsilon_a^2 - \mathbf{p}^2 \equiv M_{Da}^2(\mathbf{p}, \mathbf{r}), \tag{79}$$

where the (Dirac) mass M_{Da} here in principle depends on \mathbf{p} . Notice, that if there is no dependence of M_{Da} on \mathbf{p} , then the standard relation $\mathbf{v}_a = \mathbf{p}/\varepsilon_a$ holds.

When $V \ll 1$, transformation laws for the quasiparticle energy and momenta are [57]

$$\bar{\varepsilon}_a = \varepsilon_a - \mathbf{p}\mathbf{V}, \tag{80a}$$

$$\bar{\mathbf{p}} = \mathbf{p} - \varepsilon_a \mathbf{V}. \tag{80b}$$

and the distribution function in the moving frame is related to the LRF distribution function $\bar{f}_a(\bar{\mathbf{p}})$ as

$$f_a(\mathbf{p}) = \bar{f}_a(\bar{\mathbf{p}}). \tag{81}$$

⁴ The tensor $\Pi^{(ij)}$ coincides with the spatial components of the tensor $\Pi^{(\mu\nu)}$ in Eq. (34b) at $U^\mu \rightarrow (1, 0, 0, 0)$.

The variation of the distribution function at fixed \mathbf{p} can be written according to the chain differentiation rule

$$\delta f_a = \delta \bar{f}_a(\bar{\mathbf{p}}) + \delta \bar{\mathbf{p}} \nabla_{\bar{\mathbf{p}}} \bar{f}_a = \delta \bar{f}_a(\bar{\mathbf{p}}) - \varepsilon_a \frac{\partial \bar{\varepsilon}_a}{\partial \bar{\mathbf{p}}} \delta \mathbf{V} \frac{\partial \bar{f}_a}{\partial \varepsilon_a}, \tag{82}$$

where the variation in the first term is taken at fixed $\bar{\mathbf{p}}$. Similarly, the quasiparticle energy variation is

$$\delta \varepsilon_a = \delta \bar{\varepsilon}_a - \varepsilon_a \frac{\partial \bar{\varepsilon}_a}{\partial \bar{\mathbf{p}}} \delta \mathbf{V} + \mathbf{p} \delta \mathbf{V}. \tag{83}$$

After substitution of Eqs. (82) and (83) to Eq. (78) one can set $\mathbf{V} = 0$, $\bar{\mathbf{p}} = \mathbf{p}$, and $\bar{\varepsilon}_a = \varepsilon_a$.

The proper (i.e. independent of $\delta \mathbf{V}$) zero-order variation of the distribution function in the LRF can be written as

$$\delta f_a^{(0)} = f'_F(x_a) \left(\frac{\delta \varepsilon_a^{(0)} - \delta \mu_a}{T} + (\varepsilon_a - \mu_a) \delta \frac{1}{T} \right), \tag{84}$$

where the dimensionless quantity

$$x_a = \frac{\varepsilon_a - \mu_a}{T} \tag{85}$$

is introduced.

Collecting all terms, one obtains for the left-hand side of Eq. (78)

$$\begin{aligned} \text{l.h.s.} = -f'_F(x_a) \left\{ \frac{\varepsilon_a - h_a}{T} \mathbf{v}_a \left(\frac{\nabla T}{T} + \dot{\mathbf{V}} \right) \right. \\ \left. + \frac{1}{T} \mathbf{v}_a \left(\mathbf{d}_{(a)} + \frac{h_a}{\hbar n} [\mathbf{J} \times \mathbf{B}] \right) \right. \\ \left. \frac{p_i v_{aj}}{T} V_{ij} + \frac{1}{3} (\mathbf{p} \mathbf{v}_a) \text{div} \mathbf{V} - \frac{\partial}{\partial t} \left(\frac{\varepsilon_a^{l.e.} - \mu_a}{T} \right) \right\}, \end{aligned} \tag{86}$$

where (19c) in the limit $V \ll 1$ is used in the second line to eliminate the acceleration $\dot{\mathbf{V}}$. In Eq. (86), $\mathbf{d}_{(a)}$ is the spatial part of the four-vector $d_{(a)}^\mu$, Eq. (28b). Namely in the LRF, $d_{(a)}^\mu = (0, -\mathbf{d}_{(a)})$, where

$$\mathbf{d}_{(a)} = T \nabla \frac{\mu_a}{T} - T \frac{h_a}{\hbar} \sum_b y_b \nabla \frac{\mu_b}{T} - q_a \mathbf{E}. \tag{87}$$

The tensor V_{ij} in Eq. (86) is

$$V_{ij} = \partial_{(i} V_{j)} = \frac{1}{2} \left(\frac{\partial V_i}{\partial x_j} + \frac{\partial V_j}{\partial x_i} - \frac{2}{3} \delta_{ij} \text{div} \mathbf{V} \right) \tag{88}$$

and is the spatial part of Eq. (33b) in the limit $V \ll 1$.

Different lines in Eq. (86) correspond to different transport processes. Namely, the first line corresponds to the heat conduction while the second line to diffusion processes. These two processes are driven by the vector thermodynamic forces, and in principle they mix (Sect. 2). The third line of Eq. (86) corresponds to the shear viscosity, whose driving force is the second-order traceless tensor V_{ij} . The fourth line of Eq. (86)

corresponds to the scalar bulk viscosity processes [56]. As stated above, we do not consider bulk viscosity here, since it is mainly governed not by the quasiparticles collisions but by the reactions, and in this case in the kinetic approach a non-stationary problem should be solved. As such, we further assume that $\text{div } \mathbf{V} = 0$.

It is convenient to further transform the right-hand side of Eq. (78), defining [56]

$$\overline{\delta f_a(\mathbf{p})}^{(1)} \equiv -\frac{1}{T} f'_F(x_a) \Phi_a(\mathbf{p}), \tag{89}$$

where $\Phi_a(\mathbf{p})$ with $a = 1, \dots, r$ are unknown functions to be found. Notice that Eqs. (89) and (86) ensure formally that the deviations from the local equilibrium distribution functions are localized in the vicinity of the Fermi surface due to appearance of the term $f'_F(x)$ in these equations.

With this substitution, the magnetic operator in Eq. (78) becomes

$$\frac{q_a}{T} f'_F(x_a) [\mathbf{v}_a \times \mathbf{B}] \nabla_{\mathbf{p}} \Phi_a(\mathbf{p}), \tag{90}$$

while the collision integrals Eq. (71) take the linearized form

$$I_{ab} \text{lin}[\Phi] = -\frac{1}{T(1 + \delta_{ab})} \int_{\mathbf{p}_1'} \int_{\mathbf{p}_2} \int_{\mathbf{p}_2'} w_{ab}^{\text{eq}}(\mathbf{p}, \mathbf{p}_2; \mathbf{p}_1', \mathbf{p}_2') \times \mathcal{F}_{ab}(\Phi_1 + \Phi_2 - \Phi_{1'} - \Phi_{2'}), \tag{91}$$

where we introduced the Pauli blocking factor

$$\mathcal{F}_{ab} = f_1^{\text{eq}} f_2^{\text{eq}} (1 - f_{1'}^{\text{eq}}) (1 - f_{2'}^{\text{eq}}), \tag{92}$$

$\Phi_1 = \Phi_a(\mathbf{p})$, $\Phi_{1'} = \Phi_a(\mathbf{p}_{1'})$, $\Phi_2 = \Phi_b(\mathbf{p}_2)$, and $\Phi_{2'} = \Phi_b(\mathbf{p}_{2'})$. We will further drop the superscript ‘eq’.

The problem thus reduces to finding the functions $\Phi_a(\mathbf{p})$ from the system of the linearized transport equations

$$\begin{aligned} & -\frac{1}{T} f'_F(x_a) \left\{ (\varepsilon_a - h_a) \mathbf{v}_a \left(\frac{\nabla T}{T} + \dot{\mathbf{V}} \right) \right. \\ & \quad \left. + \mathbf{v}_a \left(\mathbf{d}_{(a)} + \frac{h_a}{\hbar n} [\mathbf{J} \times \mathbf{B}] \right) + p_i v_{aj} V_{ij} \right\} \\ & = \sum_b I_{ab} \text{lin}[\Phi] + \frac{q_a}{T} f'_F(x_a) [\mathbf{v}_a \times \mathbf{B}] \nabla_{\mathbf{p}} \Phi_a(\mathbf{p}). \end{aligned} \tag{93}$$

Consider now the entropy production rate given by Eq. (69). Linearization of the first term under the integral gives

$$\log \frac{1 - f_a}{f_a} \approx \frac{\varepsilon_a - \mu_a}{T} - \frac{1}{T} \Phi_a. \tag{94}$$

The first term correspond to the entropy exchange between the different species. When summed over species, this part of Eq. (69) vanishes (for exact collision integral, as discussed above) and one is left with

$$T \zeta = - \sum_a \int_{\mathbf{p}} \Phi_a(\mathbf{p}) I_a [\{\Phi_b\}]. \tag{95}$$

It is evident from this form of entropy production rate, that ζ is indeed second order in gradients. The linearized collision operator should be seminegative-definite in order to ensure the second law. Multiplying the left-hand side of the linearized Boltzmann Eq. (93) by $\Phi_a(\mathbf{p})$, integrating over \mathbf{p} and summing over species we obtain Eq. (27c) for the entropy generation (formally written in the LRF). Notice that the magnetic term in the right-hand side of Eq. (93) does not contribute to entropy production.

Equations (93) do not determine the functions $\Phi_a(\mathbf{p})$ completely, since the collision integrals are all zero for any set of the functions $\Phi_a^{\text{ker}} = \mathbf{a}_a + \mathbf{b}^\mu p_{(a)}^\mu$, where \mathbf{a}_a ($a = 1 \dots, r$) and \mathbf{b}^μ are arbitrary constants. These constants, which fix the solution of the homogeneous equation, should be determined by the additional conditions known as the conditions of fit [43]. Different conditions of fit can be traced to the different choices of the hydrodynamic frames [33], which is important for stability of the hydrodynamical equations, as discussed in Sect. 2. According to the general discussion, in order to find the frame-invariant collision transport coefficients at first order, it is actually possible to impose any conditions of fit. According to Eqs. (76), the uniform solutions given by a set of the constants $\{\mathbf{a}_a\}$ do not contribute to the dissipation fluxes we consider (notice, that this would not be true for the bulk viscosity). The same is true for the ‘energy’ kernel solutions in the form $\mathbf{b}^0 \varepsilon_{(a)}^0$. The conditions of fit that fix $\{\mathbf{a}_a\}$ and \mathbf{b}^0 are already contained in our definition of the local equilibrium state; they also correspond to the conditions in Eqs. (14). The remaining kernel solutions of the form $\mathbf{b} \mathbf{p}$ do not modify the heat current Eq. (76b) or the shear stress tensor Eq. (76c), but affect the dissipative particle currents Eq. (76a). Clearly, the conditions of fit for fixing the constant vector \mathbf{b} are nothing more than the conditions that fix the hydrodynamic frame. At the same time, we are interested in diffusion fluxes $\mathbf{i}_{(a)}$ that do not depend on \mathbf{b} . Therefore we suggest that the vector \mathbf{b} is fixed by imposing the Eckart condition of fit (i.e. $\mathbf{b} = 0$), when the diffusion transport coefficients can be calculated directly from (76a) in accordance with the discussion around Eq. (27). This considerations allow us to forget about the kernel solutions and assume that the deviation functions Φ_a are linear combinations of thermodynamic forces \mathcal{X}_k

$$\Phi_a(\mathbf{p}) = \sum_k \hat{\mathcal{G}}_k^a(\mathbf{p}) \cdot \mathcal{X}_k, \tag{96}$$

where $\hat{\mathcal{G}}_k^a(\mathbf{p})$ are some, in general tensor, functions.

3.3 Tensor relations

The Curie principle states that the responses to the thermodynamic forces of different tensor ranks do not mix [51]. The microscopic basis of this statement is the scalar character of the collision integral in the isotropic medium. In anisotropic

medium (i.e. anisotropic crystal) this principle can be violated. In the neutron star context this is the case when the magnetic field is very strong and the quasiparticle collisions are affected by magnetic field effects. Another example is the generic anisotropic structure, i.e. anisotropic pasta phase at the bottom of the crust, or the anisotropic pairing texture possible for the triplet neutron pairing. Both these effects are almost unexplored in the regard to NSs. Below we assume that magnetic field does not affect the quasiparticle scattering probabilities and the collision integral is isotropic. In degenerate matter the latter is a good approximation when $\omega_{BFa} \ll qv_{Fa}$, where q is the typical momentum transfer in collisions and is valid for non-quantizing fields considered in this paper.

In order to fully take into account the symmetry of the problem, it is instructive to use the irreducible tensors technique e.g., [43,66]. To this end one performs expansion over the irreducible representations of a little group corresponding to timelike vector U^μ . In the LRF this means the expansion over the irreducible representations of the group of 3D rotations. Usually in the kinetic theory the Cartesian irreducible tensor formalism is used. For our purposes, however, it is instructive to use the formalism of the irreducible spherical tensors (e.g., [70]) which allows for a simple account of the axial symmetry of the problem in the presence of the magnetic field.

Irreducible tensor set (under rotations) is a set of quantities which transform under an irreducible representation of the rotation group. Irreducible spherical tensors, in particular, transform in the same way as the eigenfunctions of the angular momentum operator, i.e. the spherical harmonics. Each vector T can be expressed as the rank-1 irreducible spherical tensor T_μ , $\mu = -1, 0, 1$, employing spherical basis [70]. The transformation law between Cartesian and spherical basis is described by the unitary matrix $U_{\mu i}$, i.e. $T_\mu = U_{\mu i} T_i$. Explicitly,

$$\begin{pmatrix} T_{-1} \\ T_0 \\ T_{+1} \end{pmatrix} = \begin{pmatrix} \frac{1}{\sqrt{2}} & -\frac{i}{\sqrt{2}} & 0 \\ 0 & 0 & 1 \\ -\frac{1}{\sqrt{2}} & -\frac{i}{\sqrt{2}} & 0 \end{pmatrix} \begin{pmatrix} T_x \\ T_y \\ T_z \end{pmatrix}. \tag{97}$$

Similarly, any second-rank tensor can be transformed to the spherical basis as

$$T_{\mu\mu'} = U_{\mu i} U_{\mu' j} T_{ij}. \tag{98}$$

Then the tensor $T_{\mu\mu'}$ can be cast over the irreducible components T_{Kq} via the unitary Clebsch–Gordan transformation

$$T_{\mu\mu'} = \sum_{Kq} i^K C_{1\mu 1\mu'}^{Kq} T_{Lq}, \quad T_{Kq} = \sum_{\mu\mu'} (-i)^K C_{1\mu 1\mu'}^{Kq} T_{\mu\mu'}, \tag{99}$$

where $C_{1\mu 1\mu'}^{Kq}$ is the Clebsch–Gordan coefficient [70]. The phase factor i^K is introduced here to ensure that the resulting

tensors behave similarly to spherical functions under complex conjugation, i.e. $(T_{Kq})^* = (-1)^q T_{K-q}$. Then

$$T_{Kq} = \sum_{\mu\mu'} (-i)^K C_{1\mu 1\mu'}^{Kq} U_{\mu i} U_{\mu' j} T_{ij}, \tag{100a}$$

$$T_{ij} = \sum_{Kq} i^K C_{1\mu 1\mu'}^{Kq} U_{\mu i}^\dagger U_{\mu' j}^\dagger T_{Kq}. \tag{100b}$$

Explicitly, for the traceless symmetric tensor of the second rank T_{ij}

$$T_{20} = -\sqrt{\frac{3}{2}} T_{zz}, \tag{101a}$$

$$T_{2\pm 1} = \pm T_{xz} + iT_{yz}, \tag{101b}$$

$$T_{2\pm 2} = \frac{1}{2} (T_{yy} - T_{xx}) \mp iT_{xy}. \tag{101c}$$

We now rewrite the linearized transport Eq. (93) in the irreducible spherical tensor formalism. The left-hand side of Eq. (93) can be written in the following general form (cf. e.g., [71])

$$-\frac{1}{T} f'_F(x) \sum_k \sqrt{\frac{4\pi}{2\ell_k + 1}} D_k^a(p) (Y_{\ell_k}(\hat{p}) \cdot (\mathcal{X}_k)_{\ell_k}), \tag{102}$$

where ℓ_k is the tensor dimension of the thermodynamic force \mathcal{X}_k , dot denotes the scalar product

$$(Y_{\ell_k}(\hat{p}) \cdot (\mathcal{X}_k)_{\ell_k}) = \sum_{m=-\ell_k}^{\ell_k} Y_{\ell_k m}^*(\hat{p}) (\mathcal{X}_k)_{\ell_k m}, \tag{103}$$

$Y_{\ell_k m}(\hat{p})$ are the spherical harmonics, \hat{p} denotes the direction of p , asterisk means complex conjugate, and $(\mathcal{X}_k)_{\ell_k m}$ is the m 'th component of the thermodynamic force \mathcal{X}_k taken in the irreducible spherical tensor form. The functions $D_k^a(p)$ in Eq. (102) contain the remaining scalar terms in Eq. (93) which depend on p but not on the direction \hat{p} . They are given in Table 1.

In order to transform the right-hand side of Eq. (93) in a similar way, the deviation function $\Phi_a(p)$ can be expanded in the spherical harmonics as

$$\Phi_a(p) = \sum_{\ell m} (\Phi_a)_{\ell m}(p) Y_{\ell m}^*(\hat{p}). \tag{104}$$

Table 1 Explicit forms of various quantities defined in the text for three thermodynamic problems, i.e. thermal conductivity ($k = \kappa$), shear viscosity ($k = \eta$), and diffusion ($k = Da$)

Force (k)	ℓ	D_k^a	\tilde{D}_k	\tilde{X}_k	ξ_k
κ	1	$v_a(\varepsilon_a - h_a)$	T	x	-1
η	2	$\sqrt{2/3}(pv_a)$	$\sqrt{2/3}pv_a$	1	+1
Da	1	v_a	1	1	+1

The collision integral in most general form in this basis is the matrix in ℓm indices

$$I_a[\{\Phi_b\}] = \sum_{\ell m \ell' m'} I_a[\{(\Phi_b)_{\ell' m'}\}]_{\ell m}^{\ell' m'} Y_{\ell m}^*(\hat{\mathbf{p}}). \tag{105}$$

However, when the collision probability is isotropic, the linearized collision integral is diagonal in ℓm and, moreover, does not depend on m

$$I_a^\ell[\{(\Phi_b)_{\ell' m'}\}]_{\ell m}^{\ell' m'} = I_a^\ell[\{(\Phi_b)_{\ell m}\}] \delta_{\ell \ell'} \delta_{m m'}. \tag{106}$$

The magnetization term Eq. (90) can be written in the irreducible form by introducing the \mathbf{p} -space angular momentum operator

$$\hat{\ell}_p = -i [\mathbf{p} \times \nabla_p]. \tag{107}$$

Then Eq. (90) becomes

$$q_a [\mathbf{v}_a \times \mathbf{B}] \nabla_p \delta f_a^{(1)} = i \frac{q_a v_a}{pT} f'_F(x_a) (\mathbf{B} \cdot \hat{\ell}_p) \Phi_a(\mathbf{p}). \tag{108}$$

This operator is diagonal in the spherical basis Eq. (104) if the direction of the magnetic field is taken as the Z axis. The equations can be solved in this frame and then rotated into the general frame, as shown below.

Thus for the isotropic collision operator, the equations for different tensor components of Φ_a decouple and for each component $(\Phi_a)_{\ell m}$ we obtain

$$\begin{aligned} & -\frac{1}{T} f'_F(x) \sum_{k|\ell_k=\ell} \sqrt{\frac{4\pi}{2\ell+1}} D_k^a(p) (\mathcal{X}_k)_{\ell m} \\ & = I_a^\ell[\{(\Phi_b)_{\ell m}\}] + i \frac{1}{T} f'_F(x) m \omega_{Ba}(p) (\Phi_a)_{\ell m}, \end{aligned} \tag{109}$$

where the summation is carried over those thermodynamic forces, that have $\ell_k = \ell$. The forces of the same rank, i.e. $\ell_k = \ell_{k'}$ are present in the left-hand side of Eq. (109) and do mix. Namely, this is the case for the thermal conductivity and diffusion processes which have $\ell_k = \ell_{Da} = 1$, see Eq. (39). As such we ‘proved’ the Curie principle for the linearized kinetic equation. Notice that the conservation of ℓ_k by the magnetic operator (108) ensures absence of the cross-term viscosity ζ_1 introduced in Eqs. (37), (38). The term ω_{Ba} in Eq. (109) is the (momentum-dependent) cyclotron frequency of the particle species a

$$\omega_{Ba} = \frac{q_a B v_a}{p}. \tag{110}$$

Therefore using the irreducible tensor formalism we have splitted the initial system of transport equations into the set of $2\ell + 1$ independent Eq. (109) for each ℓ . Owing to the isotropic character of the collision integral and a simple form of the magnetic term in Eq. (109), one observes that

$$(\Phi_a(B))_{\ell m} = (\Phi_a(mB))_{\ell 1}, \tag{111}$$

thus Eq. (109) needs to be solved only for $m = 1$. The components of Φ_a for other m ’s are obtained by a simple magnetic field rescaling $B \rightarrow mB$ [72,73].

The general solution of the irreducible linear Eq. (109) is a linear combination [cf. Eq. (96)]⁵

$$(\Phi_a)_{\ell m}(p) = \sum_k (\mathcal{G}_k^a(p))_{\ell m} (\mathcal{X}_k)_{\ell m}. \tag{112}$$

Substituting Eq. (109) to Eq. (76) using Eqs. (89) and (104) thermodynamic fluxes in spherical tensor notations reduce to

$$\begin{aligned} (\mathcal{Y}_k)_{\ell m} &= - \sum_a \int_p \frac{1}{T} f'_F(x) \sqrt{\frac{4\pi}{2\ell+1}} D_k^a(p) Y_{\ell m}(\hat{\mathbf{p}}) \Phi_a(\mathbf{p}) \\ &= - \sum_{k'} L_{\ell m}^{kk'} (\mathcal{X}_{k'})_{\ell m}, \end{aligned} \tag{113}$$

with the matrix of the kinetic coefficients $L_{\ell m}^{kk'}$ which is diagonal in ℓm . Explicitly, the matrix $L_{\ell m}^{kk'}$ is related to functions $(\mathcal{G}_k^a(p))_{\ell m}$ in Eq. (112) as

$$L_{\ell m}^{kk'} = \sum_a \frac{g_{sa}}{2\pi^2} \int p^2 dp \frac{f'_F(x)}{T} \sqrt{\frac{4\pi}{2\ell+1}} D_k^a(p) (\mathcal{G}_{k'}^a(p))_{\ell m}, \tag{114}$$

where $g_{sa} = 2$ (for fermions) is the spin statistical weight.

It is instructive to rotate the Eq. (113) to a general coordinate system in the LRF using the rotation matrices (Wigner \mathcal{D} -function [70])

$$\begin{aligned} (\mathcal{Y}_k)_{\ell m} &= \sum_{k' m' m''} (\mathcal{D}_{m m'}^\ell(\hat{\mathbf{b}}, 0))^* L_{\ell m'}^{kk'} (\mathcal{X}_{k'})_{\ell m''} \mathcal{D}_{m'' m'}^\ell(\hat{\mathbf{b}}, 0) \\ &= \sqrt{\frac{4\pi}{2\ell+1}} \sum_{k'} \sum_{K=0}^{2\ell} L_K^{kk'} [(\mathcal{X}_{k'})_\ell \otimes Y_K(\hat{\mathbf{b}})]_{\ell m}, \end{aligned} \tag{115}$$

where $\hat{\mathbf{b}} \equiv \mathbf{B}/B$, square brackets denote irreducible spherical tensor product

$$[(\mathcal{X}_{k'})_\ell \otimes Y_K(\hat{\mathbf{b}})]_{\ell m} = \sum_{m'' Q} C_{\ell m'' K Q}^{\ell m} (\mathcal{X}_{k'})_{\ell m''} Y_{K Q}(\hat{\mathbf{b}}), \tag{116}$$

and $L_K^{kk'}$ is a different set of $2\ell + 1$ kinetic coefficients linearly related to $2\ell + 1$ coefficients $L_{\ell m}^{kk'}$ as

$$L_K^{kk'} = \sum_m (-1)^{\ell-m} C_{\ell m \ell -m}^{K 0} L_{\ell m}^{kk'}. \tag{117}$$

As Eq. (115) is written in a form of an expansion over the spherical harmonics in the direction of magnetic field, it can be convenient in practice. Notice, that the component index

⁵ Notice that $(\mathcal{G}_k^a(p))_{\ell m}$ are coefficients in the linear combination Eq. (112) written in the specific frame, where \mathbf{B} is the polar axis, and are not the spherical components of the tensor \hat{G}_k^a in Eq. (96). They can be related by the transformation similar as performed in Eq. (115).

m can now be dropped in Eq. (115) since this is now the relation between the tensors for the general orientation of the LRF coordinate system with respect to \mathbf{B} . The relation (115) can be transformed from the LRF to the general frame by applying the appropriate Lorentz boosts to the tensor quantities in this relation. In this way the generalized transport coefficients (i.e. as specified in [74]) can be determined. At the end of the day they are expressed via the $(2\ell + 1)$ coefficients $L_{\ell m}^{kk'}$ or $L_K^{kk'}$ for each kk' pair. According to discussion around Eq. (111), it is enough to calculate the function

$$\tilde{L}_{kk'}(B) \equiv L_{\ell k 1}^{kk'}(B), \tag{118}$$

since $L_{\ell m}^{kk'}(B) = L_{\ell 1}^{kk'}(mB)$.

The spherical tensor formalism above can be easily connected to the Cartesian one. Let us start from the vector ($\ell = 1$) thermodynamic forces. For example, for the thermal conductivity problem (ignoring the thermal diffusion term) one gets

$$\mathcal{Y}_{qz} = -T\tilde{\kappa}(B=0)\mathcal{X}_{qz}, \tag{119a}$$

$$(\mp\mathcal{Y}_{qx} - i\mathcal{Y}_{qy}) = -T\tilde{\kappa}(\pm B)(\mp\mathcal{X}_{qx} - i\mathcal{X}_{qy}). \tag{119b}$$

Comparing with the standard definitions [52], one identifies $\kappa_{\parallel} \equiv \tilde{\kappa}(B=0)$ as the parallel component of heat conductivity, $\kappa_{\perp} \equiv \text{Re}\tilde{\kappa}(B)$ as the transverse heat conductivity, and $\kappa_{\wedge} \equiv -\text{Im}\tilde{\kappa}(B)$ as the Hall thermal conductivity component. Similar expressions hold for other transport coefficients related to the vector thermodynamic forces. The conduction parallel to magnetic field does not depend on B , while the conduction across the magnetic field depends on it.

The relations between the Cartesian components of the stress-energy tensor and the tensor V_{ij} ($\ell = 2$) are

$$\Pi_{zz} = 2\tilde{\eta}(B=0)V_{zz}, \tag{120a}$$

$$(\Pi_{zx} \pm i\Pi_{zy}) = 2\tilde{\eta}(\pm B)(V_{zx} \pm iV_{zy}), \tag{120b}$$

$$(\Pi_{xx} - \Pi_{yy} \pm 2i\Pi_{xy}) = 2\tilde{\eta}(\pm 2B) \times (V_{xx} - V_{yy} \pm 2iV_{xy}). \tag{120c}$$

Let us compare this equations with traditional formulation containing five shear viscosity coefficients $\eta_0 \dots \eta_4$ [52]

$$\Pi_{zz} = 2\eta_0 V_{zz}, \tag{121a}$$

$$\Pi_{xx} = -\eta_0 V_{zz} + \eta_1(V_{xx} - V_{yy}) + 2\eta_3 V_{xy}, \tag{121b}$$

$$\Pi_{yy} = -\eta_0 V_{zz} - \eta_1(V_{xx} - V_{yy}) - 2\eta_3 V_{xy}, \tag{121c}$$

$$\Pi_{xy} = 2\eta_1 V_{xy} - \eta_3(V_{xx} - V_{yy}), \tag{121d}$$

$$\Pi_{xz} = 2\eta_2 V_{xz} + 2\eta_4 V_{yz}, \tag{121e}$$

$$\Pi_{yz} = 2\eta_2 V_{yz} - 2\eta_4 V_{xz}. \tag{121f}$$

Then one identifies $\eta_0 = \tilde{\eta}(B=0)$, $\eta_1 = \text{Re}\tilde{\eta}(2B)$, $\eta_3 = -\text{Im}\tilde{\eta}(2B)$, $\eta_2 = \text{Re}\tilde{\eta}(B)$, $\eta_4 = -\text{Im}\tilde{\eta}(B)$.

3.4 Relaxation time approximation

The above considerations are general, but they can be analyzed in the most transparent form if the relaxation time approximation for the collision integral is used, which reads

$$I_a^{\ell}[\Phi_a] = \frac{1}{T} f'_F(x_a) \frac{(\Phi_a)_{\ell m}}{\tau_a^{(\ell)}(\varepsilon_a)}. \tag{122}$$

The covariant form of the relaxation time approximation is the Anderson-Witting model [75] where in the general frame Eq. (122) is multiplied by a factor $(p^{\mu}U_{\mu})/p^0$ (equal to 1 in the LRF). This form violates the current conservation as well as the energy and momentum conservation, respected by the collision integrals Eq. (71). In this sense it is not correct to employ the relaxation time approximation for description of transport of a closed (self-contained) plasma. In the non-relativistic case, the generalization of the relaxation time approximation was given by [76] and the current-conserving relaxation time approximations for relativistic plasmas were recently formulated by [77,78]. Here these peculiarities do not matter since we investigate the general tensor structure of the transport coefficients. One may view the relaxation time in Eq. (122) as a manifestation of the external scattering mechanisms which do not respect the conservation laws (an example is the scattering of electron off the ionic lattice in the NS crust). Within the same reasoning, we consider the single component case for simplicity, but retain the electric charge of this component. Then the electric conductivity and thermal diffusion effects are present, governed by the external scattering mechanism.

In the relaxation time approximation, the solution of the linearized Eq. (109) is given in the form Eq. (112) where simply

$$(\mathcal{G}_k^a(p))_{\ell m} = -\sqrt{\frac{4\pi}{2\ell+1}} D_k^a(p) \frac{\tau_a^{(\ell)}}{1 + im\omega_{Ba}\tau_a^{(\ell)}}, \tag{123}$$

and according to Eq. (114)

$$L_{\ell m}^{kk'} = -\frac{g_s}{2\pi^2(2\ell+1)} \int p^2 dp \frac{f'_F(x)}{T} D_k^a(p) D_{k'}^a(p) \times \frac{\tau_a^{(\ell)}}{1 + im\omega_{Ba}\tau_a^{(\ell)}}. \tag{124}$$

Three transport coefficients in the vector sector (with $k, k' = q, Da$) are

$$\left\{ \begin{array}{l} \tilde{L}_{qq}(B) \\ \tilde{L}_{qa}(B) \\ \tilde{L}_{aa}(B) \end{array} \right\} = -\frac{1}{3\pi^2} \int p^2 v_a^2 dp \frac{f'_F(x)}{T} \left\{ \begin{array}{l} (\varepsilon_a - h_a)^2 \\ (\varepsilon_a - h_a) \\ 1 \end{array} \right\} \times \frac{\tau_a^{(1)}(\varepsilon_a)}{1 + i\omega_{Ba}\tau_a^{(1)}(\varepsilon_a)}. \tag{125}$$

The coefficient \tilde{L}_{aa} when multiplied by q_a^2 is the charge conductivity, the coefficient \tilde{L}_{qa} describes thermodiffusion

effects, and \tilde{L}_{qq} is related to the heat conduction, although the traditional thermal conductivity coefficient in this case is given by

$$T\tilde{\kappa} = \tilde{L}_{qq} - \frac{\tilde{L}_{qa}^2}{\tilde{L}_{aa}}, \tag{126}$$

according to Eq. (41). In the degenerate matter, $h_a \approx \mu_a$ and the factor $f'_F(x) \approx -\delta(x)$, and integration in Eq. (125) results in

$$\tilde{\kappa} = \frac{\pi^2 n_a T}{3m_a^*} \frac{\tau_a^{(1)}(\mu_a)}{1 + i\omega_{BFa}\tau_a^{(1)}(\mu_a)}, \tag{127a}$$

$$\tilde{L}_{aa} = \frac{n_a}{m_a^*} \frac{\tau_a^{(1)}(\mu_a)}{1 + i\omega_{BFa}\tau_a^{(1)}(\mu_a)}, \tag{127b}$$

where ω_{BFa} is the cyclotron frequency at the Fermi surface defined in Eq. (1). Here we employed the fact that the thermal diffusion coefficient vanishes at the first approximation ($\tau_a^{(1)}(\epsilon_a) = \text{const}$) (see the discussion below), thus $\tilde{\kappa} \approx T^{-1}\tilde{L}_{qq}$. Equation (127b) is the Drudde formula and the Wiedemann-Franz rule $\tilde{\kappa} = \pi^2 T \tilde{L}_{aa} / 3$ holds in the degenerate case in the relaxation time approximation [79].

In the limit of large magnetization, $\omega_{BFa}\tau^{(1)}(\mu) \gg 1$, one finds

$$\kappa_{\perp} = \text{Re} \tilde{\kappa} = \frac{\pi^2 n_a T}{3m_a^*} \frac{1}{\omega_{BFa}^2 \tau_a^{(1)}(\mu_a)} \propto B^{-2} \tag{128a}$$

$$\kappa_{\wedge} = -\text{Im} \tilde{\kappa} = \frac{\pi^2 n_a T}{3m_a^*} \frac{1}{\omega_{BFa}} \propto B^{-1}. \tag{128b}$$

Notice that the limiting value of the Hall component of the thermal conductivity in Eq. (128b) does not depend on the collision mechanism and depends only on the quasiparticle number density n_a and the magnetic field B .

Similarly, for the shear viscosity ($\ell = 2$), we obtain from Eqs. (38), (124), (118), and Table 1, the following expression

$$\tilde{\eta} = -\frac{1}{15\pi^2} \int p^4 v_a^2 dp \frac{f'_F(x)}{T} \frac{\tau_a^{(2)}(\epsilon_a)}{1 + i\omega_{Ba}\tau_a^{(2)}(\epsilon_a)}, \tag{129}$$

which for the strongly degenerate matter integrates to

$$\tilde{\eta} = \frac{n_a p_{Fa}^2}{5m_a^*} \frac{\tau_a^{(2)}(\mu_a)}{1 + i\omega_{BFa}\tau_a^{(2)}(\mu_a)}. \tag{130}$$

In the limit of strong magnetization, $\omega_{BFa}\tau_a^{(2)}(\mu_a) \gg 1$, we obtain

$$\eta_1 = \frac{\eta_2}{4} = \frac{n_a p_{Fa}^2}{5m_a^*} \frac{1}{4\omega_{BFa}^2 \tau_a^{(2)}(\mu_a)}. \tag{131a}$$

$$\eta_3 = \frac{\eta_4}{2} = \frac{n_a p_{Fa}^2}{5m_a^*} \frac{1}{2\omega_{BFa}}. \tag{131b}$$

Like for the thermal conductivity, the ‘Hall’ components of the shear viscosity, η_3 and η_4 , do not depend on $\tau^{(2)}$ and depend only on the quasiparticle number density.

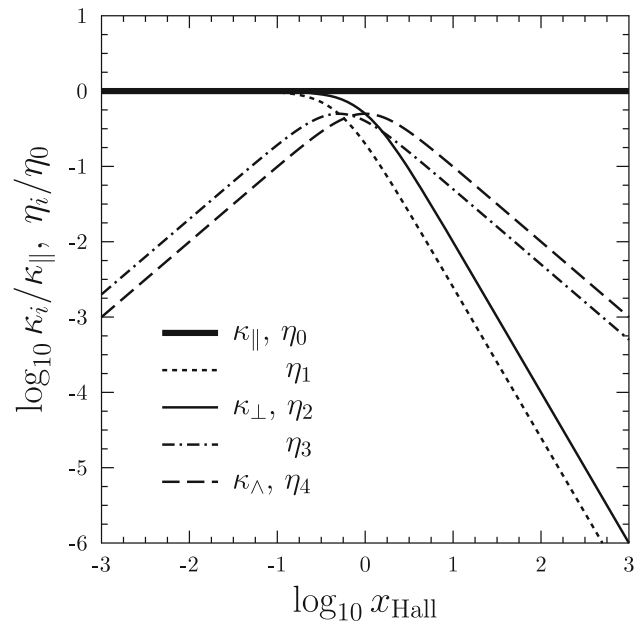


Fig. 1 Thermal conductivity components (κ_{\parallel} , κ_{\perp} , κ_{\wedge}) in units of κ_{\parallel} and shear viscosity components (η_0, \dots, η_4) in units of η_0 in relaxation-time approximation as function of the Hall parameter x_{Hall} , Eq. (132), see text for details

Although the relaxation time approximation is probably the simplest one, it catches the qualitative behavior of the tensor components of the transport coefficients with magnetic field. Let us introduce the Hall parameter

$$x_{\text{Hall}} = \omega_{BFa}\tau_a(\mu_a), \tag{132}$$

where $\tau_a(\mu_a)$ is either $\tau_a^{(1)}(\mu_a)$ or $\tau_a^{(2)}(\mu_a)$ depending on the tensor rank of the corresponding thermodynamic force. The particles are said to be magnetized when their $x_{\text{Hall}} \gtrsim 1$. In Fig. 1 we plot the dependence of various components of thermal conductivity and shear viscosity tensors on x_{Hall} following Eqs. (127) and (130). All quantities in Fig. 1 are plotted relative to the longitudinal components (η_0 or κ_{\parallel}) of the transport coefficients in question. Until $x_{\text{Hall}} \gtrsim 1$, transverse and longitudinal components of the transport coefficients are almost indistinguishable and the corresponding Hall components are small but gradually increase with x_{Hall} . At $x_{\text{Hall}} = 1$, they reach maximum with $\kappa_{\wedge}/\kappa_{\parallel} = \eta_4/\eta_0 = 1/2$. At the same point $\kappa_{\perp}/\kappa_{\parallel} = \eta_2/\eta_0 = 1/2$. For larger x_{Hall} , both transverse and Hall components of transport coefficient tensors decrease, albeit with different slopes. Namely, at large Hall parameters, one gets $\kappa_{\perp}/\kappa_{\parallel} = \eta_2/\eta_0 = x_{\text{Hall}}^{-2}$ and $\kappa_{\wedge}/\kappa_{\parallel} = \eta_4/\eta_0 = x_{\text{Hall}}^{-1}$.

In general case, the relaxation time approximation does not hold. In particular this is the situation in the NS cores, where the relaxation time approximation is not applicable (Sect. 3.6). In this case, one employs the general function $\Phi_{\ell m}$ in Eqs. (123)–(125), (129) instead of the solution (123). Before turning to the calculation of transport coefficients in

NS cores, let us briefly outline the variational method of the solution of the linearized transport equation.

3.5 Variational principle

The linearized transport Eq. (93) is the linear integral equation for the set of functions $\Phi_a, a = 1, \dots, r$, which in this section we denote collectively as Φ , that can be symbolically written as

$$X = (\hat{L} + \hat{M})\Phi, \tag{133}$$

where \hat{L} is the collision operator, which is symmetric and semi-negative definite in the Hilbert space of the functions Φ , \hat{M} is the magnetic operator which is anti-symmetric, and X is the left-hand side. \hat{L} and \hat{M} here are understood as matrices in particle species state.

The general transport Eq. (133) can rarely be solved analytically. One of the examples is the relaxation time approximation described in the previous section. For the traditional single-component Fermi-liquids, where the collision integral has the specific properties detailed in the next section, it is possible to construct the exact solutions of Eq. (133) [80–82]. This method was generalized to multicomponent problem by [71, 83] and to the non-Hermitian case in [84].

In other cases other mathematical methods are necessary, for instance quadrature methods [85]. Here we briefly outline the idea of the variational method of transport theory [43, 79, 86]. Consider first the case $\mathbf{B} = 0$, and, therefore, $\hat{M} = 0$, and define the scalar product

$$\langle \Psi | \Phi \rangle = \int_p \Psi(\mathbf{p})^* \Phi(\mathbf{p}) \tag{134}$$

(in the multicomponent system the summation over species index is understood). Left multiplying Eq. (133) with $\langle \Phi |$, one obtains

$$\langle \Phi | X \rangle = \langle \Phi | \hat{L} | \Phi \rangle, \tag{135}$$

where the right-hand side of this equation is clearly the entropy production rate according to Eq. (95)

$$T\mathcal{S} = -\langle \Phi | \hat{L} | \Phi \rangle. \tag{136}$$

It can be proved [79] that the solution of Eq. (133) maximizes Eq. (136) subject to condition Eq. (135). This is one of the equivalent formulations of the variational principle of the transport theory [79]. One observes, that it is closely related to the second law of thermodynamics (see also [86] for a review). The variational principle can be reformulated to give the boundaries on the diagonal transport coefficients in the Onsager linear relations.

In practice, the variational principle is used via the expansion of the set of test functions over some convenient finite

basis set $\{|\Phi_n\rangle\}_{n=1\dots N}$

$$\Phi = \sum_{n=1}^N c_n \Phi_n, \tag{137}$$

with coefficients c_n being the variational parameters. Then the variational equations take the form of the system of linear equations [43, 79]

$$\langle \Phi_n | X \rangle = \sum_{m=1}^N \langle \Phi_n | \hat{L} | \Phi_m \rangle c_m \tag{138}$$

which define the variational coefficients c_n . In a sense, this method approximates the integral kernel \hat{L} with some degenerate kernel [85].

Unfortunately, in the magnetized case the straightforward application of the variational principle is not possible. The physical reason is that the magnetic field term drops out of the entropy generation rate. One can formulate the similar principle for the Eq. (109) for functions $\Phi_{\ell m}$ (or using the function $\Phi(-\mathbf{B})$ in place of the complex conjugate function in Eq. (134) [79]). In this case the variational functional is only stationary (have a saddle point) but not the extremal one, however the relevant equations for the variational basis will also take the form

$$\langle \Phi_n | X \rangle = \sum_m \langle \Phi_n | \hat{L} + \hat{M} | \Phi_m \rangle c_m. \tag{139}$$

This method for non-Hermitian operators is essentially the Bubnov–Galerkin method, see e.g., [43, 85]. We are not going in the discussion of the convergence of this procedure and assume that the sufficient conditions are fulfilled. In fact, we will use below the simplest variational solution based on the single variational function ($N = 1$) which proved itself to be rather accurate under the NS conditions.

3.6 Transport coefficients for the general Fermi-liquid collision integral

For the multicomponent Fermi liquid inside NS cores the relaxation time approximations is not valid, therefore it is necessary to consider the generic linearized collision integral Eq. (91). Remember, that we assume that collision integral is scalar, i.e. the transition probability w_{ab} depends only on the relative orientations of the momenta of the colliding particles. Following the formalism of Sect. 3.3, the spherical components of the collision integral [see Eq. (106)] take the form

$$I_a^\ell[\{(\Phi_b)_{\ell m}\}] = \sum_b I_{ab}^\ell[\{(\Phi_b)_{\ell m}\}], \tag{140}$$

where (see Appendix A for details)

$$I_{ab}^\ell = -\frac{1}{T(1 + \delta_{ab})} \int_{\mathbf{p}_1'} \int_{\mathbf{p}_2} \int_{\mathbf{p}_2'} w_{ab}(\mathbf{p}_1, \mathbf{p}_2, \mathbf{p}_1', \mathbf{p}_2')$$

$$\begin{aligned} & \times \mathcal{F}_{ab} \left((\Phi_a(p_1))_{\ell m} + (\Phi_b(p_2))_{\ell m} \mathcal{P}_\ell(\hat{p}_1 \hat{p}_2) \right. \\ & - (\Phi_a(p_{1'}))_{\ell m} \mathcal{P}_\ell(\hat{p}_1 \hat{p}_{1'}) \\ & \left. - (\Phi_b(p_{2'}))_{\ell m} \mathcal{P}_\ell(\hat{p}_1 \hat{p}_{2'}) \right), \end{aligned} \tag{141}$$

an $\mathcal{P}_\ell(y)$ are Legendre polynomials of the order ℓ . Here we redefine $\mathbf{p}_1 = \mathbf{p}$ in comparison with Eq. (91), that makes the description of the scattering process as $12 \rightarrow 1'2'$ more symmetric (on the price of introducing the redundant index 1 in the left-hand side of the kinetic equation). Equation (141) is written for the elastic binary collisions, where the particle species in the input and output channels are the same. In case of the reactions (or inelastic collisions), in general deviation functions for four different species (for the reaction in a form $a + b \leftrightarrow c + d$) enter Eq. (141). This equation is still linear and the whole formalism below can be adapted to this case (assuming that the matter is in equilibrium with respect to such a reaction, i.e. $\mu_a + \mu_b = \mu_c + \mu_d$) with small modifications, although the kinematics of collisions become more involved.

The transition probability can be written as

$$w_{ab} = (2\pi)^4 \delta^{(4)}(P' - P) |T_{ab}(12 \rightarrow 1'2')|^2, \tag{142}$$

where $\delta^{(4)}(P' - P)$ represent the four-momenta conservation with $P^\mu = p_1^\mu + p_2^\mu$ and $P'^\mu = p_{1'}^\mu + p_{2'}^\mu$ being the total quasiparticle pair four-momenta before and after the collision, respectively, and $T_{ab}(12 \rightarrow 1'2')$ is the transition matrix element. Since we are considering the spin-unpolarised case, it is convenient to define the spin-averaged squared transition matrix element as

$$Q_{ab} = \frac{1}{4(1 + \delta_{ab})} \sum_{\text{spins}} |T_{ab}(12 \rightarrow 1'2')|^2. \tag{143}$$

Owing to a strong degeneracy of Fermi liquids, it is possible to decompose angular and energy integration, putting quasiparticles on the Fermi surfaces whenever possible. Moreover, only in the vicinity the Fermi surface the well-defined quasiparticles exist. Then one can express (dropping species index for brevity) $d\mathbf{p} = m^* p d\varepsilon d\Omega_p$. Moving from the energy integration to the integration over the dimensionless energy variable x , Eq. (85), one can extend the lower integration limit for x from $-\mu/T$ to $-\infty$. This allows to introduce an additional symmetry variable, namely the parity with respect to the $x \leftrightarrow -x$ inversion, which we denote as $\xi = \pm 1$. The collision integral conserves parity, therefore the perturbations that are odd and even in x decouple. As stated already, at the same level of approximation one can take $h_a \approx \mu_a$ and neglect temperature corrections to the chemical potentials. Then the heat conductivity driving term becomes odd in x , while the shear viscosity and diffusion parts are even in x . This means, in particular, that in the first approximation the thermal diffusion transport coefficients vanish and therefore thermal conductivity and diffu-

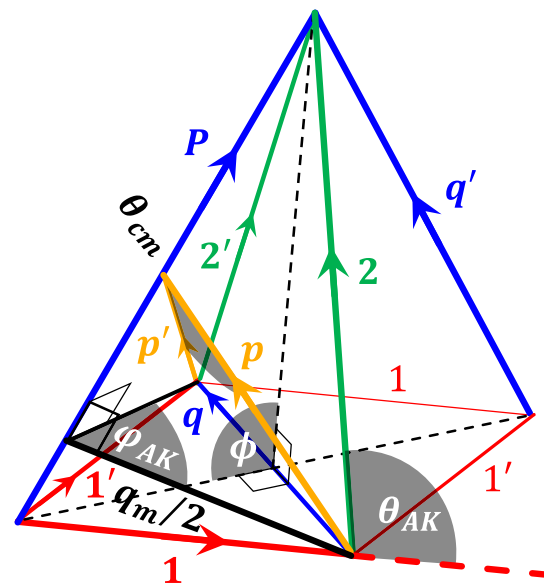


Fig. 2 Collision geometry for the process $12 \rightarrow 1'2'$ assuming $p_1 = p_{1'}$ and $p_2 = p_{2'}$. Various quasiparticle momenta and their combinations, as well as the relevant angles are identified, as discussed in the text

sion problems decouple. Based on this, we can consider the shear viscosity, thermal conductivity, and diffusion problems separately [56,71].

The relative orientation of four fixed-length vectors in space is fixed by two angular variables, see Fig. 2. Therefore of six angular integrations in Eq. (141) only two remain (formally, three integrations are eliminated by the momentum-conserving delta-function and one integration over the third Euler angle of the body-frame coordinate system, say azimuthal angle of \mathbf{p}_2 around \mathbf{p}_1 , is trivial). Different choices of these angular variables can be convenient depending on the properties of the collision matrix element. Figure 2 shows the geometry and various convenient angles and vectors. The momenta of the quasiparticles of the species a and b before the collision are \mathbf{p}_1 and \mathbf{p}_2 , respectively, while their momenta after the collision are $\mathbf{p}_{1'}$ and $\mathbf{p}_{2'}$, respectively. Total colliding pair momentum $\mathbf{P} = \mathbf{p}_1 + \mathbf{p}_2 = \mathbf{p}_{1'} + \mathbf{p}_{2'}$ is conserved during collisions. The momentum transferred in collision from b quasiparticle to a quasiparticle is $\mathbf{q} = \mathbf{p}_{1'} - \mathbf{p}_1 = \mathbf{p}_2 - \mathbf{p}_{2'}$ and the transferred energy is $\omega = \varepsilon_{1'} - \varepsilon_1 = \varepsilon_2 - \varepsilon_{2'}$. In degenerate matter, the transferred energy is of the order of temperature [due to the Pauli blocking factor \mathcal{F}_{ab} in Eq. (141)] and therefore is small. In addition, one defines the momentum $\mathbf{q}' = \mathbf{p}_{2'} - \mathbf{p}_1$ which describes the momentum transfer in exchange channel.

In what follows it is convenient to define the angular average of some function $A(\{\mathbf{p}_i\})$ as⁶

⁶ Actually, this expression is not exactly an average, since for $A = 1$ it gives $\pi(q_{\max} - q_{\min})$, see (145) below. This definition, however, reduces the number of unnecessary factors in expressions.

$$\langle A(\{\mathbf{p}_i\}) \rangle = \frac{p_1 p_2 p_{1'} p_{2'}}{16\pi^2} \int d\hat{\mathbf{p}}_1 d\hat{\mathbf{p}}_{1'} d\hat{\mathbf{p}}_2 d\hat{\mathbf{p}}_{2'} A(\{\mathbf{p}_i\}) \times \delta(\mathbf{p}_{1'} + \mathbf{p}_{2'} - \mathbf{p}_1 - \mathbf{p}_2). \tag{144}$$

If the function $A(\{\mathbf{p}_i\})$ depends only on the relative orientations of the quasiparticle momenta, as in Eq. (141), the integration over $\hat{\mathbf{p}}_1$ gives just 4π , and can be excluded from Eq. (144).

Scattering matrices are frequently obtained from the microscopic theory as functions of the transferred momentum \mathbf{q} . Therefore, one of the convenient angular variables is $q = |\mathbf{q}|$ and for the second one one can use the angle ϕ between the planes $(\mathbf{p}_1 \mathbf{p}_{1'})$ and $(\mathbf{p}_2 \mathbf{p}_{2'})$, see Fig. 2. In this case the angular averages reduce to the integration over q and ϕ :

$$\langle A(\{\mathbf{p}_i\}) \rangle = \int_{q_{\min}}^{q_{\max}} dq \int_0^\pi d\phi A(\{\mathbf{p}_i\}), \tag{145}$$

where $q_{\max} = \min(p_1 + p_{1'}, p_2 + p_{2'})$ and $q_{\min} = \max(|p_1 - p_{1'}|, |p_2 - p_{2'}|)$. In NS cores one has $|\omega|v_{Fa,b} \ll q$ and $q_{\min} \approx \max(|\omega|/v_{Fa}, |\omega|/v_{Fb})$ [1]. One can set $p_1 \approx p_{1'} \approx p_{Fa}$, $p_2 \approx p_{2'} \approx p_{Fb}$, $q_{\min} = 0$ and $q_{\max} = \min(2p_{Fa}, 2p_{Fb})$.

Alternatively, we notice that the cross-sections for the in-medium problems are frequently calculated from microscopic theory as a function of the total momentum P . In this case it is convenient to use P and the Abrikosov–Khalatnikov angle ϕ_{AK} [87] (see Fig. 2) instead of q and ϕ . The angle ϕ_{AK} is the angle between the $(\mathbf{p}_1 \mathbf{p}_2)$ and $(\mathbf{p}_{1'} \mathbf{p}_{2'})$ planes. In this case, the angular average becomes

$$\langle A(\{\mathbf{p}_i\}) \rangle = \int_{P_{\min}}^{P_{\max}} dP \int_0^\pi d\phi_{AK} A(\{\mathbf{p}_i\}), \tag{146}$$

where $P_{\min} = |p_{Fa} - p_{Fb}|$ and $P_{\max} = p_{Fa} + p_{Fb}$. One can relate P to the second Abrikosov-Khalatnikov angle, namely the angle θ_{AK} between \mathbf{p}_2 and \mathbf{p}_1 via

$$P^2 = p_1^2 + p_2^2 + 2p_1 p_2 \cos \theta_{AK}, \tag{147}$$

which is convenient when w_{ab} is known as a function of θ_{AK} and ϕ_{AK} . In this case one obtains the standard definitions of angular averages of the Fermi-liquid theory [56, 71].

Finally, it can be convenient to use P and q as the integration variables. This is achieved by utilizing the relation

$$q = q_m \sin \frac{\phi_{AK}}{2}, \tag{148}$$

where $q_m(P)$ is the maximal value of q for a given P and is equal to twice the height in the (p_1, p_2, P) triangle (see Fig. 2)

$$q_m = \frac{2p_1 p_2 \sin \Theta_{AK}}{P} = \frac{\sqrt{4p_{Fa}^2 p_{Fb}^2 - (p_{Fa}^2 + p_{Fb}^2 - P^2)^2}}{P}. \tag{149}$$

Then

$$\langle A(\{\mathbf{p}_i\}) \rangle = 2 \int_{P_{\min}}^{P_{\max}} dP \int_0^{q_m} \frac{dq}{\sqrt{q_m^2 - q^2}} A(\{\mathbf{p}_i\}). \tag{150}$$

The concise description of the different choices of the angular variables can be found in [84].

The remaining integration is performed over energy variables, or over x_i , $i = (1, 2, 1', 2')$, in the dimensionless form. One integration is eliminated by the energy conservation and generally only the two integrations remain. One of them can be carried out further if the transition probability can be placed on shell, i.e., if it does not depend on the transferred energy $\omega = \varepsilon_{1'} - \varepsilon_1$. This is the standard approximation for the traditional Fermi-liquids [56]. However, in principle, transition probability can depend on the transferred energy. This is the typical situation encountered in the classical, non-degenerate plasmas. But, it turns out that the electromagnetic interaction in the relativistic plasma (and also the QCD interactions for the quark matter) also possesses this property [88].

To proceed further, it is convenient to express

$$D_k^a(p_1) \approx v_{Fa} \tilde{D}_k(p_{Fa}) \tilde{X}_k(x_1), \tag{151}$$

where $\tilde{X}_k(x_1)$ is the x -dependent part of the driving term (namely, x_1 for the thermal conductivity and 1 for other processes considered), and $\tilde{D}_k(p_{Fa})$ is the remainder, which depends on the on-shell momentum p_{Fa} . This decomposition is possible since we work in the vicinity of the Fermi surface which is guaranteed by the presence of the factor $f'_F(x)$ in all integral expressions for physical quantities. The functions entering Eq. (152) are also given in Table 1.

Consider now the thermal conductivity or shear viscosity problems. As said above, these transport problems can be considered separately owing to the symmetry restrictions. The diffusion problem will be treated later. The irreducible spherical components of the deviation function Φ_a^k can be represented ($k = \kappa, \eta$) as

$$\left(\Phi_a^k(p_1) \right)_{\ell m} = -\sqrt{\frac{4\pi}{2\ell + 1}} \tilde{D}_k(p_{Fa}) (\mathcal{X}_k)_{\ell m} \times \lambda_a^{(k, \text{eff})} \left(\Psi_a^k(x_1) \right)_{\ell m}, \tag{152}$$

where $(\Psi_a^k(x_1))_{\ell m}$ are the dimensionless functions of the energy variable. Notice that there is no summation over k in comparison to Eq. (123) due to decoupling of the transport phenomena considered.

The quantities $\lambda_a^{(k, \text{eff})}$ in Eq. (152) are the auxiliary effective mean free paths. Traditionally, in the Fermi-liquid transport theory one utilizes the concept of the effective relaxation times (e.g., [56], see also Sect. 3.3), which are related to the effective mean free paths as $\lambda_{\text{eff}} = v_F \tau_{\text{eff}}$. Since the NS cores contain the relativistic leptons with Fermi velocities of the order of the speed of light and the heavy non-relativistic

baryons (e.g., protons), the relaxation times for these quasiparticles are quite different, while the effective mean free paths are closer [89], and usage of λ_{eff} instead of τ_{eff} seems to be more convenient, although this is of course a matter of taste. In the standard approach, one takes the single quasiparticle excitation mean free path (relaxation time) for $\lambda_a^{(k,\text{eff})}$ [56, 71]. However this approach is problematic in the relativistic plasma in NS cores, since this quantity diverges at the Fermi surface due to the properties of the long-range electromagnetic interaction (e.g., [90]). This potentially could present a problem for the whole theory, however the transport is governed by the quasiparticles slightly distorted from the Fermi surface and the resulting transport mean free path stays finite. In principle, the auxiliary effective mean free paths $\lambda_a^{(k,\text{eff})}$ are then selected based on the aesthetic arguments (e.g. in such a way that the system of transport equations is made maximally compact).

Once the functions $\Psi_a^k(x)$ defined in Eq. (152) are found from the solution of the linearized transport equation, the complex thermal conductivity and shear viscosity coefficients can be found. The corresponding expressions are given by Eqs. (A.5) and (A.6) in Appendix A. The complete systems of linearized transport equation for thermal conductivity and shear viscosity problems for the case when the scattering probability can depend on the transferred energy ω are rather lengthy and are given in Appendix A. Notice, that when w_{ab} does not depend on ω , the situation simplifies significantly and the exact solution of the system of the multicomponent transport equations can be constructed [71]. In general situation, the exact analytical solution is not known.

Here we employ the simplest variational solution based on the one-parametric family of the test functions as described in Sect. 3.5. In this respect, we consider the equation for $m = 1$ (Sect. 3.3) and replace

$$\lambda_a^{(k,\text{eff})}(\Psi_a^k(x_1))_{\ell 1} \rightarrow \tilde{\lambda}_a^k \tilde{X}_k(x_1) \tag{153}$$

in Eq. (152), where $\tilde{\lambda}_a^k$ is now a (complex) variational parameter. The tilde above $\tilde{\lambda}_a^k$ has the same meaning as in Eq. (118). Substitution Eq. (153) is a simplest one which respects the parity of the function $\tilde{\Psi}(x_1)$ and clearly resembles the solution (123) obtained in the relaxation time approximation.

Using Eqs. (137) and (139) with $N = 1$ and evaluating the scalar products one obtains the following system of equations for $k = \kappa, \eta$

$$1 = \sum_b \left(\Lambda_{ab}^k \tilde{\lambda}_a^k + \Lambda'_{ab}{}^k \tilde{\lambda}_b^k \right) + i \frac{\omega_{\text{BF}a}}{v_{\text{F}a}} \tilde{\lambda}_a^k \tag{154}$$

at the lowest order variational solution. The matrices Λ_{ab}^k and $\Lambda'_{ab}{}^k$ contain all information about the quasiparticle collisions and are related to the transport cross-section in the system. They differ for the different transport problems considered, see below, but the general structure is the same. We

will call further Λ_{ab}^k as transport matrix. Equation (154) is written in the form that isolates different pair collision mechanisms. It is instructive to rewrite it in an explicit form of the $r \times r$ linear system for $\tilde{\lambda}_a^k$

$$1 = \left(\Lambda_a^k + i \frac{\omega_{\text{BF}a}}{v_{\text{F}a}} \right) \tilde{\lambda}_a^k + \sum_{b \neq a} \Lambda_{ab}^k \tilde{\lambda}_b^k, \quad a = 1 \dots r, \tag{155}$$

where the diagonal elements of the (transport) matrix of the system are

$$\Lambda_a^k = \sum_b \Lambda_{ab}^k + \Lambda'_{aa}{}^k. \tag{156}$$

Once the parameters $\tilde{\lambda}_a^k$ are found from the system of equations (155), the partial thermal conductivity and shear viscosity are given by the standard expressions [cf. Eqs. (127a) and (130)]

$$\tilde{\kappa}_a = \frac{\pi^2 n_a T}{3 p_{\text{F}a}} \tilde{\lambda}_a^\kappa, \tag{157}$$

$$\tilde{\eta}_a = \frac{n_a p_{\text{F}a}}{5} \tilde{\lambda}_a^\eta. \tag{158}$$

According to Eq. (114), the total κ and η are given by a sum of the partial contributions over particle species.

The transport matrices Λ_{ab}^k in Eq. (154) are given by the angular averages of the transition matrix element with certain angular factors depending on the transport coefficient considered. Specifically, for the thermal conductivity, $k = \kappa$ ($\ell = 1, \xi = 1$)

$$\Lambda_{ab}^\kappa = \frac{3T^2 m_a^{*2} m_b^{*2}}{4\pi^4 p_{\text{F}a}^2} \int_w \left\langle \left(\frac{w^2}{\pi^2} + \left[\frac{1}{3} - \frac{w^2}{6\pi^2} \right] \frac{q^2}{p_{\text{F}a}^2} \right) Q_{ab} \right\rangle, \tag{159a}$$

$$\Lambda'^{\kappa}_{ab} = -\frac{3T^2 m_a^{*2} m_b^{*2}}{4\pi^4 p_{\text{F}a}^2} \int_w \frac{w^2}{\pi^2} \left\langle \left(\frac{\mathbf{p}_1(\mathbf{p}_2 + \mathbf{p}_2')}{2 p_{\text{F}a} p_{\text{F}b}} \right) Q_{ab} \right\rangle, \tag{159b}$$

where $w = \omega/T$ is the dimensionless transferred energy and the abbreviation

$$\int_w = \int_0^\infty dw \frac{(w/2)^2}{\sinh^2(w/2)} \tag{160}$$

is introduced.

For the shear viscosity, $k = \eta$ ($\ell = 2, \xi = +1$) the transport matrix elements are

$$\Lambda_{ab}^\eta = \frac{3T^2 m_a^{*2} m_b^{*2}}{4\pi^4 p_{\text{F}a}^2} \int_w \left\langle \frac{q^2}{p_{\text{F}a}^2} \left(1 - \frac{q^2}{4 p_{\text{F}a}^2} \right) Q_{ab} \right\rangle, \tag{161a}$$

$$\Lambda'^{\eta}_{ab} = -\frac{3T^2 m_a^{*2} m_b^{*2}}{4\pi^4 p_{\text{F}a}^2} \int_w \left\langle \frac{q^2}{p_{\text{F}a}^2} \left(\frac{\mathbf{p}_1(\mathbf{p}_2 + \mathbf{p}_2')}{2 p_{\text{F}a} p_{\text{F}b}} \right) Q_{ab} \right\rangle. \tag{161b}$$

In principle, the determination of the diffusion coefficients should proceed in similar way. The certain care is needed since there are $r - 1$ independent forces in the left-hand side of the Boltzman equation and one needs to employ the additional condition of fit (as discussed in Sect. 2), the conditions specifying the Eckart frame can be used). There are different strategies for treating this problem, e.g., [91] (see also the appendix in Ref. [74]). However, in the lowest-order variational approximation it is instructive to employ the Stephan–Maxwell scheme Eq. (44) and express $\mathbf{d}_{(a)}$ through the diffusion fluxes. This is easily achieved by writing

$$\Phi_a(\mathbf{p}_1) = \mathbf{p}_1 \mathbf{w}_{(a)} \tag{162}$$

with constant vectors $\mathbf{w}_{(a)}$ which have the meaning of the diffusion velocity since in this case

$$\Delta \mathbf{j}_{(a)} = n_a \mathbf{w}_{(a)}. \tag{163}$$

Integration of the linearized transport equation multiplied with \mathbf{p}_1 results in

$$\begin{aligned} n_a \left(\mathbf{d}_{(a)} + \frac{\hbar_a}{\hbar n} [\mathbf{J} \times \mathbf{B}] \right) &= \int_{\mathbf{p}_1} \mathbf{p}_1 I_a[\{\Phi_b\}] \\ &+ q_a [\Delta \mathbf{j}_{(a)} \times \mathbf{B}] = \sum_b J_{ab} (\mathbf{w}_b - \mathbf{w}_a) \\ &+ n_a q_a [\mathbf{w}_a \times \mathbf{B}], \end{aligned} \tag{164}$$

where

$$J_{ab} = \frac{T^2 m_a^{*2} m_b^{*2}}{12\pi^6} \int_w \langle q^2 \mathcal{Q}_{ab} \rangle \tag{165}$$

are the momentum transfer rates (or friction coefficients). In this simplest case the friction coefficients J_{ab} do not depend on the magnetic field. Going beyond Eq. (162) in principle results in tensor structure of the coefficients J_{ab} , characteristic for the vector transport coefficients (Sect. 3.3). The equation of motions (164) serve as a part of the input for the studies of the magnetic field evolution in NS cores, e.g. [92–97]. When the diffusion driving forces $\mathbf{d}_{(a)}$ contain only the electric field contribution (no chemical gradients), sometimes it is desirable to invert Eq. (164) and find the relation $\mathbf{J} = \hat{\sigma} \mathbf{E}$, where $\hat{\sigma}$ is the electrical conductivity tensor. Electrical conductivity depends on the momentum transfer rates J_{ab} in a non-trivial way, see, e.g., [8]. A problem of inversion of Eq. (164) is discussed in Appendix C where also a practical expression for the electrical conductivity for a specific case of $npe\mu$ matter is given.

In traditional Fermi liquids, the squared transition matrix element \mathcal{Q}_{ab} does not depend on $\omega = wT$. Then integrals over w in Eqs. (159), (161), and (165) can be taken analytically and one obtains instead of Eqs. (159a)–(165) the following expressions:

$$A_{ab}^\kappa = \frac{T^2 m_a^{*2} m_b^{*2}}{5\pi^2 p_{Fa}^2} \left\langle \left(1 + \frac{q^2}{4p_{Fa}^2} \right) \mathcal{Q}_{ab} \right\rangle, \tag{166a}$$

$$A_{ab}^{\prime\kappa} = - \frac{T^2 m_a^{*2} m_b^{*2}}{5\pi^2 p_{Fa}^2} \left\langle \left(\frac{\mathbf{p}_1(\mathbf{p}_2 + \mathbf{p}_{2'})}{2p_{Fa} p_{Fb}} \right) \mathcal{Q}_{ab} \right\rangle. \tag{166b}$$

$$A_{ab}^\eta = \frac{T^2 m_a^{*2} m_b^{*2}}{4\pi^2 p_{Fa}^2} \left\langle \frac{q^2}{p_{Fa}^2} \left(1 - \frac{q^2}{4p_{Fa}^2} \right) \mathcal{Q}_{ab} \right\rangle, \tag{167a}$$

$$A_{ab}^{\prime\eta} = - \frac{T^2 m_a^{*2} m_b^{*2}}{4\pi^2 p_{Fa}^2} \left\langle \frac{q^2}{p_{Fa}^2} \left(\frac{\mathbf{p}_1(\mathbf{p}_2 + \mathbf{p}_{2'})}{2p_{Fa} p_{Fb}} \right) \mathcal{Q}_{ab} \right\rangle, \tag{167b}$$

$$J_{ab} = \frac{T^2 m_a^{*2} m_b^{*2}}{36\pi^4} \langle q^2 \mathcal{Q}_{ab} \rangle. \tag{168}$$

In general, as stated above, in this case it is possible to obtain exact solutions of the system of transport equations analytically [71, 84], but the properties of electromagnetic interactions in NS cores spoil this picture.

Therefore, in order to find the transport coefficients of the magnetized multicomponent liquid inside the NS cores one needs to be supplied by the quasiparticle spectra (effective masses) and the squared matrix element $\mathcal{Q}_{ab}(\omega, q, \phi)$. The discussion of the latter one is the subject of the next section.

4 Microphysics of quasiparticle collisions in NS cores

We assume here that the NS cores contain light leptonic component (electrons and muons) and heavy baryon component. For the transport properties of the quark NS core see, e.g., review in [1] and references therein. Leptons interact between themselves and with charged baryons via the electromagnetic forces, while baryons mainly interact by the strong forces. The presence of the dense medium modifies the properties of both these interaction channels. When collisions of charged baryons are considered, in principle, the interference between the electromagnetic and strong interaction channels needs to be taken into account [98]. However, it was found that the charged baryons usually give negligible contribution to the transport coefficients [83, 89, 99, 100]. Therefore, we neglect the interference contribution and consider the electromagnetic and strong channels separately for simplicity.

4.1 Electromagnetic interactions

The properties of the electromagnetic interaction are strongly affected by the character of the plasma screening. In the relativistic plasma the magnetic part of the interaction becomes dominant which in the leading order is screened dynamically. This changes considerably the behavior of the transport cross-sections in cold relativistic plasmas resulting in their non-Fermi liquid temperature dependence. This was realized in Refs. [88, 101, 102] and applied to the nucleonic NS core matter by [103–106], see [1] for a review.

The transition matrix at the one-loop level is given as

$$T_{ab} \rightarrow M_{ab} = 4\pi\alpha_f \left(\frac{\mathcal{J}_a^0 \mathcal{J}_b^0}{q^2 + \Pi_l(\omega, q)} - \frac{\mathcal{J}_{a,t} \mathcal{J}_{b,t}}{q^2 + \Pi_t(\omega, q)} \right), \tag{169}$$

where α_f is the fine-structure constant, $\mathcal{J}_{a,t}$ is the transverse with respect to \mathbf{q} component of the spatial part of the transition current, \mathcal{J}_a^0 is the timelike component of the transition current, and $\Pi_l(\omega, q)$ and $\Pi_t(\omega, q)$ are the longitudinal and transverse polarization operators of the photon in medium, respectively. When $a = b$, the exchange contribution needs to be taken into account according to

$$T_{ab}(12 \rightarrow 1'2') \rightarrow M_{ab}(12 \rightarrow 1'2') - M_{ab}(12 \rightarrow 2'1'), \tag{170}$$

which leads to appearance of the exchange-interference terms in the squared matrix element. However these interference terms lead only to small corrections to the transport cross-sections (due to dominance of the small-angle collisions) and can be neglected [103, 104].

Remember that the relevant energy transfer in the collisions is of the order of temperature due to Pauli blocking. Therefore it is enough to take the polarization operators in the limits ($\omega, q \ll p_{Fa}$) and $\omega v_{Fa} \ll q$. In this case the longitudinal polarization operator is simply the squared Debye mass

$$\Pi_l(\omega, q) = q_l^2 \equiv \frac{4\alpha_f}{\pi} \sum_a Z_a^2 m_a^* p_{Fa}, \tag{171}$$

where Z_a is the quasiparticle charge number so that $q_a = Z_a e$. In NS cores, $Z_a = \pm 1$. Notice the appearance of the quasiparticle effective mass in Eq. (171). In contrast, the transverse screening is not static, and in the leading order it is governed by the Landau damping. The transverse polarization operator is

$$\Pi_t(\omega, q) = i \frac{\pi}{4} \frac{\omega}{q} q_t^2 \equiv i \frac{\omega}{q} \alpha_f \sum_a Z_a^2 p_{Fa}^2 \equiv i \Lambda^3 / q, \tag{172}$$

where the characteristic momentum scale Λ is introduced, which obeys $\Lambda \ll q_l \ll p_{Fa}$. At high temperatures ($T \gtrsim q_l$), the static limit breaks down and one needs to consider more general structure of the polarization operator [102]. Notice that the detailed analysis of the impact of various approximations to Π_l and Π_t is performed by [106, 107], where it is found that the so-called hard dense loop result for the in-medium polarization functions is always a good approximation in the NS core context.

In order to calculate \mathcal{Q}_{ab} , it is necessary to take the spin trace of the squared matrix element Eq. (169). The electromagnetic transition current in free space is given by

$$\mathcal{J}_a^\mu = \bar{u}_a(p_{1'}) \left(F_{a1}(-q^2) \gamma^\mu + i \frac{F_{a2}(-q^2)}{2m_a} \sigma^{\mu\nu} q_\nu \right) u_a(p_1), \tag{173}$$

where $\sigma^{\mu\nu} = i/2[\gamma^\mu, \gamma^\nu]$, $F_{a1}(-q^2)$ and $F_{a2}(-q^2)$ are electromagnetic form-factors, m_a is the bare particle mass, and the $u_a(p_1)$ is the Dirac bispinor normalized as

$$\bar{u}_a u_a = \frac{m_a}{\varepsilon_a}. \tag{174}$$

This normalization is used in order to keep the notations for transition matrix elements close in relativistic and non-relativistic cases.

Defining

$$G_a^{\mu\nu} = \frac{1}{2} \sum_{\text{spins}} \mathcal{J}_a^\mu \mathcal{J}_a^\nu \tag{175}$$

one obtains

$$G_a^{\mu\nu} = \frac{F_{a1}^2(-q^2) + F_{a2}^2(-q^2) q^2 / (4m_a^2)}{4\varepsilon_a^2} P_a^\mu P_a^\nu + \frac{F_{a,m}^2(-q^2)}{4\varepsilon_a^2} \left(Q^2 g^{\mu\nu} - Q^\mu Q^\nu \right), \tag{176}$$

where $F_{a,m}(-q^2) = F_{a1}(-q^2) + F_{a2}(-q^2)$ is the Sachs magnetic form-factor, $P_a^\mu = p_1^\mu + p_{1'}^\mu$ and $Q^\mu = p_1^\mu - p_{1'}^\mu$. Notice that for leptons the form factors are $F_{\ell 1} = F_{\ell m} = 1$, $F_{\ell 2} = 0$ (neglecting QED corrections), while for proton $F_{p1}(0) = 1$, $F_{pm}(0) = 2.79$, and for the neutron $F_{n1}(0) = 0$, $F_{nm}(0) = -1.91$.

The squared transition matrix element is then

$$\mathcal{Q}_{ab} = 16\pi^2 \alpha_f^2 \left(\frac{G_a^{00} G_b^{00}}{|q^2 + \Pi_l(\omega, q)|^2} - 2\text{Re} \frac{G_a^{k0} G_b^{k0}}{(q^2 + \Pi_l(\omega, q))(q^2 + \Pi_t(\omega, q))^*} + \frac{G_a^{kl} G_b^{kl}}{|q^2 + \Pi_t(\omega, q)|^2} \right), \tag{177}$$

where we neglected exchange-interference term for identical particles ($a = b$) and took into account that $\mathcal{J}_{a,t} \approx \mathcal{J}_a$ in the limit $\omega v_{Fa} \ll 1$ since $Q = (0, \mathbf{q})$, $Q^2 = -q^2$, and the spatial component of P_a is transverse to \mathbf{q} .

Equation (176) is obtained for the free non-interacting particles and can be modified by the Fermi-liquid effects. For degenerate leptons which form almost ideal gas, it is enough to use Eq. (176). Since we are interested in the transition probabilities in the vicinity of the Fermi surface, we can set $\varepsilon_a = m_a^*$.

The situation is different for baryons. However, the main contribution to the scattering probabilities comes from the small-angle collisions, where $q \ll p_{Fa}$. In non-relativistic limit (applicable well for protons in NS cores) this also means

that $q \ll m_a$. For charged baryons (protons) this allows one to neglect the magnetic term containing $F_{a,m}^2$ and do not discuss its renormalization in a first approximation. At the same level of approximation, one can neglect the kinematic structure of the form-factors and the anomalous magnetic moment interaction and set $F_{a1}(-q^2) \approx F_{a1}(0) = 1$, $F_{a2}(-q^2) \approx F_{a2}(0) = 0$. Then the same expressions for lepton and lepton-baryon scattering can be used. Finally, notice that the transition current is the matrix element of the velocity operator. That means that in vicinity of the Fermi surface one should substitute $\epsilon_a \rightarrow m_a^*$ in denominator in Eq. (176) as in the case of free particles. These considerations are not valid for neutrons which are chargeless particles. However their electromagnetic interaction with other charged particles is small and can be neglected.

Therefore, using Eqs. (176), (177), one finds the following expression for Q_{ab}

$$Q_{ab} = 16\pi^2 \alpha_f^2 Z_a^2 Z_b^2 \left(\frac{L_l}{|q^2 + \Pi_l(\omega, q)|^2} - 2\text{Re} \frac{v_{Fa} v_{Fb} L_{tl}}{(q^2 + \Pi_l(\omega, q))(q^2 + \Pi_t(\omega, q))^*} + \frac{v_{Fa}^2 v_{Fb}^2 L_t}{|q^2 + \Pi_t(\omega, q)|^2} \right), \tag{178}$$

where the kinematic numerators are

$$L_l = \left(1 - \frac{q^2}{4m_a^{*2}} \right) \left(1 - \frac{q^2}{4m_b^{*2}} \right), \tag{179a}$$

$$L_{tl} = \sqrt{\left(1 - \frac{q^2}{4p_{Fa}^2} \right) \left(1 - \frac{q^2}{4p_{Fb}^2} \right)} \cos \phi, \tag{179b}$$

$$L_t = \left(1 - \frac{q^2}{4p_{Fa}^2} \right) \left(1 - \frac{q^2}{4p_{Fb}^2} \right) \cos^2 \phi + \frac{q^2}{4p_{Fa}^2} + \frac{q^2}{4p_{Fb}^2}. \tag{179c}$$

The Eqs. (178), (179) needs to be substituted into the expressions for the various transport matrix components, Eqs. (159), (161), and (165). We need to perform three integrations (over q , ϕ , and w). The integration over ϕ is trivial since the angular weighting factors in ‘direct’ transport matrices Eqs. (159a), (161a), and (165) do not depend on ϕ , while the weighting factor in the non-diagonal transport matrices Λ_{ab}^k in Eqs. (159b) and (161b) in contrast are proportional to $\cos \phi$. Therefore the longitudinal (L_l) and transverse (L_t) channels contribute to transport matrices Λ_{ab}^k , J_{ab} , so one can decompose $\Lambda_{ab}^k = \Lambda_{ab}^{k,l} + \Lambda_{ab}^{k,t}$, while the non-diagonal matrices Λ_{ab}^k contain only the mixed (L_{tl}) channel. After the ϕ integration, Eq. (178) contains only the polynomial in q^2 terms in the numerator. The integrals over q [see Eq. (145)] will

depend on the following rational integrals for three terms in Eq. (178)

$$I_l^{(n)} = \int_0^{q_m} \frac{q^n dq}{|q^2 + \Pi_l|^2} = \int_0^{q_m} \frac{q^n dq}{|q^2 + q_l^2|^2}, \tag{180}$$

$$I_t^{(n)} = \int_0^{q_m} \frac{q^n dq}{|q^2 + \Pi_t|^2} = \int_0^{q_m} \frac{q^{n+2} dq}{q^6 + \Lambda^6}, \tag{181}$$

$$I_{tl}^{(n)} = \int_0^{q_m} \text{Re} \frac{q^n dq}{(q^2 + \Pi_l)(q^2 + \Pi_t)^*} = \int_0^{q_m} \frac{q^{n+4} dq}{(q^2 + q_l^2)(q^6 + \Lambda^6)}, \tag{182}$$

which all can be taken analytically. We do not give these lengthy expressions here,⁷ but notice that since the characteristic transverse screening momentum Λ is small, only the leading terms in Λ are needed in practice. Then

$$I_t^{(0)} = \frac{\pi}{6\Lambda^3} + \mathcal{O}(\Lambda^{-1}), \quad I_t^{(2)} = \frac{\pi}{3\Lambda} + \mathcal{O}(\Lambda), \tag{183}$$

$$I_{tl}^{(0)} = \frac{\pi^2}{3q_l^2 \Lambda} + \mathcal{O}(\Lambda^0), \tag{184}$$

but for the mixed integral and $n \geq 2$, the transverse screening can be neglected and

$$I_{tl}^{(n)} = I_l^{(n)} + q_l^2 I_l^{(n-2)} + \mathcal{O}(\Lambda), \quad n \geq 2. \tag{185}$$

The longitudinal part of the squared matrix element does not depend on Λ at all. The only dependence on w in expressions is contained in the Λ -dependent terms. When the leading contribution in Λ is identified, the integral over w can be performed analytically. Collecting all results, we find for the transport matrices for the thermal conductivity problem

$$\Lambda_{ab}^k = \Lambda_{ab}^{k,t} + \Lambda_{ab}^{k,l}, \tag{186}$$

where the transverse contribution is

$$\Lambda_{ab}^{k,t} = \frac{24\zeta(3)T}{\pi^3 q_l^2} \alpha_f^2 Z_a^2 Z_b^2 p_{Fb}^2, \tag{187}$$

where $\zeta(3)$ is the Riemann zeta-function, while for the longitudinal contribution one obtains rather lengthy, but simple expression

$$\Lambda_{ab}^{k,l} = \frac{16\pi \alpha_f^2 Z_a^2 Z_b^2 T^2 m_a^{*2} m_b^{*2}}{5p_{Fa}^2} \left(I_l^{(0)} + \frac{1}{4} \left(\frac{1}{p_{Fa}^2} - \frac{1}{m_a^{*2}} - \frac{1}{m_b^{*2}} \right) I_l^{(2)} - \frac{1}{16} \left(\frac{1}{p_{Fa}^2 m_a^{*2}} - \frac{1}{m_a^{*2} m_b^{*2}} + \frac{1}{p_{Fa}^2 m_b^{*2}} \right) I_l^{(4)} + \frac{1}{64 p_{Fa}^2 m_a^{*2} m_b^{*2}} I_l^{(6)} \right). \tag{188}$$

⁷ Explicit expressions for some of these integrals are given in Appendix B.

In practice it is enough to restrict the calculations to the first line in Eq. (188). Keeping explicitly only the leading term in q_l , one gets

$$\Lambda_{ab}^{\kappa,l} = \frac{4\pi^2 \alpha_f^2 Z_a^2 Z_b^2 T^2 m_a^{*2} m_b^{*2}}{5 p_{Fa}^2 q_l^3} + \mathcal{O}(q_l^{-1}), \tag{189}$$

however it is not recommended to use this limit, since the correction induced by the exact expression for $I_l^{(0)}$ can be significant. Other integrals in Eq. (188) are written for completeness. The non-diagonal term for thermal conductivity, Eq. (159b), contains only the mixed (tl) contribution. Keeping the leading order in Λ results in

$$\Lambda_{ab}^{\kappa} = \left(\frac{4}{\pi}\right)^{1/3} \Gamma(11/3) \zeta(8/3) \alpha_f^2 Z_a^2 Z_b^2 \frac{m_a^* m_b^* p_{Fb} T^{5/3}}{p_{Fa} q_l^2 q_t^{2/3}}, \tag{190}$$

where $\Gamma(11/3)$ is the Euler gamma-function, and this result is exact in q_l .

Similarly, for the shear viscosity transport matrices,

$$\Lambda_{ab}^{\eta} = \Lambda_{ab}^{\eta,t} + \Lambda_{ab}^{\eta,l}, \tag{191}$$

where the transverse contribution is

$$\Lambda_{ab}^{\eta,t} = 2 \left(\frac{4}{\pi}\right)^{1/3} \Gamma(8/3) \zeta(5/3) \alpha_f^2 Z_a^2 Z_b^2 \frac{p_{Fb}^2 T^{5/3}}{p_{Fa} q_l^2 q_t^{2/3}}. \tag{192}$$

Notice the different power of temperature in comparison with Eq. (187). This is a result of an additional q^2 factor in Eq. (161a) which leads to different contribution of plasma screening to the final result. The longitudinal contribution with account for all kinematic corrections is given by

$$\begin{aligned} \Lambda_{ab}^{\eta,l} = & \frac{4\pi \alpha_f^2 Z_a^2 Z_b^2 T^2 m_a^{*2} m_b^{*2}}{p_{Fa}^4} \left(I_l^{(2)} \right. \\ & - \frac{1}{4} \left(\frac{1}{p_{Fa}^2} + \frac{1}{m_a^{*2}} + \frac{1}{m_b^{*2}} \right) I_l^{(4)} \\ & + \frac{1}{16} \left(\frac{1}{p_{Fa}^2 m_a^{*2}} + \frac{1}{m_a^{*2} m_b^{*2}} + \frac{1}{p_{Fa}^2 m_b^{*2}} \right) I_l^{(6)} \\ & \left. - \frac{1}{64 p_{Fa}^2 m_a^{*2} m_b^{*2}} I_l^{(8)} \right). \end{aligned} \tag{193}$$

The leading contribution is given by the first line in Eq. (193). Retaining the leading order in q_l , Eq. (193) reads

$$\Lambda_{ab}^{\eta,l} = \frac{\pi^2 \alpha_f^2 Z_a^2 Z_b^2 T^2 m_a^{*2} m_b^{*2}}{p_{Fa}^4 q_l} + \mathcal{O}(q_l). \tag{194}$$

In contrast to the thermal conductivity case, for the shear viscosity problem the non-diagonal matrix element Λ_{ab}^{η} does not depend on the transverse screening in the leading order

and has the same order in q_l as the longitudinal part, namely

$$\begin{aligned} \Lambda_{ab}^{\eta} = & \frac{4\pi \alpha_f^2 Z_a^2 Z_b^2 T^2 m_a^* m_b^* p_{Fb}}{p_{Fa}^3} \\ & \left(I_{tl}^{(2)} - \frac{1}{4} \left(\frac{1}{p_{Fa}^2} + \frac{1}{p_{Fb}^2} \right) I_{tl}^{(4)} \right. \\ & \left. + \frac{1}{16 p_{Fa}^2 p_{Fb}^2} I_{tl}^{(6)} \right), \end{aligned} \tag{195}$$

and, keeping the leading order in q_l ,

$$\Lambda_{ab}^{\eta} = \frac{2\pi^2 \alpha_f^2 Z_a^2 Z_b^2 T^2 m_a^* m_b^* p_b}{p_{Fa}^3 q_l} + \mathcal{O}(q_l). \tag{196}$$

Finally, performing the same integration for the momentum transfer rates in Eq. (165), one finds

$$J_{ab} = J_{ab}^l + J_{ab}^t, \tag{197}$$

i.e. there is no mixed longitudinal-transverse contributions in this case. The transverse term J_{ab}^t in Eq. (197) is

$$J_{ab}^t = \frac{n_a p_{Fa}}{3} \Lambda_{ab}^{\eta,t} \tag{198}$$

and the longitudinal one is

$$\begin{aligned} J_{ab}^l = & \frac{4}{9\pi} \alpha_f^2 Z_a^2 Z_b^2 T^2 m_a^{*2} m_b^{*2} \\ & \left(I_l^{(2)} - \frac{1}{4} \left(\frac{1}{m_a^{*2}} + \frac{1}{m_b^{*2}} \right) I_l^{(4)} \right. \\ & \left. + \frac{1}{16 m_a^{*2} m_b^{*2}} I_l^{(6)} \right). \end{aligned} \tag{199}$$

These contributions behave similarly as the transport matrix for the shear viscosity problem. Indeed, according to Eqs. (161a) and (165), if the kinematical corrections in Eq. (161a) can be neglected (extremely weak screening case), one finds $n_a p_{Fa} \Lambda_{ab}^{\eta} = 3 J_{ab}$. Keeping, as above, the leading order in q_l , the longitudinal contribution to J_{ab} reads

$$J_{ab}^l = \frac{\alpha_f^2 Z_a^2 Z_b^2 T^2 m_a^{*2} m_b^{*2}}{9 q_l} + \mathcal{O}(q_l). \tag{200}$$

In practice, the transverse contributions to Λ_{ab}^{κ} , Λ_{ab}^{η} , and J_{ab} always dominate over the longitudinal contributions. This leads to the non-Fermi-liquid behaviour of the transport matrices and hence of the transport coefficients [1, 102]. However, while for the thermal conductivity one can just neglect the longitudinal contribution, for the shear viscosity and momentum transfer rates this dominance is not dramatic and both contributions should be kept at realistic values of temperature. Moreover, it is not enough to retain only the leading order in q_l and the reasonable approximation is to keep the integral I_n^l with lowest order n for each expression above.

In principle, there are also contributions to the transport matrix due to lepton–neutron scatterings, namely Λ_{en}^k and $\Lambda_{\mu n}^k$ terms. They arise from the interaction of the lepton with the anomalous neutron magnetic moment [F_{a2} term in Eq. (173)]. It is much less effective than lepton–proton interaction. Thus we expect Λ_{en}^k and $\Lambda_{\mu n}^k$ to give negligible contributions to viscosity and thermal conductivity and do not consider these transport matrix elements in this work. The only quantities, for which the lepton–neutron interaction is important, are the friction coefficients J_{en} and $J_{\mu n}$. These coefficients can be found in section VII of the Ref. [74] and references therein.

Practical expressions for calculating the electromagnetic contribution to transport coefficients based on the results of this section are given in Appendix B.

4.2 Strong interactions

Description of collisions in the strong sector is hampered by the poorly known impact of many-body effects on the baryon interactions at supranuclear densities. Different approaches to the problem in the context of the NS cores transport are reviewed in [1]. Remember, that the necessary transport matrices Λ_{ab}^k depend on the in-medium effective masses of quasiparticles and the scattering matrix elements \mathcal{Q}_{ab} .

One approach is to forget about all in-medium modifications or include them only in the effective masses and employ the free-space scattering matrix elements. The simplest model of the strong interaction is the free one-pion exchange model (FOPE). For completeness we briefly discuss it in Sect. 4.2.2, since in principle it can serve as a starting model for the in-medium modifications.

It is well-known, however, that the free one-pion exchange model in the first Born approximation overestimates the scattering cross-sections so it does not serve as a good approximation for calculation of \mathcal{Q}_{ab} . Therefore the next level of approximation is to extract \mathcal{Q}_{ab} directly from the experimental data on the scattering experiments or from the accurate free-space calculations that reproduce the experimental data. The latter approach was elaborated in a range of studies [9, 83, 104, 105, 108], we consider it in Sect. 4.2.3.

Of course, this is a ‘poor man solution’ to the problem of in-medium transport cross-sections. Both effective masses and scattering probabilities need to be calculated from the same microscopic model (and the same as the EOS). Unfortunately, model dependence of results is quite substantial, especially at large densities (e.g., [1, 89]). Several approaches were proposed for calculation of the in-medium scattering rates in NS cores [1]. In pure neutron matter approximation these include thermodynamic T -matrix approach [109] or effective quasiparticle interaction [110]. Effective interaction construction on a basis of the variational methods and subsequent application to NS matter was performed in [111–113].

The calculations within the Brueckner-Hartree-Fock (BHF) theory [114] were also carried out [89, 99, 100, 111, 115, 116]. Frequently a partial wave expansion of the scattering problem is used and we show how this expansion enters the calculations in Sect. 4.2.4.

A different approach is known as the medium-modified one-pion exchange (MOPE) model derived in the framework of the Landau-Migdal Fermi-liquid theory for nuclear matter [117]. In this model the modification (softening) of the pionic mode by the in-medium effects is explicitly introduced in the theory. At present, up to our knowledge, the calculations of transport coefficients of dense nuclear matter within this model exist for pure neutron matter only. For thermal conductivity this was done by [118] and for shear viscosity by [119]. The review of the MOPE model is outside the scope of the present manuscript.

4.2.1 Kinematics of collisions

For the collisions mediated by the strong interactions, the static case ($\omega = 0$) can be employed and one needs to calculate the angular averages given in Eqs. (166)–(168). It turns out that it is convenient to use the (Pq) representation of angular averages given in Eq. (150). The total momentum P of the colliding pair with respect to surrounding medium can be used to parameterize the in-medium effects. On the other hand, the scattering is frequently described in the center of mass (c.m.) frame by defining the relative p momenta of the colliding pair [$\mathbf{p} = \frac{1}{2}(\mathbf{p}_1 - \mathbf{p}_2)$, see Fig. 2], and the center of mass scattering angle θ_{cm} given by (see Fig. 2)

$$\cos \theta_{\text{cm}} = 1 - \frac{q^2}{2p^2}. \tag{201}$$

Notice that the total and relative momenta are related via

$$P^2 + 4p^2 = 2(p_{Fa}^2 + p_{Fb}^2), \tag{202}$$

in addition the following useful equality holds

$$\mathbf{p}_1(\mathbf{p}_2 + \mathbf{p}_2') = P^2 - p_{Fa}^2 - p_{Fb}^2 + \frac{q^2}{2}. \tag{203}$$

Then the angular weighting factors in Eqs. (166)–(168) are observed to be polynomial in P and q . This suggests that it is convenient to introduce the averages⁸ [99]

$$\mathcal{Q}_{ab}^{(ij)} \equiv \left\langle \mathcal{Q}_{ab} P^i q^j \right\rangle. \tag{204}$$

The relevant transport matrices in Eqs. (166)–(168) in terms of averages $\mathcal{Q}_{ab}^{(ij)}$ are given as [116]

$$A_{ab}^k = \frac{T^2 m_a^{*2} m_b^{*2}}{5\pi^2 p_{Fa}^2} \left(\mathcal{Q}_{ab}^{(00)} + \frac{1}{4p_{Fa}^2} \mathcal{Q}_{ab}^{(02)} \right), \tag{205a}$$

⁸ Notice that the angular averages in [99, 116] differ by a factor of 2 from Eq. (204) since this factor in Eq. (150) was taken out in those references, which is not convenient here.

$$\Lambda'^{\kappa}_{ab} = \frac{T^2 m_a^{*2} m_b^{*2}}{10\pi^2 p_{Fa}^3 p_{Fb}} \left((p_{Fa}^2 + p_{Fb}^2) \mathcal{Q}_{ab}^{(00)} - \mathcal{Q}_{ab}^{(20)} - \frac{1}{2} \mathcal{Q}_{ab}^{(02)} \right), \tag{205b}$$

$$\Lambda^{\kappa}_{aa} + \Lambda'^{\kappa}_{aa} = \frac{T^2 m_a^{*4}}{10\pi^2 p_{Fa}^4} \left(4p_{Fa}^2 \mathcal{Q}_{aa}^{(00)} - \mathcal{Q}_{aa}^{(20)} \right), \tag{205c}$$

$$\Lambda^{\eta}_{ab} = \frac{T^2 m_a^{*2} m_b^{*2}}{4\pi^2 p_{Fa}^4} \left(\mathcal{Q}_{ab}^{(02)} - \frac{1}{4p_{Fa}^2} \mathcal{Q}_{ab}^{(04)} \right), \tag{205d}$$

$$\Lambda'^{\eta}_{ab} = \frac{T^2 m_a^{*2} m_b^{*2}}{8\pi^2 p_{Fa}^5 p_{Fb}} \left((p_{Fa}^2 + p_{Fb}^2) \mathcal{Q}_{ab}^{(02)} - \mathcal{Q}_{ab}^{(22)} - \frac{1}{2} \mathcal{Q}_{ab}^{(04)} \right), \tag{205e}$$

$$\Lambda^{\eta}_{aa} + \Lambda'^{\eta}_{aa} = \frac{T^2 m_a^{*4}}{8\pi^2 p_{Fa}^6} \left(4p_{Fa}^2 \mathcal{Q}_{aa}^{(02)} - \mathcal{Q}_{aa}^{(04)} - \mathcal{Q}_{aa}^{(22)} \right), \tag{205f}$$

$$J_{ab} = \frac{T^2 m_a^{*2} m_b^{*2}}{36\pi^4} \mathcal{Q}_{ab}^{(02)}. \tag{205g}$$

In Eqs. (205c) and (205f) we combined the direct and primed transport matrix elements for like species since it is in this form in which they couple to $\tilde{\lambda}_a^k$ in Eqs. (154)–(155).

4.2.2 Free one-pion exchange

The simplest model of the strong NN -interaction is the one-pion exchange (OPE) model. It appeals to a simple phenomenological low-energy Lagrangian of the πN interaction

$$\mathcal{L}_{\pi N} = g_{ab} \varphi_{\pi} \bar{\psi}_a \gamma^5 \psi_b, \tag{206}$$

where ψ_a and ψ_b are the wavefunctions of incoming and outgoing nucleons a and b , and φ_{π} is the pion field (charged or neutral, depending on what the nucleons a and b are). For πpp and πnn -scatterings, $g_{pp} = -g_{nn} \approx 13.1$ and for πnp -scattering $g_{np} = g_{pp} \sqrt{2}$ (see, e.g., sec. 4.1.1. in Ref. [98]). In this section we restrict ourselves to the free OPE interaction in the first Born approximation. In this case the transition matrix element for NN -scattering is [cf. Eq. (169)]

$$T_{ab}(12 \rightarrow 1'2') = M_{ab}(12 \rightarrow 1'2') - M_{ab}(12 \rightarrow 2'1'). \tag{207}$$

The direct and exchange parts of the matrix element are⁹

$$M_{ab}(12 \rightarrow 1'2') = g_{aa} g_{bb} \bar{u}_a(p'_1) \gamma^5 u_a(p_1) \times D_{\pi}(p'_1 - p_1) \bar{u}_b(p'_2) \gamma^5 u_b(p_2), \tag{208a}$$

$$M_{ab}(12 \rightarrow 2'1') = g_{ab}^2 \bar{u}_b(p'_2) \gamma^5 u_a(p_1) \times D_{\pi}(p'_2 - p_1) \bar{u}_a(p'_1) \gamma^5 u_b(p_2), \tag{208b}$$

where D_{π} is the pion propagator. Consequently,

$$\mathcal{Q}_{ab} = \frac{\mathcal{A}^2(q^2) + \mathcal{B}^2(q^2) + \mathcal{A}(q^2)\mathcal{B}(q^2)}{16(1 + \delta_{ab})\varepsilon_a^2 \varepsilon_b^2}, \tag{209a}$$

⁹ We employ the bispinor normalization Eq. (174).

where

$$\mathcal{A} = g_{aa} g_{bb} q^2 D_{\pi}(-q^2), \tag{209b}$$

$$\mathcal{B} = g_{ab}^2 \left[q'^2 + (m_a - m_b)^2 - (\varepsilon_a - \varepsilon_b)^2 \right] D_{\pi} \left((\varepsilon_a - \varepsilon_b)^2 - q^2 \right). \tag{209c}$$

In the latter three formulas \mathbf{q} and \mathbf{q}' are the 3-momentum transfers defined in Sect. 3.6.

The formula for \mathcal{Q}_{ab} could be simplified for non-relativistic collisions of nucleons. In this case one can set $m_a = m_b = m_N$, where we adopt $m_N = 939$ MeV as a typical nucleon mass, and $\varepsilon_a \approx \varepsilon_b$. In-vacuum pion propagator reads $D_{\pi}(-q^2) = (-q^2 - m_{\pi}^2)^{-1}$, which is of course a crude estimate. Then \mathcal{Q}_{ab} reduces to a standard form of the squared matrix element of one pion exchange nuclear potential

$$\mathcal{Q}_{ab} = \frac{1}{16(1 + \delta_{ab})\varepsilon_a^2 \varepsilon_b^2} \left[\frac{g_{aa}^2 g_{bb}^2 q^4}{(q^2 + m_{\pi}^2)^2} + \frac{g_{ab}^4 q'^4}{(q'^2 + m_{\pi}^2)^2} + \frac{g_{aa} g_{bb} g_{ab}^2 q^2 q'^2}{(q^2 + m_{\pi}^2)(q'^2 + m_{\pi}^2)} \right]. \tag{210}$$

We can now calculate the averages $\mathcal{Q}_{ab}^{(ij)}$ in Eq. (204) and hence the OPE transport matrices in Eq. (205). After transferring Eq. (210) to the (Pq) variables by employing the relation

$$q^2 + q'^2 = 4p^2 = 2(p_{Fa}^2 + p_{Fb}^2) - P^2, \tag{211}$$

the integrations, in principle, this can be performed analytically, but the results are by no means illuminating. We therefore do not give the explicit expressions here, and illustrate the results in Sect. 5.

4.2.3 In-vacuum cross-sections

In this section we restrict ourselves to the nuclear composition of the NS core matter. In other words, we consider only scattering within the np subsystem. Neglecting relativistic corrections, one relates the differential cross-section to the squared matrix element as

$$\frac{d\sigma_{ab}}{d\Omega}(E_{\text{lab}}, \theta_{\text{cm}}) = \frac{m_N^2}{16\pi^2} (1 + \delta_{ab}) \mathcal{Q}_{ab}, \tag{212}$$

where $\cos \theta_{\text{cm}}$ is given by Eq. (201) and $E_{\text{lab}} = 2p^2/m_N$. Assuming that the differential cross-sections are known, one can use them to calculate the transport matrices in Eq. (150).

Using this approach, Baiko et al. [108] defined for neutron-neutron collisions in thermal conductivity problem

$$\Lambda^{\kappa}_{nn} + \Lambda'^{\kappa}_{nn} = \frac{64T^2 m_n^{*4}}{5m_N^2 p_{Fn}} S_{nn2} \tag{213}$$

where S_{nn2} is an effective transport cross-section with a dimension of area,

$$S_{nn2} = \frac{m_N^2}{128\pi^2 p_{Fn}^3} \langle (q^2 + q'^2) \mathcal{Q}_{nn} \rangle. \tag{214}$$

We use here the variables q and q' inside the angular brackets to make a clear connection with Ref. [108] who also used the notation S_{n2} for S_{nn2} . Notice that in vacuum S_{nn2} depends only on one argument, the neutron Fermi-momentum p_{Fn} .

Baiko et al. [108] were interested in the neutron contribution to the transport coefficients and protons were considered as passive scatterers. While this is a good approximation for the non-magnetized case, the proton transport, in principle, can be significant in presence of the magnetic field. If we neglect the charge dependence of nucleon interactions (i.e. consider the electromagnetic forces separately), then Eqs. (213) and (214) can be also used for the proton-proton collisions by substituting $p_{Fn} \rightarrow p_{Fp}$, namely

$$A_{pp}^\kappa + A_{pp}^{\prime\kappa} = \frac{64T^2 m_p^{*4}}{5m_N^2 p_{Fp}} S_{pp2}, \tag{215}$$

where $S_{pp2} = S_{nn2}|_{p_{Fn} \rightarrow p_{Fp}}$.

For the neutron-proton scattering in thermal conductivity problem one has [108]

$$A_{np}^\kappa = \frac{64T^2 m_n^{*2} m_p^{*2}}{5m_N^2 p_{Fn}} (S_{np1} + S_{np2}), \tag{216}$$

where two effective np cross-sections are defined:

$$S_{np1} = \frac{m_N^2}{64\pi^2 p_{Fn}} \langle \mathcal{Q}_{np} \rangle \tag{217}$$

and

$$S_{np2} = \frac{m_N^2}{256\pi^2 p_{Fn}^3} \langle q^2 \mathcal{Q}_{np} \rangle. \tag{218}$$

Second of them, Eq. (218), also enters the expression for the momentum transfer rates [105]

$$J_{np} = J_{pn} = \frac{64}{9\pi^2} T^2 \frac{m_n^{*2} m_p^{*2}}{m_N^2} p_{Fn}^3 S_{np2}. \tag{219}$$

The same effective cross-sections define the transposed (pn) matrix elements for the thermal conductivity problem

$$A_{pn}^\kappa = \frac{64T^2 m_n^{*2} m_p^{*2} p_{Fn}}{5m_N^2 p_{Fp}^2} \left(S_{np1} + \frac{p_{Fn}^2}{p_{Fp}^2} S_{np2} \right). \tag{220}$$

This spurious asymmetry results from the asymmetric definition of the effective transport cross-sections in [108].

The shear viscosity problem was treated in a similar way in [104]. Equation (205f) for nn or pp collisions is rewritten as ($a = n, p$)

$$A_{aa}^\eta + A_{aa}^{\prime\eta} = \frac{64T^2 m_a^{*4}}{m_N^2 p_{Fa}} S_{aa4} \tag{221}$$

with

$$S_{aa4} = \frac{m_N^2}{16\pi^2} \frac{1}{(2p_{Fa})^5} \langle q^2 q'^2 \mathcal{Q}_{aa} \rangle. \tag{222}$$

Here we modified slightly the definition of S_{aa4} (with $a = n$) compared to the quantity S_{nn}^{SY08} introduced in [104], namely $S_{nn4} = S_{nn}^{\text{SY08}}/12$. Notice that like S_{nn2} and S_{pp2} above, S_{nn4} and S_{pp4} are actually the values of the same function $S_{aa4}(p_{Fa})$ evaluated at p_{Fn} or p_{Fp} , respectively.

For the np scattering in the shear viscosity problem we can write

$$A_{np}^\eta = \frac{64T^2 m_n^{*2} m_p^{*2}}{m_N^2 p_{Fn}} (S_{np2} - S_{np4}), \tag{223}$$

where

$$S_{np4} = \frac{m_N^2}{16\pi^2} \frac{1}{2(2p_{Fn})^5} \langle q^4 \mathcal{Q}_{np} \rangle. \tag{224}$$

Shternin and Yakovlev [104] did not separate S_{np2} and S_{np4} , their $S_{np}^{\text{SY08}} = 6(S_{np2} - S_{np4})$.

In [104] like in [108] only neutron transport was considered. However the pn components of the transport matrix can be expressed via the functions S_{np2} and S_{np4} as

$$A_{pn}^\eta = \frac{64T^2 m_n^{*2} m_p^{*2}}{m_N^2 p_{Fp}} \left(\frac{p_{Fn}^3}{p_{Fp}^3} S_{np2} - \frac{p_{Fn}^5}{p_{Fp}^5} S_{np4} \right). \tag{225}$$

The primed elements of the transport matrices which mix neutron and proton transport were not considered in [104, 108]. In order to keep a close analogy with their notations we express

$$A_{np}^{\prime\kappa} = \frac{p_{Fp}^2}{p_{Fn}^2} A_{pn}^{\prime\kappa} = \frac{64T^2 m_n^{*2} m_p^{*2}}{5m_N^2 p_{Fp}} S'_{np2} \tag{226}$$

and

$$A_{np}^{\prime\eta} = \frac{p_{Fp}^4}{p_{Fn}^4} A_{pn}^{\prime\eta} = \frac{64T^2 m_n^{*2} m_p^{*2}}{m_N^2 p_{Fp}} S'_{np4}, \tag{227}$$

where

$$S'_{np2} = \frac{m_N^2}{16\pi^2} \frac{1}{8p_{Fn}^3} \left\langle \left((p_{Fn}^2 + p_{Fp}^2) - P^2 - \frac{q^2}{2} \right) \mathcal{Q}_{np} \right\rangle \tag{228}$$

and

$$S'_{np4} = \frac{m_N^2}{16\pi^2} \frac{1}{32p_{Fn}^5} \left\langle q^2 \left((p_{Fn}^2 + p_{Fp}^2) - P^2 - \frac{q^2}{2} \right) \mathcal{Q}_{np} \right\rangle. \tag{229}$$

The functions S_{nn2} , S_{np1} , S_{np2} , S_{nn4} , and $S_{np2} - S_{np4}$ were fitted in Refs. [104, 108] on the basis of the free-space cross-sections obtained in Refs. [120, 121] based in turn on the realistic Bonn potential [122] which accurately reproduces observed NN scattering data and properties of a few-nucleon

systems. Available range of fitting parameters in [104, 108] is insufficient for consideration of the pp collisions, therefore we refitted these functions (and fitted the complementary ones) on a larger parameter space. Specifically, we took the free-space cross-section calculated in [99] based on the realistic free-space Argonne v18 potential [123]. Resulting fit expressions are given in Appendix B.

4.2.4 Partial wave expansion

In many cases when the quasiparticle scattering matrix is obtained from the microscopic theory, it is given in the partial wave basis in the center of mass frame of the scattering baryons. Let us denote the in-medium scattering matrix by G_{ab} in this case instead of T_{ab} (having in mind the G -matrix of the Brueckner–Hartree–Fock theory as a prototype). The partial wave basis depends on the total momentum P and the relative momentum p of the colliding pair and the angular momentum quantum numbers. Namely, the partial wave state is $|P, p; J \ell SM_J\rangle$, where S is the pair total spin, ℓ is the pair orbital momentum, J is its total angular momentum, and M_J is the total angular momentum projection.

Let $G_{\ell\ell'}^J(P, p)$ be the matrix element of the scattering matrix which is diagonal in P, p, J , and S and do not depend on M_J . Then the quantity Q_{ab} can be expanded in the series in Legendre polynomials $\mathcal{P}_L(\cos \theta_{\text{cm}})$:

$$Q_{ab}(q, P) = \frac{1}{1 + \delta_{ab}} \sum_L Q_{ab}^{(L)}(P) \mathcal{P}_L(\cos \theta_{\text{cm}}), \quad (230)$$

where $\cos \theta_{\text{cm}}$ is given in Eq. (201) and the coefficients of expansion are related to the matrix elements of the transition amplitude in the partial wave basis as [99]

$$\begin{aligned} Q_{ab}^{(L)}(P) &= \frac{1}{16\pi^2} \sum i^{\ell' - \ell + \bar{\ell} - \bar{\ell}'} \Pi_{\ell\ell'} \Pi_{\bar{\ell}\bar{\ell}'} \Pi_{JJ}^2 C_{\ell'0\bar{\ell}'0}^{L'0} C_{\ell0\bar{\ell}0}^{L0} \\ &\times \begin{Bmatrix} \bar{\ell} & S & \bar{J} \\ J & L & \ell \end{Bmatrix} \begin{Bmatrix} \bar{\ell}' & S & \bar{J} \\ J & L & \ell' \end{Bmatrix} \\ &\times \left(1 + \delta_{ab}(-1)^{S+\ell}\right) \left(1 + \delta_{ab}(-1)^{S+\bar{\ell}}\right) \\ &\times G_{\ell\ell'}^J(P, p) \left(G_{\bar{\ell}\bar{\ell}'}^{\bar{J}}(P, p)\right)^*. \end{aligned} \quad (231)$$

Here $\Pi_{fg} \equiv \sqrt{(2f+1)(2g+1)}$, terms in curly brackets are $6j$ -symbols of the quantum angular momentum theory [70], terms in the third line take into account exchange contributions, and the pair index ab is omitted at the scattering matrix elements for brevity. The summation in Eq. (231) is carried over all angular momenta and spin variables, except L .

The medium effects enter Eqs. (230) and (231) via the dependence of the scattering matrix on the total pair momentum P which breaks the translation invariance. The expansion (230) together with Eq. (201) allow us to perform the integration over q in Eq. (204) analytically with the help of the following relation [99]

$$\begin{aligned} \int_0^{q_m} \frac{q^j dq}{\sqrt{q_m^2 - q^2}} \mathcal{P}_L\left(1 - \frac{q^2}{2p^2}\right) &= \frac{q_m^j}{2} B\left(\frac{j+1}{2}, \frac{1}{2}\right) \\ &\times {}_3F_2\left(-L, L+1, \frac{j+1}{2}; 1, \frac{j}{2}+1; \frac{q_m^2}{4p^2}\right), \end{aligned} \quad (232)$$

where $B\left(\frac{j+1}{2}, \frac{1}{2}\right)$ is the beta-function, and ${}_3F_2$ is the generalized hypergeometric function. It reduces to the $L-1$ order polynomial in $q_m^2/(4p^2)$, as its first argument, $-L$, is a negative integer. The remaining integral over P in Eq. (204) in general should be performed numerically.

5 Discussion

Section 3.6 identifies key quantities that are needed from the microscopic theory for calculating the diffusive transport coefficients in the NS core in the weak-coupling regime. Namely, these are the effective masses m_a^* of the quasiparticles presented in the matter and the values of transport matrices $\Lambda_{ab}^k, \Lambda_{ab}^{\bar{k}}$, which are found from the angular averaging of quasiparticle scattering probabilities. With these quantities available, the transport coefficients of the non-magnetized matter can be easily found from the solution of the system Eq. (155) or, in case of the momentum transfer rates, directly from the corresponding Eqs. (165) or (168). Magnetic field does not modify this procedure significantly if the irreducible spherical tensor formalism is used and the transport coefficients are expressed via the complex functions (118). The inclusion of the magnetic field in this formalism is achieved by a simple addition of the imaginary diagonal matrix to the system Eq. (155).

5.1 Transport matrices and momentum transfer rates

The electromagnetic part of the transport matrices can be calculated in the universal form, independent on the particular EOS of the dense matter inside the NS cores. The necessary microscopic ingredients are the particle fractions and the quasiparticle effective masses at Fermi surface. The lepton effective masses are ones for free particles, $m_\ell^* = \sqrt{m_\ell^2 + p_{F\ell}^2}$ for $\ell = e, \mu$. The proton (or other charged baryon) effective masses should be provided along with the EOS. For instance, some of the EOSs in the ComPOSE database already contain the information about m^* . Otherwise one needs to assume some typical value of the proton effective mass, say $m_p^* = 0.8m_N$. In this case the electromagnetic contribution to Eq. (154) can be readily calculated. For convenience, we give practical expressions for the electromagnetic contribution in Appendix B.

For the strong sector the situation is much less certain. Ideally, the averages (204) and hence the elements of the

transport matrices need to be calculated on the basis of the same microphysics as the EOS. In reality this is rarely accessible for a modelling practitioners and they need to extract transport coefficients and EOS from unrelated sources.

Let us illustrate this uncertainty following [89, 116]. Assume that we take some EOS of the dense matter and want to calculate the transport coefficients. For certainty, we take the BSk21 EOS from the Brussels–Skyrme EOS family [124] which has a convenient analytical parametrization of the particle fractions. In Fig. 3 we plot the effective transport cross-sections defined in Sect. 4.2.3 as functions of density for various models of nuclear interaction. Blue dash-dotted lines show the results of the free OPE model in the first Born approximation of Sect. 4.2.2, while red solid lines show the results of the in-vacuum cross-sections calculated as described in Sect. 4.2.3. Clearly the free OPE model in Born approximation, as expected, is a bad approximation for the effective transport cross-sections.

Other solid lines in Fig. 3 show the results of [89] who calculated effective nucleon transport mean free paths on a grid of baryon densities and proton fractions ($x_p > 0.05$ and $n_B < 0.6 \text{ fm}^{-3}$) for five nuclear interactions models in the non-relativistic BHF approach. Each interaction results in its own EOS and, specifically, in its own proton fraction for NS core matter in the beta equilibrium. These proton fractions are also different from those for the BSk21 EOS.

The NN interactions considered in [89] are based on two realistic two-body potentials: the Argonne v18 (Av18 for short) potential [123] and the charge-dependent Bonn (CD-Bonn for short) potential [125] and two models for the three-body interactions, i.e. the phenomenological Urbana IX (UIX for short) model [126] and the microscopic three-body force (Tbmic for short) model based on the meson-nucleon theory of the nucleon interaction [127, 128]. Combinations of these interactions result in five interaction models (see [89] for details) which we denote as Av18, CDBonn, Av18 + UIX, CDBonn + UIX, and Av18 + Tbmic. In these calculations, effective masses and in-medium scattering matrices were calculated in a self-consistent way within the BHF framework and included in transport mean free paths.

One sees a considerable scatter in the effective transport cross-sections in Fig. 3, especially at high n_B . For most of those, the in-vacuum interaction (red solid lines) provides a poor approximation. One of the exceptions is the S_{np2} cross-sections [panel (f) in Fig. 3] related to the friction coefficient J_{np} and can be used in calculations (see, e.g., [74]).

Somewhat better results can be achieved by combining the effective transport cross-sections with the results of the effective mass calculations for the microscopic models (e.g., [129]). The latter ones are available more frequently. We illustrate this with the dotted lines in Fig. 3 that show the combinations $m_a^{*2} m_b^{*2} S_\alpha / m_N^4$ where $m_{a,b}^*$ are the effective masses for five microscopic interactions considered and

effective transport cross-sections S_α with $\alpha = nn2, nn4, pp2, pp4, np1, np2, np4, np2',$ and $np4'$ are calculated with the in-vacuum interaction. The difference of these results from the complete calculations (colored solid lined) is solely due to in-medium Q_{ab} and not in $m_{a,b}^*$. We observe, that the agreement with the complete calculations is poor, but better than that for pure in-vacuum interactions. Thus it can be recommended to use the fits for the in-vacuum cross-sections given in Appendix B together with microscopic values of effective masses, if available. If not, one can use some typical values, e.g., $m_n^* = m_p^* = 0.8m_N$, see below.

Notice that here only five interaction models within a single many-body method (non-relativistic BHF) are explored. In reality, the uncertainty in microscopic treatment can be considerably larger (e.g., when the calculations are performed within the MOPE model [118, 119]).

Let us focus now on the dependence of the in-vacuum transport cross-sections on EOS of NS core matter. To this end we downloaded several EOSs from the ‘Cold neutron star EOS’ section of the ComPOSE database. Specifically we restricted ourselves to the models with purely nucleonic composition, and also to those where the composition is stored in the database. These include 16 models of the unified Skyrme group [130] denoted as ‘RG(Name)’ in ComPOSE, where ‘Name’ is the label of the interaction model, three relativistic mean field (RMF) models from [131, 132], denoted as DS(CMF)-2, DS(CMF)-4, and DS(CMF)-J6, and the BHF calculations based on the chiral perturbation theory from [133].

We extended our EOS bank beyond the current ComPOSE database. Namely, we added two EOSs denoted by DDME2 and NL3 $\omega\rho$ in [134], the Skyrme-based EOS SLy4 from [135], and the microscopic BHF EOS from [136].

We also employed several models from the BSk family which have convenient analytical representations. Specifically, we used the models BSk20–22 and BSk24–26 [124, 137]. We also added a celebrated variational EOS APR [138] and four EOSs built upon the analytical parameterization of the APREOS of [139, 140], specifically those denoted by APR I–IV in [141] or HHJ I–IV in [134]. Finally we included four analytical PAL models from [142, 143], which differ by the functional form of the density dependence of the symmetry energy, see appendix D in [144] for details.

In total, our EOS bank contains 39 models summarized in Table 2. The proton fractions x_p as functions of the baryon density n_B are given in Fig. 4 by the black solid lines.¹⁰ Notice that some EOSs result in quite large (and probably unrealistic) proton fractions for beta-equilibrium matter. In the same figure with the thick red line we plot the approximate

¹⁰ A prominent jump in one of the black curves seen in Fig. 4 corresponds to the phase transition in the original APR EOS [138].

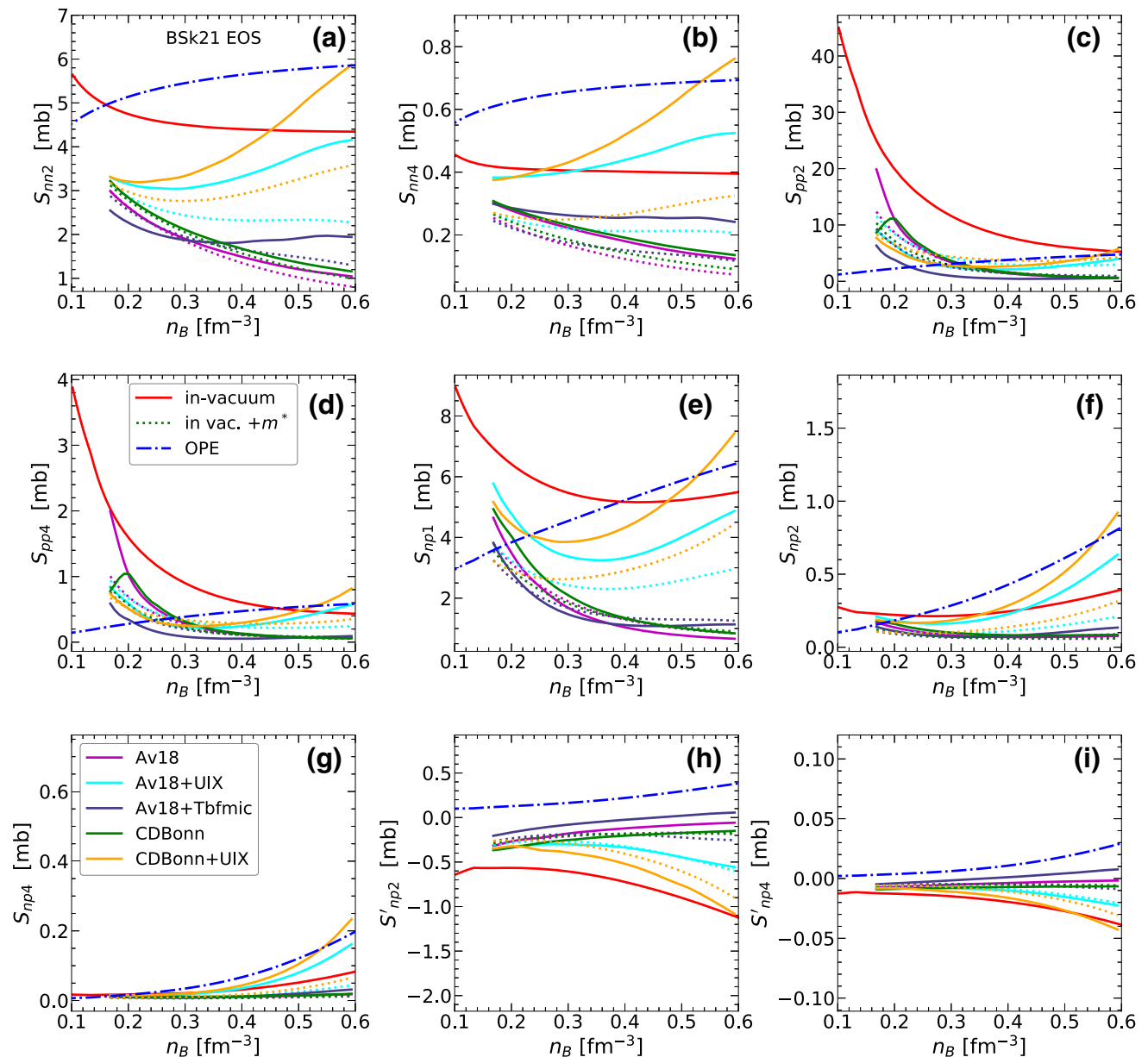


Fig. 3 Effective transport cross-sections defined in Sect. 4.2.3 as functions of density for the BSk21 EOS. Blue dash-dotted line show OPE results, red solid line shows the in-vacuum cross-sections. Coloured solid lines correspond to different microscopic models of nuclear inter-

actions as coded in the legend in panel (g) and described in the text. Dotted lines show in-vacuum effective transport cross-sections combined with the nucleon effective masses for the microscopic interactions (with the same color coding as the respective solid lines), see text for details

expression

$$x_p = 0.05 \left(\frac{n_B}{n_0} \right)^{0.65}, \tag{233}$$

where $n_0 = 0.16 \text{ fm}^{-3}$, proposed in [153] as a qualitative estimate of the proton fraction inside a beta-equilibrium nucleonic NS core. We will use this model as a toy model below.

In Fig. 5 we plot the same effective transport cross-sections as in Fig. 3 for the in-vacuum interaction for all EOS considered here (black lines). Thick red lines correspond to

the ‘toy model’ composition of Eq. (233). One observes that the effective transport cross-sections for the collisions of like particles S_{nn2} , S_{nn4} , and to a lesser extent, S_{pp2} , S_{pp4} are described by the toy model relatively well, in contrast to the cross-sections that involve np collisions. This is a direct consequence of the large scatter of the proton fraction within the EOS bank, see Fig. 4. Relatively small scatter of S_{pp2} and S_{pp4} around the toy model is because the main phase-space dependence is accounted for by the normalization factors in definitions (214) and (222). Notice that the furthest curves from the thick red line are those with the largest proton

Table 2 Summary of EOSs used in the paper. First part corresponds to models taken from CompOSE database, second for additional models not in CompOSE

Name	Composition	Type	References
CompOSE			
RG(KDE0v)	$npe\mu$	Skyrme	[130,145]
RG(KDE0v1)	$npe\mu$	Skyrme	[130,145]
RG(Rs)	$npe\mu$	Skyrme	[130,146]
RG(SK255)	$npe\mu$	Skyrme	[130,145]
RG(SK272)	$npe\mu$	Skyrme	[130,145]
RG(SKa)	$npe\mu$	Skyrme	[130,147]
RG(SKb)	$npe\mu$	Skyrme	[130,147]
RG(SKI 2–5)	$npe\mu$	Skyrme	[130,148]
RG(SKI 6)	$npe\mu$	Skyrme	[130,149]
RG(SKMp)	$npe\mu$	Skyrme	[130,150]
RG(SKOp)	$npe\mu$	Skyrme	[130,151]
RG(SLy2)	$npe\mu$	Skyrme	[130,152]
RG(SLy9)	$npe\mu$	Skyrme	[130,152]
DS(CMF)-2,4,6	npe	RMF	[131,132]
BL	$npe\mu$	BHF	[133]
Not in CompOSE			
DDME2	$npe\mu$	RMF	[134]
NL3 $\omega\rho$	$npe\mu$	RMF	[134]
SLy4	$npe\mu$	Skyrme	[135]
BHF	$npe\mu$	BHF	[136]
BSk 20–21	$npe\mu$	Skyrme	[124]
BSk 22, 24–26	$npe\mu$	Skyrme	[137]
APR	$npe\mu$	Var.	[138]
HHJ I–IV	$npe\mu$	Phen.	[134,139,140]
PAL I–III	$npe\mu$	Phen.	[142,144]
PAL-IV	$npe\mu$	Phen.	[143,144]

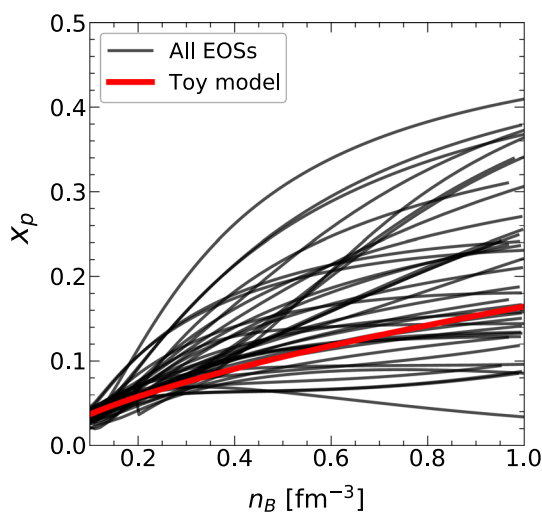


Fig. 4 Proton fraction x_p versus density for all EOSs considered in the paper (black solid lines). Thick red line shows the toy model of Eq. (233)

fractions. Nevertheless the toy model is expected to give an acceptable estimate for the transport coefficients of nucleonic NS core matter when more sophisticated calculations are not available.

For the sake of illustration we combine the results shown in Figs. 3 and 5 in Fig. 6. Here we compare the in-vacuum effective transport cross-sections (black lines) with the effective transport cross-sections for the microscopic models from [89] (colored lines). The OPE cross-sections for the toy model (233) are given by the blue dash-dotted lines, while the in-vacuum cross-sections for this model are shown with the thick red lines. In addition, with the thick red dashed lines we show the effective transport cross-sections for in-vacuum interaction but assuming $m_n^* = m_p^* = 0.8m_N$. Figure 6 looks rather cumbersome and basically illustrates that until the microscopic calculations of transport properties are available alongside the EOSs, all ‘simple’ calculations are mere qualitative estimates rather than the quantitative ones. We can range the levels of approximation as toy model plus $m_{n,p}^* = 0.8m_N$, in-vacuum fits for the actual composition plus $m_{n,p}^* = 0.8m_N$ and in-vacuum fits with somehow known $m_{n,p}^*$. Below we continue with first two options.

In Fig. 7, panels (a)–(h) we plot (in the logarithmic scale) the elements of the transport matrices which enter the system of Eq. (155) for the np subsystem and in the panel (i) we plot the neutron–proton momentum transfer rate J_{np} which is given by the similar angular average expression, see Sect. 4.2.1. All quantities are calculated within the in-vacuum interaction model for $T = 10^8$ K and $m_n^* = m_p^* = 0.8m_N$. Remember that each Λ_{ab} in Fig. 7 scales as $\Lambda_{ab} \propto m_a^{*2} m_b^{*2} T^2$. As in Fig. 4, black solid lines show results for a complete EOS bank described here, while thick red lines correspond to the toy model composition. We see that the typical transport mean free paths for nucleons due to collisions mediated by strong interactions in NS cores are of the order of $10^{-6} T_8^{-2}$ cm, where $T_8 = T/(10^8$ K).

For comparison, in Fig. 8 we plot the electromagnetic contributions to the transport matrices in the $e\mu p$ subsystem as function of n_B . Black and blue lines correspond to thermal conductivity ($k = \kappa$) and shear viscosity ($k = \eta$) problems, respectively, for all EOSs considered here. Thick red and orange lines show the toy model results for κ and η transport matrices, respectively. Since the transport matrices for shear viscosity, in general, contain additional factor q^2 in angular averages (see Sect. 4.1), the values of Λ^η are couple orders of magnitude smaller than Λ^κ . Remember that due to dominance of the dynamically-screened transverse part of the electromagnetic interaction, the temperature dependence of Λ_{ab}^k plotted in Fig. 8 differs from the Fermi-liquid law $\Lambda_{ab}^k \propto T^2$. Approximate scaling for the diagonal components is $\Lambda_a^\kappa \propto T$ and $\Lambda_a^\eta \propto T^{5/3}$, although in the latter case this scaling works worse as discussed in Sect. 4.1. One

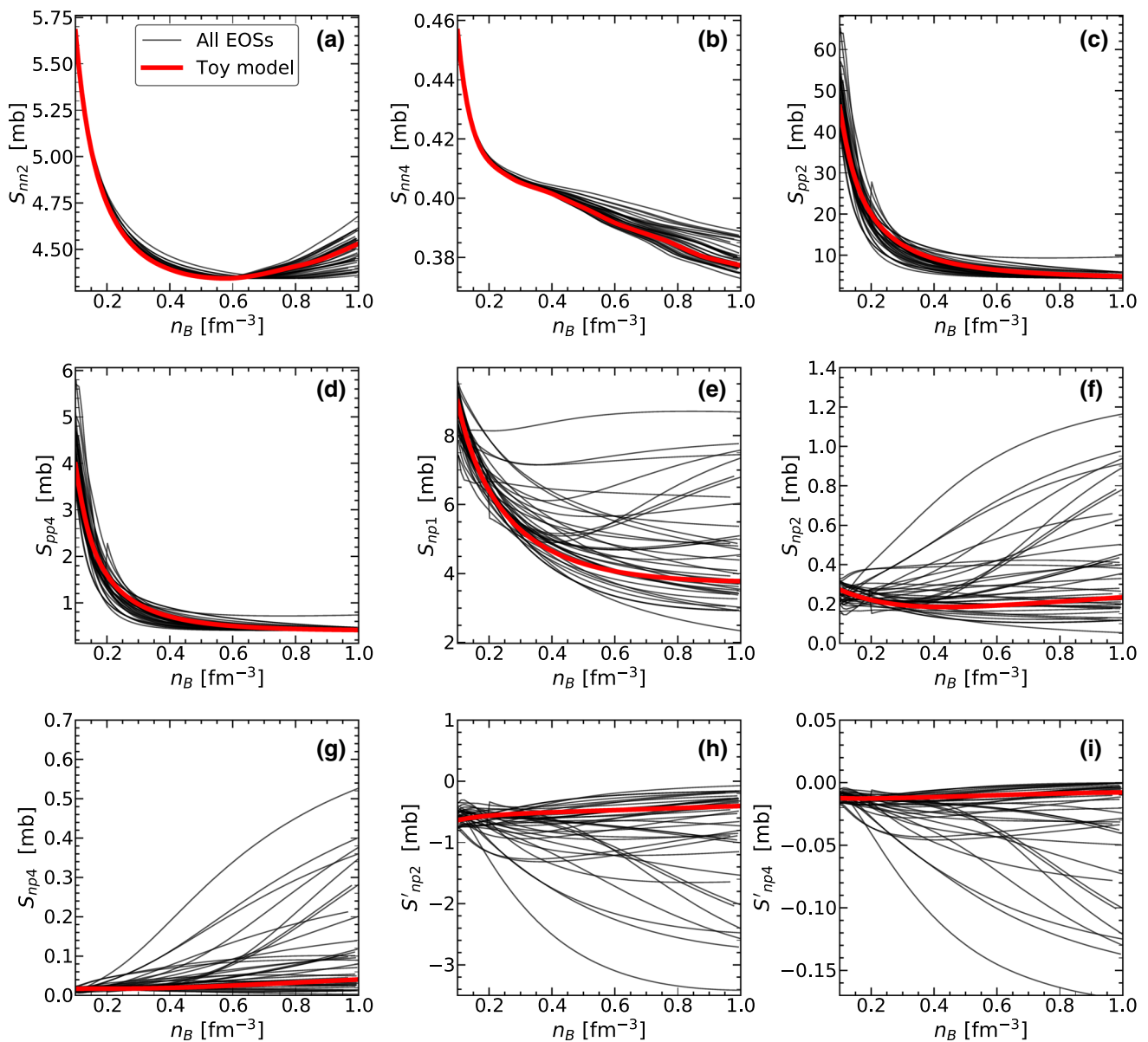


Fig. 5 Effective transport cross-sections defined in Sect. 4.2.3 as functions of density for all EOS described in the text and the in-vacuum interaction (black solid lines). Thick red solid lines show the results for the toy model with the proton fraction from Eq. (233)

observes that the diagonal components of the transport matrix for electromagnetic interaction are always much larger than the non-diagonal components which can be neglected in the first approximation. Protons interact both via the strong and electromagnetic forces therefore in Fig. 8(i) we plot with dashed lines the total Λ_p^κ (red dashed lines) and Λ_p^η (red orange lines). While strong interactions dominate the effective proton mean free path for the shear viscosity problem, this is not so for the thermal conductivity problem, where the contributions from the electromagnetic and strong sectors are comparable. Figures 7 and 8 show that it is always a good approximation to treat protons as the passive scatterers.

5.2 Shear viscosity and thermal conductivity at $\mathbf{B} = 0$

Now we have all in hand to calculate the shear viscosity and the thermal conductivity in the NS cores. Figure 9 shows the parallel components of the shear viscosity, η_0 [panel (a)] and thermal conductivity κ_{\parallel} [panel (b)] which do not depend on \mathbf{B} . These components are equal to the isotropic transport coefficients in absence of the magnetic field. As for Fig. 7, we set $T = 10^8$ K and $m_n^* = m_p^* = 0.8m_N$ and plot the results for all EOS with black lines and the result for the toy model composition with the thick red line. As the electromagnetic contribution and strong sector contribution have different temperature dependencies, there is no general simple temperature scaling for these coefficients (however, see

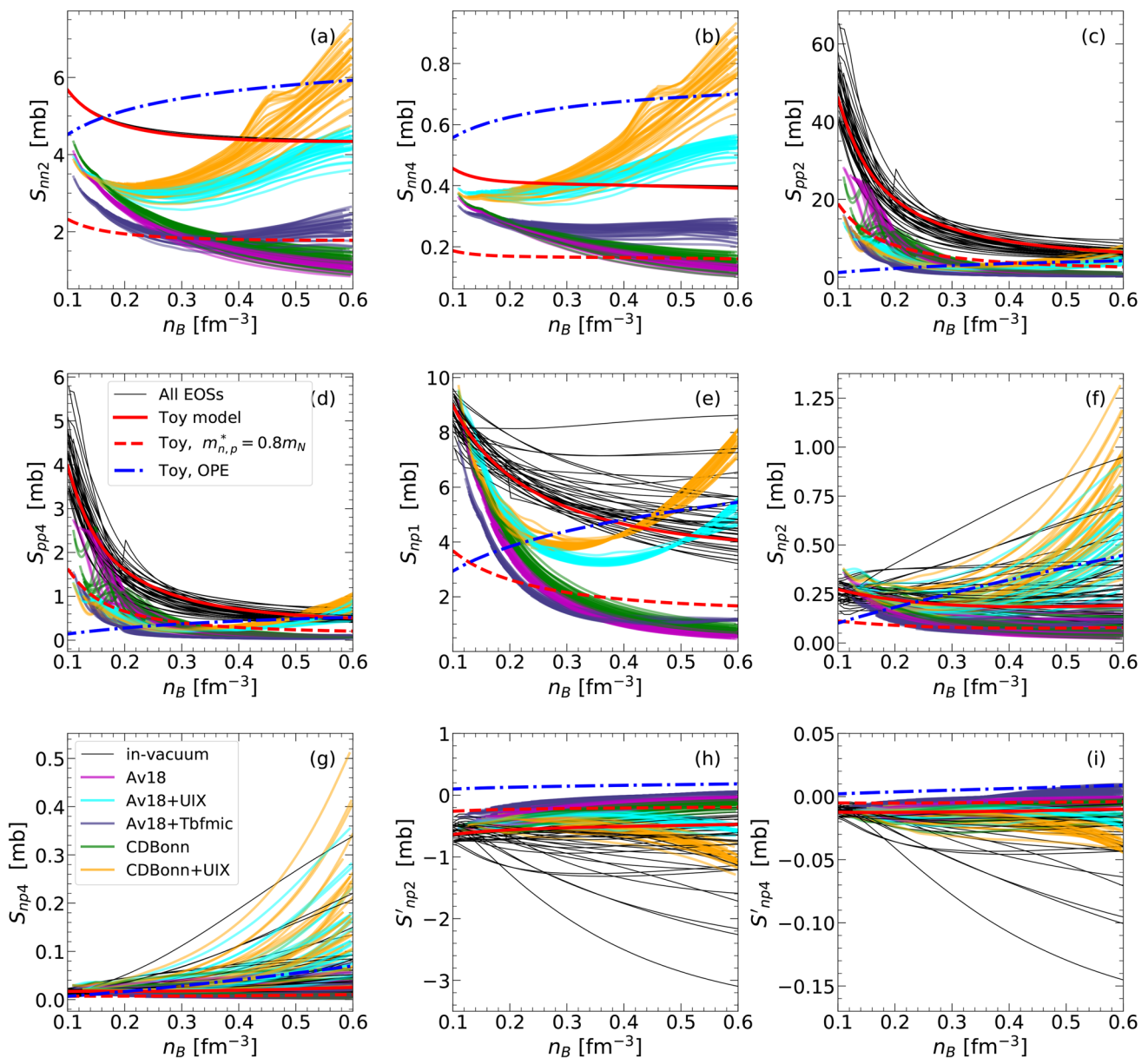


Fig. 6 Same as Fig. 5 with addition of the results for various microscopic potentials applied to all EOSs considered in the paper (cf. Fig. 3 for BSk21 EOS). Different microscopic interactions are coded as in

Fig. 3. Thick lines show the toy model (233) results for the OPE (blue dash-dotted), in-vacuum (red solid), and in-vacuum with constant $m_{n,p}^* = 0.8m_N$ (red dashed)

below). One observes qualitatively similar behavior of the transport coefficients with density for all considered EOSs.

The partial contributions to η_0 and κ_{\parallel} are shown in Fig. 10 in panels (a, b), respectively, for the toy model composition, $T = 10^8$ K, and $m_n^* = m_p^* = 0.8m_N$. Other, more realistic EOSs, show similar behavior. Notice that the thermal conductivity, Fig. 10b, is almost completely determined by the neutron contribution [1]. This is due to the strong dominance of the transverse channel of the electromagnetic interaction which suppresses the lepton thermal conductivity and also makes it temperature-independent, Sect. 4.1. The neutron contribution, in contrast, scales as T^{-1} . Thus, only at

high temperatures, $T \gtrsim 3 \times 10^9$ K, leptons start to play some role in heat conduction in the non-superfluid matter [1, 103]. The neutron thermal conductivity is determined by the Λ_n^{κ} transport matrix element shown in Fig. 7a. Its relatively small scatter over EOSs transforms to the relatively small scatter for κ_{\parallel} in Fig. 9b. It is clear that the modification of the microscopic interaction results in large changes in κ_{\parallel} [89]. Anyway, the important fact for practical applications is that the thermal conductivity in NS cores is large, effectively washing out the temperature gradients.

The situation is in some sense opposite for the shear viscosity. According to Fig. 10a, leptons give the main con-

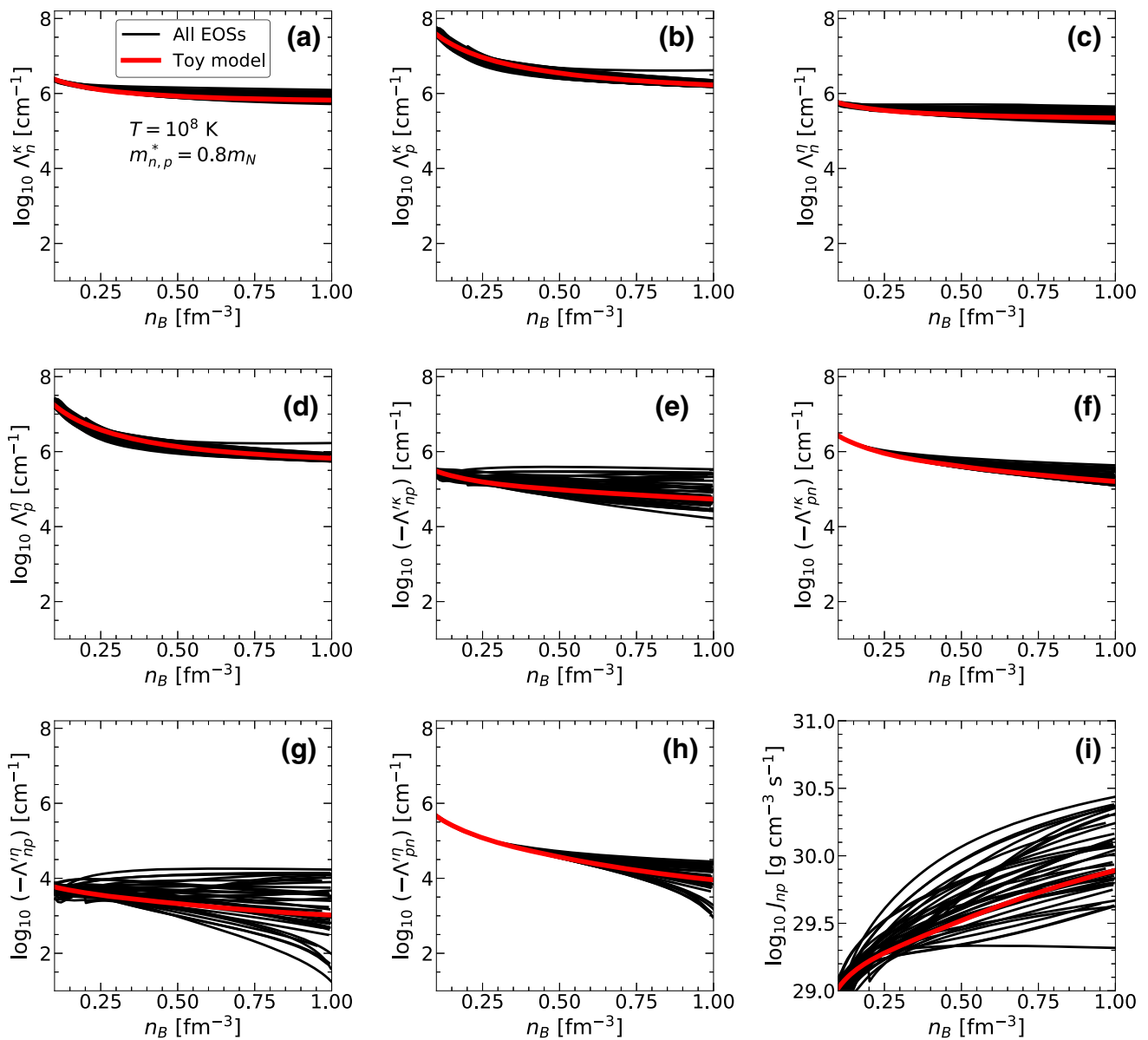


Fig. 7 Transport matrix elements for strong interaction in the np subsystem (panels **a–h**) and the momentum transfer rate J_{np} (panel **i**) as functions of baryon number density. Results are shown for all EOS con-

sidered in the paper and in-vacuum interaction (black solid lines). Thick red line shows the toy model (233) result. In all cases, $T = 10^8$ K and $m_{n,p}^* = 0.8m_N$

tribution to η_0 , while neutron contribution is less important [1,89]. The difference with the thermal conductivity case is due to considerably larger transport lepton mean free paths for the shear viscosity problem than for the thermal conductivity (in other words $\Lambda_\ell^\eta \ll \Lambda_\ell^k$) due to different kinematics, see Fig. 8 and the discussion in Sect. 5.1. Notice, that the conclusion $\eta_\ell \gg \eta_n$ does not depend on temperature, since the temperature dependencies of the lepton and neutron contributions are close. Namely, the neutron shear viscosity scales as T^{-2} , while the non-Fermi liquid effects in the electromagnetic interactions modify this scaling for leptons at most to $T^{-5/3}$ at lowest temperatures [1,104] (see also Fig. 12a

below). The gross result of the realistic microscopic interaction, at least for the models considered here, is the further reduction of the neutron contribution to η_0 [89,99]. In this respect, a considerable scatter in the results for various EOSs seen in Fig. 9a results from the scatter in proton (and hence lepton) fractions, see Fig. 4, and not from the scatter in S_α . This means that the knowledge of the proton effective mass and the particle fractions is enough for reliable calculation of the shear viscosity coefficient η_0 (i.e., shear viscosity in the absence of magnetic field) in non-superfluid NS core matter.

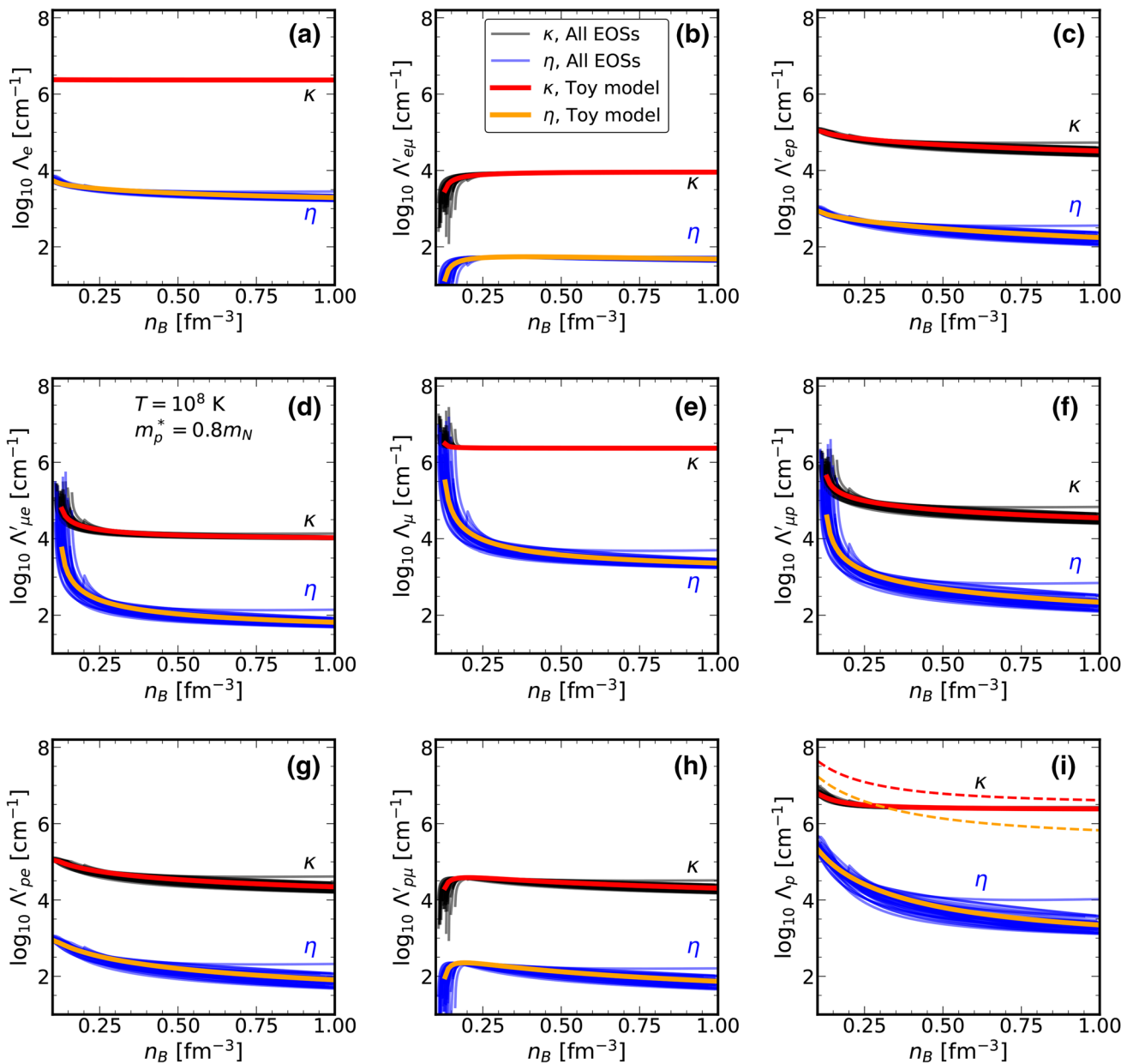


Fig. 8 Transport matrix elements for electromagnetic interaction in the $e\mu p$ subsystem as functions of baryon number density. Results for all EOS considered in the paper are shown with black solid lines for thermal conductivity and blue solid lines for shear viscosity, as marked in the plot. Thick red and orange line shows the toy model e (233) results

for κ and η , respectively. Dashed red and orange lines in panel (i) show total $\Lambda_p = (\Lambda_p)^{\text{strong}} + (\Lambda_p)^{\text{em}}$ for thermal conductivity and shear viscosity for the toy model, respectively. In all cases, $T = 10^8$ K and $m_p^* = 0.8m_N$

5.3 Shear viscosity and thermal conductivity of magnetized NS cores

We now turn to the transport coefficients in presence of the magnetic field. Remember, that at the lowest variational order there is no magnetic field dependence and no tensor structure in the momentum transfer rates J_{ab} (this is of course not true for the electric conductivity tensor that can be obtained by inverting the generalized Ohm law (164), see, e.g., [8] and

Appendix C). Therefore we refer the reader to Ref. [89] and sec. VII of Ref. [74] for the detailed discussion of the momentum transfer rates in the non-superfluid $npe\mu$ NS cores which extends the discussion here.

In the magnetic field, components of the thermal conductivity and shear viscosity tensors are described by the complex functions $\tilde{\kappa}(B)$ and $\tilde{\eta}(B)$ (Sects. 3.3 and 3.6). We have already discussed the longitudinal contributions $\kappa_{\parallel} = \tilde{\kappa}(B = 0)$ and $\eta_0 = \tilde{\eta}(B = 0)$. In Fig. 11 we plot real and imaginary

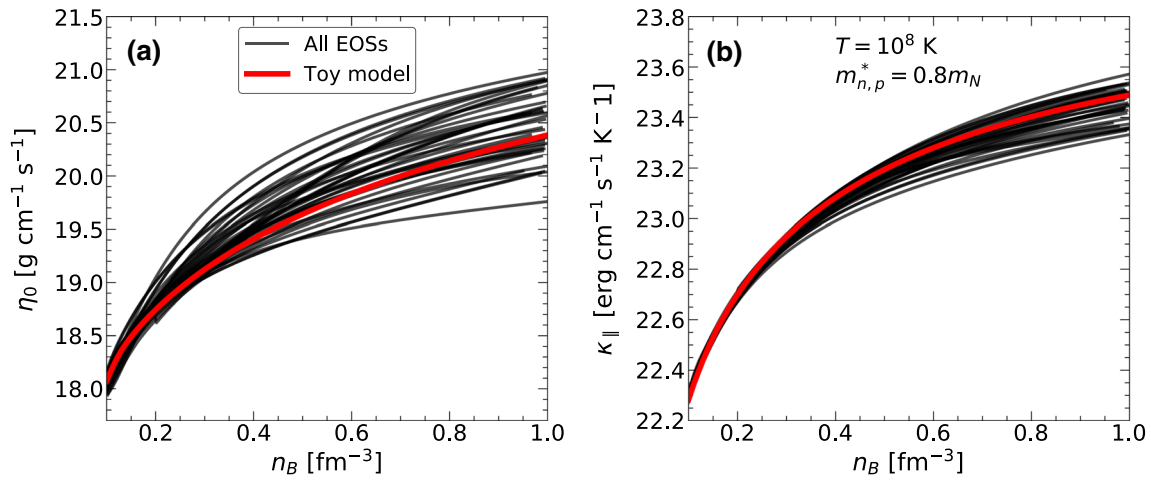


Fig. 9 Longitudinal component of the shear viscosity η_0 (panel **a**) and longitudinal component of the thermal conductivity κ_{\parallel} (panel **b**) as functions of density for all EOSs considered in the paper (black solid lines) and the toy model (233) (thick red solid line). In all cases, $T = 10^8$ K and $m_{n,p}^* = 0.8m_N$

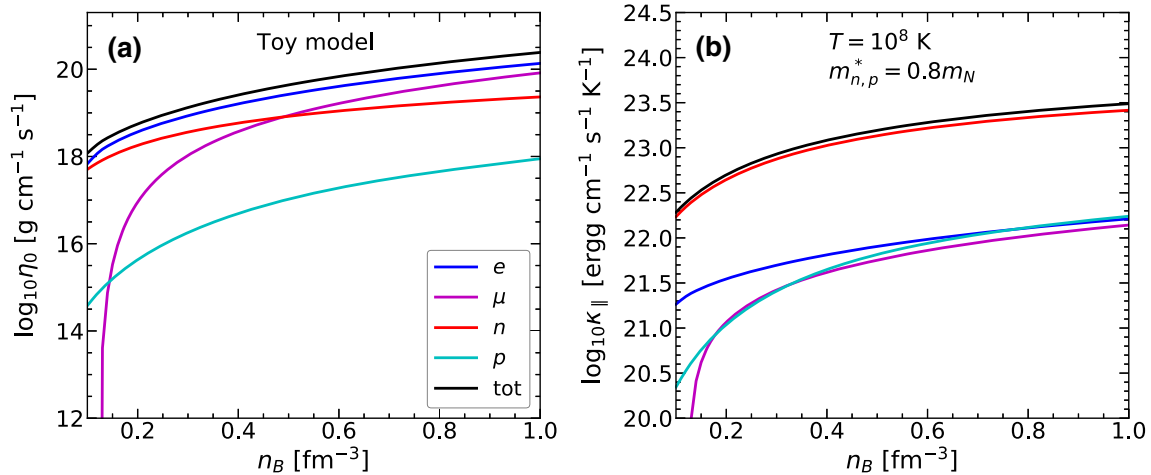


Fig. 10 Partial contributions to the longitudinal component of the shear viscosity η_0 (panel **a**) and longitudinal component of the thermal conductivity κ_{\parallel} (panel **b**) as functions of density for the toy model

(233) and the $npe\mu$ composition. Total contribution and partial contributions are color coded as indicated in the legend on the panel (a). In this calculation, $T = 10^8$ K and $m_{n,p}^* = 0.8m_N$

parts of $\tilde{\kappa}(B)$ and $\tilde{\eta}(B)$ and corresponding partial contributions from different particle species as functions of B . Recall that the Cartesian components of the thermal conductivity are $\kappa_{\perp} = \text{Re } \tilde{\kappa}(B)$ and $\kappa_{\parallel} = -\text{Im } \tilde{\kappa}(B)$, while for the shear viscosity $\eta_1 = \text{Re } \tilde{\eta}(2B)$, $\eta_3 = -\text{Im } \tilde{\eta}(2B)$, $\eta_2 = \text{Re } \tilde{\eta}(B)$, and $\eta_4 = -\text{Im } \tilde{\eta}(B)$. As above, we use the toy model composition at a characteristic baryon density $n_B = 0.35 \text{ fm}^{-3}$. We also set $T = 10^8$ K and $m_n^* = m_p^* = 0.8m_N$. The behavior of the transport coefficients can be understood by comparing Fig. 11 with Fig. 1 which is plotted in the relaxation-time approximation.

Indeed, the results of Sect. 4.1 for electromagnetic collisions suggest that the non-diagonal (primed) components of the transport matrices for electromagnetic interactions are significantly smaller than the diagonal components, as seen in Fig. 8. Therefore in the first approximation one can neglect

mixing between leptons and other species and the lepton mean free paths can be determined from the simple equation of the effective relaxation time form, namely

$$\tilde{\lambda}_{\ell}^k = \frac{1}{\Lambda_{\ell}^k + i\omega_{\text{BF}\ell}/v_{\text{F}\ell}}, \quad \ell = e, \mu \tag{234}$$

for $k = \kappa, \eta$. Therefore lepton transport coefficients behave as shown in Fig. 1 where the effective Hall parameters are $x_{\text{Hall}\ell} = \omega_{\text{BF}\ell} (\Lambda_{\ell}^k v_{\text{F}\ell})^{-1}$. In a strong sector situation is not so simple. Dashed lines in Fig. 8i can be viewed as an estimate for the real part of inverse proton mean free paths. Comparing it with the non-diagonal components of the transport matrices Λ_{np}^k in Fig. 7, one can assume that protons do not influence the real part of the equation for neutron effective mean free path $\tilde{\lambda}_n^k$ (but not the imaginary part, since neutrons are electrically neutral, see below). Therefore, one can write

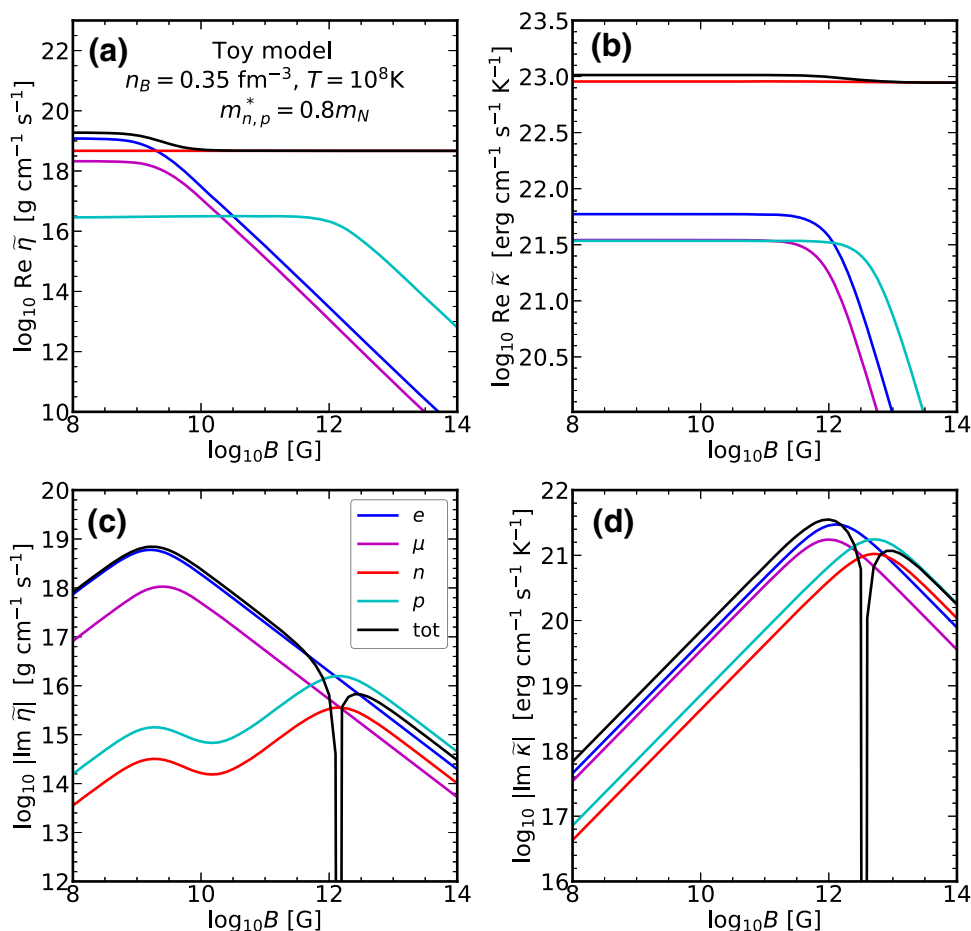


Fig. 11 Partial contributions to the complex shear viscosity $\tilde{\eta}$ and thermal conductivity $\tilde{\kappa}$ coefficients as functions of the magnetic field. Panels a–d show, respectively, $\text{Re } \tilde{\eta}(B)$, $|\text{Im } \tilde{\eta}(B)|$, $\text{Re } \tilde{\kappa}(B)$, and $|\text{Im } \tilde{\kappa}(B)|$. Results are plotted for the toy model (233), $npe\mu$ composition, $T = 10^8$ K, $n_B = 0.35 \text{ fm}^{-3}$ and $m_{n,p}^* = 0.8m_N$. Black solid line marked

$B = 0$ in panel (a) and lines marked $B < 10^{12}$ G in panel (b) also represent the longitudinal components η_0 and κ_{\parallel} , respectively. Dashed line marked $e\mu$ ($B = 0$) in panel (b) shows the electron and muon contribution to κ_{\parallel} . Discontinuities in the Hall contributions (panels c, d) indicate the sign change of these components, see text for details

for neutrons the relaxation-time type expression

$$\text{Re } \tilde{\lambda}_n^k = \frac{1}{\Lambda_n^k}, \tag{235}$$

which does not depend on the magnetic field. According to Fig. 7, inverse neutron mean free path Λ_n^k [see Eq. (235)] can be comparable to the non-diagonal components of the transport matrices Λ_{pn}^k , therefore this mixing can affect proton mean free paths. In this approximation, one finds

$$\text{Re } \tilde{\lambda}_p^k = \text{Re } \frac{1 - \Lambda_{pn}^k / \Lambda_n^k}{\Lambda_p^k + i\omega_{\text{BF}p} / v_{\text{FP}}}. \tag{236}$$

Equation (236) has the effective relaxation-time form with the Hall parameter $x_{\text{Hall}p} = \omega_{\text{BF}p} (\Lambda_p^k v_{\text{FP}})^{-1}$, but with numerator different from unity.

Consider now the transverse components of the shear viscosity shown in Fig. 11a. At low magnetic field ($B \lesssim 3 \times 10^9$ G for conditions in Fig. 11) leptons are not magnetized,

i.e. $x_{\text{Hall}e,\mu} < 1$. In this case, $\text{Re } \tilde{\eta}(B) \approx \eta_0 \approx \eta_{0e\mu}$, see Fig. 11a. When $x_{\text{Hall}e,\mu}$ reaches unity and starts to increase with increasing B , leptons become strongly magnetized and their contribution to $\text{Re } \tilde{\eta}$ (i.e., to the transverse components of the shear viscosity tensor) rapidly diminishes (see blue and magenta lines in Fig. 11a). At this point ($B \gtrsim 10^{10}$ G for conditions in Fig. 11), $\text{Re } \tilde{\eta}$ is fully determined by neutrons according to Eq. (235). Protons become magnetized at larger fields when $x_{\text{Hall}p} \gtrsim 1$, but their contribution to $\text{Re } \tilde{\eta}$ is negligible.

A simpler behavior is observed for the transverse component of the thermal conductivity, $\text{Re } \tilde{\kappa}$, plotted in Fig. 11b. According to Fig. 10b, the lepton contribution to the thermal conductivity is negligible (at least at the selected temperature, see below) and their magnetization results in almost no changes in $\text{Re } \tilde{\kappa}$ (Fig. 11b, black line). Notice that the lepton Hall parameters for thermal conductivity reach unity at much larger magnetic fields B than those for shear viscosity. This is due to smaller effective transport mean free paths for ther-

mal conductivity due to stronger dominance of the transverse channel of electromagnetic interactions.

Consider now the Hall components, $\text{Im } \tilde{\eta}$ and $\text{Im } \tilde{\kappa}$, plotted in Fig. 11c, d, respectively. Until protons are magnetized, the Hall components are fully determined by leptons and follow the relaxation-time expressions (234). They reach maxima at $x_{\text{Halle},\mu} \approx 1$, cf. Fig. 1. According to Eqs. (131b) and (128b), asymptotic values of Hall components of shear viscosity and thermal conductivity at $x_{\text{Halle},\mu} \gg 1$ (but $x_{\text{Hall}p} \ll 1$) are given by the universal expressions

$$\text{Im } \tilde{\eta} \approx \text{Im } \tilde{\eta}_{e\mu} = -\frac{n_e p_{Fe}^2 + n_\mu p_{F\mu}^2}{5eB}, \tag{237a}$$

$$\text{Im } \tilde{\kappa} \approx \text{Im } \tilde{\kappa}_{e\mu} = -\frac{\pi^2 T}{3} \frac{n_e + n_\mu}{eB}. \tag{237b}$$

In Fig. 11c, d we plot the Hall components in the logarithmic scale, so their sign is not shown. The Hall contribution of leptons have negative sign due to negative charges of leptons, while the proton contribution is positive. Figure 11a, c show that at $x_{\text{Halle},\mu} \approx 1$, the Hall components of the shear viscosity are comparable to the transverse components. For thermal conductivity, $\text{Im } \tilde{\kappa}$ is always much smaller than $\text{Re } \tilde{\kappa}$ (Fig. 11b, d).

From Eq. (154) for electrically neutral ($q_n = 0$) neutrons, for $k = \eta, \kappa$ one obtains

$$\text{Im } \tilde{\lambda}_n^k = -\frac{\Lambda_{np}^k}{\Lambda_n^k} \text{Im } \tilde{\lambda}_p^k, \tag{238}$$

i.e. despite being charge neutral, neutrons contribute to the Hall components of thermal conductivity or shear viscosity due to their interaction with protons. Depending on the sign of (Λ_{np}^k) which can be either positive or negative, the neutron contribution to the total $\text{Im } \tilde{\eta}$ or $\text{Im } \tilde{\kappa}$ can be positive or negative. For the specific case shown in Fig. 11, both proton and neutron contributions are positive and larger than those for leptons, leading to change in sign of this component at $x_{\text{Hall}p} \gtrsim 1$, which is seen as a discontinuities in total Hall components shown in Fig. 11c, d.

Proton contribution to the Hall components of transport coefficients, and hence the neutron contribution as well show more complicated behavior around $x_{\text{Halle},\mu} \sim 1$ in Fig. 11c, d than follows from a simple relaxation-time approximation. This can be understood as follows. Taking into account Eq. (238), the equation for $\text{Im } \tilde{\lambda}_p^k$ reads

$$\left(\Lambda_p^k - \frac{\Lambda_{np}^k \Lambda_{pn}^k}{\Lambda_n^k} \right) \text{Im } \tilde{\lambda}_p^k = -\frac{\omega_{BFp}}{v_{Fp}} \text{Re } \tilde{\lambda}_p^k - \Lambda_{pe}^k \text{Im } \tilde{\lambda}_e^k - \Lambda_{p\mu}^k \text{Im } \tilde{\lambda}_\mu^k. \tag{239}$$

Assuming that $\tilde{\lambda}_e^k, \tilde{\lambda}_\mu^k$, and $\text{Re } \tilde{\lambda}_p^k$ are determined by Eqs. (234) and (236), the imaginary part $\text{Im } \tilde{\lambda}_p^k$ can be cal-

culated from Eq. (239). Until $x_{\text{Halle},\mu,p} < 1$, $\text{Im } \tilde{\lambda}_\ell^k \propto \omega_{BF\ell}$ and one has $\text{Im } \tilde{\lambda}_p^k \propto B$. When leptons become magnetized, $x_{\text{Halle},\mu} \sim 1$, but still $x_{\text{Hall}p} < 1$, lepton contribution to right-hand side of Eq. (239) drops down that is clearly visible in cyan and red lines in Fig. 11c. For thermal conductivity, this effect is not visible in Fig. 11d since the protons and leptons have similar Hall parameters here. Finally, when all charged particles are magnetized, $\text{Im } \tilde{\lambda}_\ell^k \propto \omega_{BF\ell}^{-1}$, $\text{Re } \tilde{\lambda}_p^k \propto \omega_{BFp}^{-2}$ so that $\text{Im } \tilde{\lambda}_p^k \propto B^{-1}$, but with the proportionality coefficient which contains combination of the components of transport matrices. Therefore the total Hall components of shear viscosity and thermal conductivity do not reach universal asymptotics in the large Hall parameter regime analogous to Eq. (237). Almost complete cancellation of the lepton and neutron contributions to $\text{Im } \tilde{\kappa}$ seen at large B in Fig. 11d is a chance coincidence which breaks down at other densities.

Finally, in Fig. 12 we explore the temperature dependence of $\tilde{\eta}$ and $\tilde{\kappa}$ for $B = 10^8, 10^9, \dots, 10^{14}$ G; the values of $\log_{10} B$ [G] are shown near the respective curves. As in Fig. 11, we use the toy model composition at $n_B = 0.35 \text{ fm}^{-3}$ and $m_n^* = m_p^* = 0.8m_N$.

In Fig. 12a we show $\text{Re } \tilde{\eta}$ component of the shear viscosity tensor. According to the discussion above, at $B = 0$ [black solid line in Fig. 12a marked $B = 0$], leptons give the dominant contribution to the shear viscosity [89]. At low temperatures, the shear viscosity obeys the $\eta \propto T^{-5/3}$ asymptotic instead of the standard Fermi-liquid result $\eta \propto T^{-2}$ due to the dominance of the transverse channel of the electromagnetic collisions, see Eq. (192). At higher temperatures, the contribution of the longitudinal channel to the lepton shear viscosity is significant and the slope of the $\eta(T)$ dependence lies in between the $\propto T^{-5/3}$ and $\propto T^{-2}$ powerlaws. At each given $B > 0$ the behavior of $\text{Re } \tilde{\eta}(B)$ is similar. Since the effective mean free paths increase with decrease of temperature, the effective Hall parameters for leptons also increase. Until $x_{\text{Halle},\mu} = 1$, magnetic field does not influence the transport significantly and $\text{Re } \tilde{\eta}(B) \approx \tilde{\eta}(B = 0)$, see Fig. 11. With lowering temperature, leptons become magnetized and their contribution to $\text{Re } \tilde{\eta}$ decreases until the transverse shear viscosity components become completely determined by neutrons. In Fig. 12a this is the line corresponding to the highest $B = 10^{14}$ G plotted. At this point, $\text{Re } \tilde{\eta} \approx \text{Re } \tilde{\eta}_n \propto T^{-2}$ and does not depend on B (see Fig. 11).

The Hall components of the shear viscosity, i.e. $\text{Im } \tilde{\eta}$, are plotted in Fig. 12c. This figure can be understood in the same way as Fig. 11c. At a given B , starting from large temperatures, $\text{Im } \tilde{\eta}$ is governed by leptons and basically follow the relaxation-time approximation law Eq. (130). When leptons are magnetized, $\text{Im } \tilde{\eta}$ is given by (237a) and does not depend on temperature until the magnetization of protons occur. After that, $\text{Im } \tilde{\eta}$ changes sign rapidly (in present

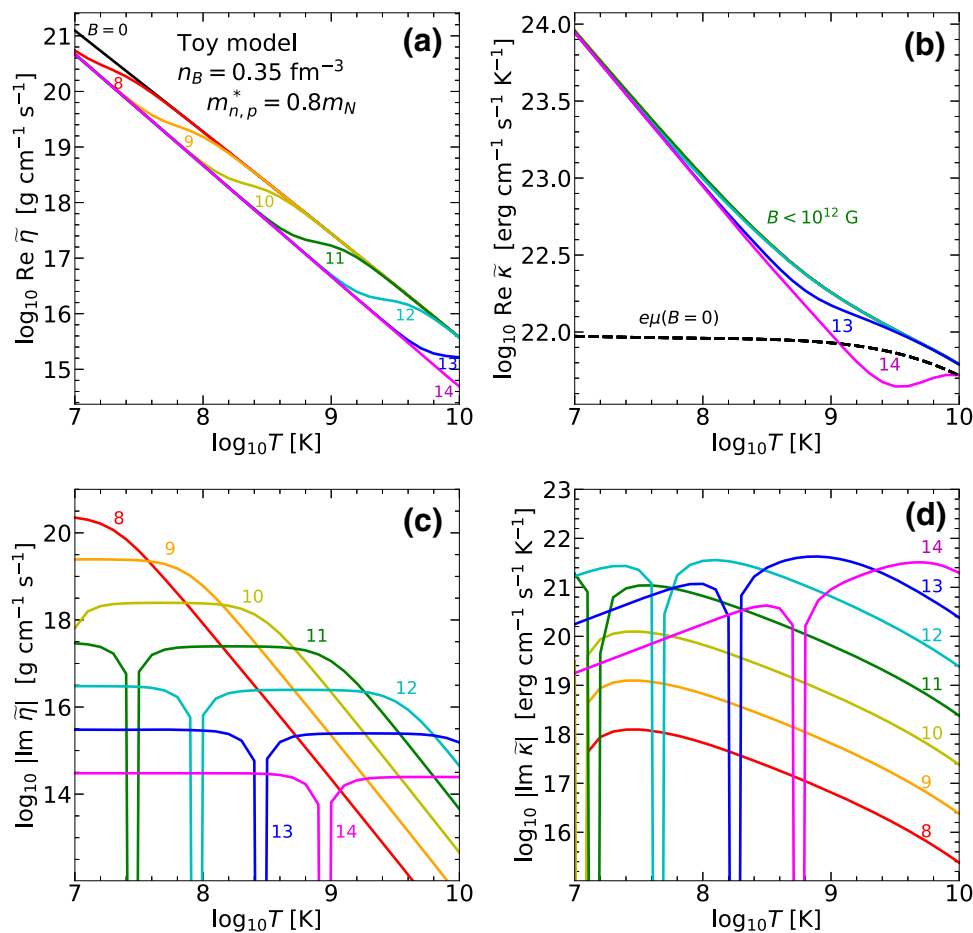


Fig. 12 Temperature dependence of the complex shear viscosity $\tilde{\eta}$ and thermal conductivity $\tilde{\kappa}$ coefficients for various values of the magnetic field B . Different values of B are shown in different colors and indicated by $\log_{10} B[\text{G}]$ near the respective curves. Panels **a–d** show, respec-

tively, $\text{Re } \tilde{\eta}(B)$, $|\text{Im } \tilde{\eta}(B)|$, $\text{Re } \tilde{\kappa}(B)$, and $|\text{Im } \tilde{\kappa}(B)|$. Results are plotted for the toy model (233), $npe\mu$ composition, $n_B = 0.35 \text{ fm}^{-3}$ and $m_{n,p}^* = 0.8m_N$

model) and become determined by all particle species. At low temperatures, $\text{Im } \tilde{\eta}$ stays constant, which is however not universal and depends on the transport scattering cross-sections as follows from above [see Eq. (239)].

Less interesting situation is observed for the thermal conductivity. In Fig. 12b we show $\text{Re } \tilde{\kappa}$ component of the thermal conductivity tensor. Since at $B = 0$ thermal conductivity is governed by neutrons (Figs. 10b, 11b), magnetic field does not influence it considerably and for $B < 10^{12} \text{ G}$ for conditions shown in Fig. 12b, $\text{Re } \tilde{\kappa}(B) \approx \text{Re } \tilde{\kappa}(B = 0) = \kappa_n$. The lepton contribution to thermal conductivity at $B = 0$ is shown with dashed line in Fig. 12b. At lower temperatures it is temperature-independent and start to transit to the standard Fermi-liquid behavior $\kappa \propto T^{-1}$ at large T . At large $B \gtrsim 10^{12} \text{ G}$, the lepton magnetization starts at high temperatures, where the lepton contribution to the total thermal conductivity is sizable. Therefore, for $B \gtrsim 10^{13} \text{ G}$ one observes the drop in $\text{Re } \tilde{\kappa}$ representing basically the neutron contribution. In any case, thermal conductivity perpendicular to the magnetic field stays large.

The behavior of the Hall component of thermal conductivity, $\text{Im } \tilde{\kappa}$, shown in Fig. 12d is qualitatively similar to the behavior of $\text{Im } \tilde{\eta}$. In the limit of large magnetization, the only difference is the appearance of temperature in the limiting expressions Eq. (128b) and (237b) leading to $\text{Im } \tilde{\kappa} \propto T$ limiting behavior at low temperatures. In the opposite limit of weak magnetization (large T), $\text{Im } \tilde{\kappa}$ is determined by leptons and basically have relaxation-time approximation behavior according to Eqs. (127a) and (234). The change of the slope of $\text{Im } \tilde{\kappa}(T)$ curve seen in Fig. 12d reflects the change of the Λ_ℓ^c temperature dependence (seen also with the dashed line in Fig. 12b). This is a result of increasing contribution of the longitudinal plasmon exchange to lepton scattering at large T .

6 Conclusion

In this paper we reviewed the framework for calculating the first-order transport coefficients (shear viscosity, thermal conductivity, and momentum transfer rates) of the multi-

component non-superfluid NS core matter in the presence of the strong magnetic field. In this case, transport coefficients become tensor quantities which can be most economically calculated utilizing the spherical tensor formalism. In this approach, each tensorial transport coefficient is described by a single complex function of the magnetic field as discussed in Sect. 3.3.

At the simplest variational level, thermal conductivity and shear viscosity are given by Eqs. (157) and (158), where the effective generalized complex mean free paths are found from the system of linear algebraic equations (154) or (155). The core of this system is the transport matrix elements Λ_{ab}^k and Λ'_{ab}^k ($k = \kappa, \eta$, and a, b indicate particle species) which are expressed by the angular averages of the scattering probabilities with certain weighting factors depending on the transport problem in question. The definitions of these matrix elements are given in Eqs. (159)–(161). The momentum transfer rates are also expressed via the corresponding transport matrix element, Eq. (168).

The transport matrices depend on the interactions between the constituents of the NS core liquid and need to be calculated from the microscopic theory. Leptons interact via the electromagnetic forces, the corresponding ‘electromagnetic’ contribution to transport matrices can be calculated in the relatively model-independent way, provided composition and effective masses of charged baryons are known. In contrast, baryons interact mainly through the strong force channel. In this case calculations of EOS and the transport properties should be performed in consistent way. Ideally, public EOS databases such as CompOSE, should also provide the transport matrices for each EOS. When such calculations are not available, one is forced to use the approximate approaches.

We applied the developed formalism to the $npe\mu$ composition of the NS cores. Utilizing 39 EOS models and five microscopic interactions (not consistent with these EOSs), we investigated the uncertainty range that can be expected in realistic calculations. We then compared these results with the approximate approach based on the in-vacuum cross-sections of the nucleon scattering. We expect that these results (supplemented with the nucleon effective masses if available) give qualitatively correct picture of transport properties of the NS core matter. We provide (Appendix B) the practical fitting expressions that can be used for any EOS of dense matter. In addition we provide the ‘toy model’ fits based on the crude estimate (233) for the proton fraction that allow one to estimate the transport matrices and hence the transport coefficients at a given baryon density.

Magnetic field more strongly affects the motion of light leptons than the baryonic component of the matter. Therefore magnetic field effects are more prominent for the shear viscosity, where leptons dominate the transport at $B = 0$, than for the thermal conductivity, where the situation is opposite

[1]. We find that the shear viscosity can be strongly influenced even by the moderate $B \gtrsim 10^{10}$ G. At sufficiently low temperatures, the shear viscosity in the plane transverse to magnetic field becomes fully determined by neutrons. In this sense it can vary significantly for the different models of the nuclear interaction. The ‘parallel’ shear viscosity coefficient η_0 is not affected by the magnetic field and is dominated by the lepton contribution. Thermal conductivity is less affected by the magnetic field, basically the perpendicular component of the conductivity is affected in the high-temperature and high-magnetic field region of the parameter space studied.

Notice that while these conclusions were illustrated in the paper for the ‘toy’ model under the approximation of the in-vacuum nucleon scattering, they are expected to be qualitatively valid if more accurate calculations are available.

In our study we ignored the possibility of inelastic collisions (i.e. reactions). The formalism outlined here can be extended to this case by considering particle non-conserving collision integrals in the system of Fermi-liquid transport equations. Reactions lead to appearance of the corresponding terms in the entropy generation rate and corresponding scalar transport coefficients. These processes are in the mutual interaction with the bulk viscosity coefficients. Moreover in this case a dynamical problem needs to be considered. The reaction-driven bulk viscosity in the dynamical regime can be derived without relying on the kinetic equations, see, e.g., [1] for a review.

We illustrated the formalism described in the paper exclusively for nucleonic NS core composition. In principle, NS cores can have richer composition. For instance, the hyperonic NS cores are widely discussed, see, e.g. [154] for a review. Transport coefficients for the hypernuclear NS cores can be, in principle, calculated using the similar formalism as studied here. For the non-magnetized case this was done by [100] for two models of hypernuclear interaction. The momentum transfer rates within the free-particle model and $npe\Sigma^-$ composition were considered in [9]. When several hyperon species are present, in principle, there is a possibility of strong inelastic collisions (neglected in [100]). In this case, even when the matter is in the equilibrium state with respect to these reactions, they can contribute to the transport cross-sections. In the presence of inelastic collisions, the system (155), which determine transport mean free paths, has the same form, but the transport matrices receive additional contributions. These contributions can be determined following the lines of Sect. 3.6, but the kinematic expressions for the transport matrix elements and angular averages will be more involved, because all four Fermi-momenta of the quasiparticles participating in collisions are different in this case.

In this study we did not consider the transport properties of the NS core matter in presence of superfluidity/superconductivity. It is known that baryons in NS core matter can form Cooper pairs due to the presence of the attrac-

tive character of some partial wave channels of the baryon interaction, see [155] for a review. This pairing may lead to the existence of superflows and supercurrents. In this case the hydrodynamic equations become much more complicated, and multifluid consideration is necessary, see e.g., [13, 156], and references therein. Additional complications arise since the pairing in NS cores, like for the superfluid He³, can have the anisotropic pattern. For instance, the neutrons in NS core are thought to pair in the ³P₂–³F₂ channel. Even in the superfluid case, the flows of the normal part of the fluid are subject to the dissipative processes. In principle the relevant transport coefficients can be calculated based on the the kinetic theory for the anisotropic superfluids e.g. [157], although it is severely more complicated task than the non-superfluid problem.

Superfluidity modifies the transport coefficients on NS core matter in several ways, e.g. [1], which we outline briefly. The relevant excitations of the normal component in the superfluid matter are not the usual quasiparticles, but rather the Bogoliubov quasiparticles, which spectra have a gap at the Fermi surface. In addition, the number of such quasiparticles does not necessarily conserve in collisions. The main effect of these modifications results in the exponential suppression of the scattering rates for the processes in which the superfluid species participate. Moreover, if the paired species are charged (e.g., protons) this modifies the properties of the electromagnetic screening. This affects the scattering of all charged species, for instance, leptons [1, 89]. At low temperatures, another excitations, namely the superfluid phonons, can contribute to the transport properties of NS core matter. This contribution is reviewed in, e.g., [158].

Even more complicated is the case of the magnetized superfluid/superconducting matter. Under a certain conditions, the matter can be in the type II superconducting state where the magnetic field is confined in the topological defects called Abrikosov vortices. This introduces another mesoscopic scale on the stage and additional terms in dissipative hydrodynamics, e.g. [15].

A detailed discussion of all these effects is left for future studies.

Acknowledgements The authors are grateful to Dima Yakovlev for discussions.

Data Availability Statement This manuscript has no associated data or the data will not be deposited. [Authors' comment: This is a theoretical study and there are no data associated to it.]

Appendix A: Linearized kinetic equations

Let us outline derivation of Eq. (141) from Eq. (91). Functions $\Phi(\mathbf{p}_i)$ are expanded in spherical harmonics according to Eq. (104). These spherical harmonics can be rotated to the body frame which has $\hat{\mathbf{p}}_1$ as a polar axis via

$$Y_{\ell m}(\hat{\mathbf{p}}_i) = \sum_{m'} \left(\mathcal{D}_{mm'}^\ell(\hat{\mathbf{p}}_1, \varphi) \right)^* Y_{\ell m'}(\hat{\mathbf{p}}_i \hat{\mathbf{p}}_1, \varphi_i), \tag{A.1}$$

where φ is the azimuthal angle of the body frame system with respect to the laboratory system, φ_i is the azimuthal angle of \mathbf{p}_i in the body-frame coordinate system. Isotropy of the collision probability in Eq. (141) means, in particular, that it does not depend on φ however angular integration contains integration over φ . Therefore only $m' = 0$ term in Eq. (A.1) survives and one has

$$Y_{\ell m}(\hat{\mathbf{p}}_i) \rightarrow Y_{\ell m}(\hat{\mathbf{p}}_1) \mathcal{P}_\ell(\hat{\mathbf{p}}_i \hat{\mathbf{p}}_1) \tag{A.2}$$

resulting in Eq. (141).

Complete system of the linearized transport equations for the thermal conductivity or the shear viscosity of multicomponent Fermi-liquid is obtained by substituting Eqs. (152) and (140) to Eq. (109) and placing all quasiparticles on respective Fermi surfaces using energy-angular decomposition. It is convenient to substitute $x_2 \rightarrow -x_2$ in the collision integral and exchange $x_2 \leftrightarrow x_{2'}$ in terms containing $\tilde{\Psi}_b(x_{2'})$. Finally, one obtains

$$\begin{aligned} -f'_F(x_1) \tilde{X}_k(x_1) &= \frac{T^2 m_a^{*2}}{4\pi^4 p_{Fa}^2 \tilde{D}_k(p_{Fa})} \int dx_{1'} dx_2 dx_{2'} \\ &\times f_F(x_1) f_F(-x_{1'}) f_F(-x_2) f_F(-x_{2'}) \\ &\times \delta(x_1 - x_2 - x_{1'} - x_{2'}) \\ &\times \left(\tilde{D}_k(p_{Fa}) \tilde{\Psi}_a^k(x_1) \lambda_a^{(k, \text{eff})} \sum_b m_b^{*2} \langle Q_{ab} \rangle \right. \\ &- \tilde{D}_k(p_{Fa}) \tilde{\Psi}_a^k(x_{1'}) \lambda_a^{(k, \text{eff})} \sum_b m_b^{*2} \langle Q_{ab} \mathcal{P}_\ell(\hat{\mathbf{p}}_1 \hat{\mathbf{p}}_{1'}) \rangle \\ &- \sum_b m_b^{*2} \tilde{D}_k(p_{Fb}) \tilde{\Psi}_b^k(x_2) \lambda_b^{(k, \text{eff})} \\ &\left. \times \langle Q_{ab} (\mathcal{P}_\ell(\hat{\mathbf{p}}_1 \hat{\mathbf{p}}_{2'}) - (-1)^{\xi k} \mathcal{P}_\ell(\hat{\mathbf{p}}_1 \hat{\mathbf{p}}_2)) \rangle \right) \\ &+ i f'_F(x_1) \frac{\omega_{BFa}}{v_{Fa}} \lambda_a^{(k, \text{eff})} \tilde{\Psi}_a^k(x_1), \tag{A.3} \end{aligned}$$

where the symmetry of the transport problem due to x inversion is used (hence appearance of the phase $(-1)^{\xi k}$) and angular integrations are encapsulated in the angular brackets according to Eq. (144). This equation for $\ell = 1, 2$ contains the following angular averages that should be provided by the microscopic theory

$$\begin{aligned} &\langle Q_{ab} \rangle, \quad \langle Q_{ab} P_1(\hat{\mathbf{p}}_1 \hat{\mathbf{p}}_{1'}) \rangle, \quad \langle Q_{ab} P_2(\hat{\mathbf{p}}_1 \hat{\mathbf{p}}_{1'}) \rangle, \\ &\langle Q_{ab} (P_1(\hat{\mathbf{p}}_1 \hat{\mathbf{p}}_2) \pm P_1(\hat{\mathbf{p}}_1 \hat{\mathbf{p}}_{2'})) \rangle, \\ &\langle Q_{ab} (P_2(\hat{\mathbf{p}}_1 \hat{\mathbf{p}}_{2'}) - P_2(\hat{\mathbf{p}}_1 \hat{\mathbf{p}}_2)) \rangle. \tag{A.4} \end{aligned}$$

Notice that the averages $\langle Q_{aa} \rangle$ (i.e. without angular factors) do not enter the simplest variational solution, but are necessary for solution of (A.3). If the squared matrix element Q_{ab} does not depend on $w = x_{1'} - x_1$, two of three integrations

over x_i can be performed analytically and Eq. (A.3) reduces to much simpler integral equation given in [71] that allows for exact solution. In principle, one can integrate over x_2 and $x_{2'}$ in the terms containing $\tilde{\Psi}_a$ in Eq. (A.3), but in general two energy integrations remain in terms containing $\Psi_b(x_2)$.

After the solution of the system of kinetic equations (A.3), the complex thermal conductivity and shear viscosity coefficients are given by [cf. Eqs. (157) and (158)]

$$\tilde{\kappa}_a = \frac{\pi^2 n_a T}{3 p_{Fa}} \lambda_{\text{eff}}^{\kappa,a} \times \frac{3}{\pi^2} \int dx (-f'_F(x)) x^2 \tilde{\Psi}_a^\kappa(x), \quad (\text{A.5})$$

$$\tilde{\eta}_a = \frac{n_a p_{Fa}}{5} \lambda_{\text{eff}}^{\eta,a} \times \int dx (-f'_F(x)) \tilde{\Psi}_a^\eta(x). \quad (\text{A.6})$$

For the diffusion problem the general transport equation is even more cumbersome, since it contains the summation over k . Moreover when solving these equations one needs to carefully account for the conditions of fit that get rid of the kernel solutions [91]. We do not write these equations here; the formal equations can be easily written via the methods described in Sect. 3. The respective equations for the normal Fermi-liquid case where w_{ab} does not depend on ω can be found in [71] (without the magnetic field).

Appendix B: Practical formulae for nuclear NS core matter

In this appendix we give practical expressions for calculating transport coefficients considered in the paper, namely, thermal conductivity $\hat{\kappa}$, shear viscosity $\hat{\eta}$ tensors, and momentum transfer rates J_{ab} , $a \neq b$, in the nucleonic ($npe\mu$) NS cores.

Independent components of the thermal conductivity and shear viscosity tensors are determined by the complex functions $\tilde{\kappa}(B)$ and $\tilde{\eta}(B)$, respectively, as

$$\kappa_{\parallel} = \tilde{\kappa}(B = 0), \quad (\text{B.7a})$$

$$\kappa_{\perp} = \text{Re} \tilde{\kappa}(B), \quad (\text{B.7b})$$

$$\kappa_{\wedge} = -\text{Im} \tilde{\kappa}(B), \quad (\text{B.7c})$$

$$\eta_0 = \tilde{\eta}(B = 0), \quad (\text{B.8a})$$

$$\eta_1 = \text{Re} \tilde{\eta}(2B), \quad (\text{B.8b})$$

$$\eta_3 = -\text{Im} \tilde{\eta}(2B), \quad (\text{B.8c})$$

$$\eta_2 = \text{Re} \tilde{\eta}(B), \quad (\text{B.8d})$$

$$\eta_4 = -\text{Im} \tilde{\eta}(B). \quad (\text{B.8e})$$

Complex functions $\tilde{\kappa}$, $\tilde{\eta}$ are sums of the partial contributions, $a = n, p, e, \mu$

$$\tilde{\kappa} = \sum_a \tilde{\kappa}_a, \quad (\text{B.9})$$

$$\tilde{\eta} = \sum_a \tilde{\eta}_a, \quad (\text{B.10})$$

where

$$\tilde{\kappa}_a = 5.66 \times 10^{22} \left(\frac{n_a}{n_0}\right)^{2/3} T_8 \frac{\tilde{\lambda}_a^\kappa}{10^{-6} \text{ cm}} \text{ erg cm}^{-1} \text{ s}^{-1} \text{ K}^{-1}, \quad (\text{B.11})$$

$$\tilde{\eta}_a = 5.66 \times 10^{17} \left(\frac{n_a}{n_0}\right)^{4/3} \frac{\tilde{\lambda}_a^\eta}{10^{-6} \text{ cm}} \text{ g cm}^{-1} \text{ s}^{-1}, \quad (\text{B.12})$$

$n_0 = 0.16 \text{ fm}^{-3}$, $T_8 = T/(10^8 \text{ K})$ and $\tilde{\lambda}_a^k$ with $k = \kappa, \eta$ are generalized complex effective mean free paths of quasiparticles.

Effective mean free paths are found from the solution of a system of linear equations ($k = \kappa, \eta$)

$$1 = \left(\Lambda_a^k + i \frac{\omega_{BFa}}{v_{Fa}}\right) \tilde{\lambda}_a^k + \sum_{b \neq a} \Lambda_{ab}^k \tilde{\lambda}_b^k, \quad (\text{B.13})$$

where magnetic field enters through the inverse gyroradii

$$\frac{\omega_{BFa}}{v_{Fa}} = \frac{q_a B}{p_{Fa} c} = 9.04 \times 10^5 Z_a B_{12} \left(\frac{n_a}{n_0}\right)^{-1/3} \text{ cm}^{-1}, \quad (\text{B.14})$$

where $B_{12} = B/(10^{12} \text{ G})$ and charge numbers $Z_a = 0, \pm 1$ in $npe\mu$ matter.

Coefficients Λ_a^k in Eq. (B.13) are

$$\Lambda_a^k = \sum_b \Lambda_{ab}^k + \Lambda_{aa}^k. \quad (\text{B.15})$$

Transport matrix elements $\Lambda_{ab}^k, \Lambda_{ab}^{\prime k}$ in general contain contributions from all interaction channels between the particle species a and b . In the model considered here, leptons ($\ell = e, \mu$) participate in electromagnetic interactions, neutrons in strong interactions, and protons in both. In latter case one needs to sum both contributions. Below we give the practical expressions for the transport matrix elements and related momentum transfer rates J_{ab} for electromagnetic and strong channels separately. In this Appendix, $x_a \equiv n_a/n_B$, where n_B is the total baryon density.

Appendix B.1: Electromagnetic channel

In the electromagnetic sector, $a, b = e, \mu, p$. Expressions below are based on the results described in detail in Sect. 4.1.

Practical expressions for the screening wavenumbers are

$$q_l = 0.27 \left(\frac{n_B}{n_0}\right)^{1/6} \sqrt{\sum_a Z_a^2 x_a^{1/3} \frac{m_a^*}{m_N}} \text{ fm}^{-1}, \quad (\text{B.16a})$$

$$q_t = 0.16 \left(\frac{n_B}{n_0}\right)^{1/3} \sqrt{\sum_a Z_a^2 x_a^{2/3}} \text{ fm}^{-1}. \quad (\text{B.16b})$$

The effective mass for leptons is $m_\ell^* = \sqrt{m_\ell^2 + p_{F\ell}^2/c^2}$, while for protons one needs to use the Landau effective mass on the Fermi surface here.

In what follows we normalize screening momenta over fm^{-1} : $\bar{q}_l = q_l/(\text{fm}^{-1})$, $\bar{q}_t = q_t/(\text{fm}^{-1})$.

We need the following integrals

$$I_l^{(0)} = \frac{1}{2\bar{q}_l^3} \left[\arctan \frac{q_m}{q_l} + \frac{q_m q_l}{q_m^2 + q_l^2} \right], \tag{B.17a}$$

$$I_l^{(2)} = \frac{1}{2\bar{q}_l} \left[\arctan \frac{q_m}{q_l} - \frac{q_m q_l}{q_m^2 + q_l^2} \right], \tag{B.17b}$$

$$I_{tl}^{(2)} = I_l^{(2)} + \bar{q}_l^2 I_l^{(0)} = \frac{1}{\bar{q}_l} \arctan \frac{q_m}{q_l}, \tag{B.17c}$$

where $q_m = 2 \min(p_{Fa}, p_{Fb})$.

Now the transport matrix elements for the thermal conductivity are

$$[\Lambda_{ab}^\kappa]^{\text{em}} = \Lambda_{ab}^{\kappa,t} + \Lambda_{ab}^{\kappa,l}, \tag{B.18}$$

where the transverse contribution is

$$\Lambda_{ab}^{\kappa,t} = 6.10 \times 10^4 T_8 x_b^{2/3} \left(\frac{n_B}{n_0}\right)^{2/3} \bar{q}_t^{-2} \text{cm}^{-1}, \tag{B.19}$$

and the longitudinal contribution is

$$\Lambda_{ab}^{\kappa,l} = 1.86 \times 10^3 T_8^2 \left(\frac{m_a^* m_b^*}{m_N^2}\right)^2 \left(\frac{n_B}{n_0}\right)^{-2/3} \times x_a^{-2/3} I_l^{(0)} \text{cm}^{-1}. \tag{B.20}$$

Non-diagonal coefficients in Eq. (B.13) for thermal conductivity are

$$[\Lambda'_{ab}{}^\kappa]^{\text{em}} = 3.65 \times 10^3 \frac{T_8^{5/3}}{\bar{q}_l^2 \bar{q}_t^{2/3}} \frac{m_a^* m_b^* x_b^{1/3}}{m_N^2 x_a^{1/3}} \text{cm}^{-1}. \tag{B.21}$$

Similar expressions for shear viscosity problem read

$$[\Lambda_{ab}^\eta]^{\text{em}} = \Lambda_{ab}^{\eta,t} + \Lambda_{ab}^{\eta,l}, \tag{B.22}$$

where

$$\Lambda_{ab}^{\eta,t} = 200 T_8^{5/3} \frac{x_b^{2/3}}{x_a^{2/3} \bar{q}_t} \text{cm}^{-1}, \tag{B.23}$$

and

$$\Lambda_{ab}^{\eta,l} = 822 T_8^2 \left(\frac{m_a^* m_b^*}{m_N^2}\right)^2 \left(\frac{n_B}{n_0}\right)^{-4/3} x_a^{-4/3} I_l^{(2)} \text{cm}^{-1}. \tag{B.24}$$

Non-diagonal elements are

$$[\Lambda'_{ab}{}^\eta]^{\text{em}} = 102 T_8^2 \frac{m_a^* m_b^*}{m_N^2} \left(\frac{n_B}{n_0}\right)^{-2/3} \frac{x_b^{1/3}}{x_a} I_{tl}^{(2)} \text{cm}^{-1}. \tag{B.25}$$

The momentum transfer rates J_{ab} appearing in the diffusion problems are calculated in a similar way:

$$[J_{ab}]^{\text{em}} = J_{ab}^l + J_{ab}^t, \tag{B.26}$$

where

$$J_{ab}^t = 1.89 \times 10^{26} T_8^{5/3} \left(\frac{n_B}{n_0}\right)^{4/3} \frac{x_a^{2/3} x_b^{2/3}}{\bar{q}_t^{2/3}} \text{g cm}^{-3} \text{s}^{-1}, \tag{B.27a}$$

$$J_{ab}^l = 7.78 \times 10^{26} T_8^2 \left(\frac{m_a^* m_b^*}{m_N^2}\right)^2 I_l^{(2)} \text{g cm}^{-3} \text{s}^{-1}. \tag{B.27b}$$

Appendix B.2: Strong channel

The strong interaction operates in the subsystem of protons and neutrons. We define

$$C_\Lambda = 1.65 \times 10^6 T_8^2 \left(\frac{n_B}{n_0}\right)^{-1/3} \text{cm}^{-1}. \tag{B.28}$$

Then, for the thermal conductivity and $a = n, p$

$$\Lambda_{aa}^\kappa + \Lambda'_{aa}{}^\kappa = \frac{1}{5} C_\Lambda \left(\frac{m_a^*}{m_N}\right)^4 x_a^{-1/3} \frac{S_{aa2}}{\text{mb}}, \tag{B.29a}$$

$$\Lambda_{np}^\kappa = \frac{1}{5} C_\Lambda \left(\frac{m_p^* m_n^*}{m_N^2}\right)^2 x_n^{-1/3} \frac{S_{np1} + S_{np2}}{\text{mb}}, \tag{B.29b}$$

$$\Lambda_{pn}^\kappa = \frac{1}{5} C_\Lambda \left(\frac{m_p^* m_n^*}{m_N^2}\right)^2 \frac{x_n^{1/3}}{x_p^{2/3}} \left(\frac{S_{np1}}{\text{mb}} + \frac{x_n^{2/3}}{x_p^{2/3}} \frac{S_{np2}}{\text{mb}}\right), \tag{B.29c}$$

$$\Lambda'_{np}{}^\kappa = \frac{x_p^{2/3}}{x_n^{2/3}} \Lambda'_{pn}{}^\kappa = \frac{1}{5} C_\Lambda \left(\frac{m_p^* m_n^*}{m_N^2}\right)^2 x_p^{-1/3} \frac{S'_{np2}}{\text{mb}}. \tag{B.29d}$$

For the shear viscosity

$$\Lambda_{aa}^\eta + \Lambda'_{aa}{}^\eta = C_\Lambda \left(\frac{m_a^*}{m_N}\right)^4 x_a^{-1/3} \frac{S_{aa4}}{\text{mb}}, \tag{B.30a}$$

$$\Lambda_{np}^\eta = C_\Lambda \left(\frac{m_p^* m_n^*}{m_N^2}\right)^2 x_n^{-1/3} \frac{S_{np2} - S_{np4}}{\text{mb}}, \tag{B.30b}$$

$$\Lambda_{pn}^\eta = C_\Lambda \left(\frac{m_p^* m_n^*}{m_N^2}\right)^2 x_p^{-1/3} \left(\frac{x_n}{x_p} \frac{S_{np2}}{\text{mb}} - \frac{x_n^{5/3}}{x_p^{5/3}} \frac{S_{np4}}{\text{mb}}\right), \tag{B.30c}$$

$$\Lambda'_{np}{}^\eta = \frac{x_p^{4/3}}{x_n^{4/3}} \Lambda'_{pn}{}^\eta = C_\Lambda \left(\frac{m_p^* m_n^*}{m_N^2}\right)^2 x_p^{-1/3} \frac{S'_{np4}}{\text{mb}}. \tag{B.30d}$$

The momentum transfer rates (here only J_{np} coefficient exists)

$$J_{np} = 1.56 \times 10^{30} T_8^2 \left(\frac{m_p^* m_n^*}{m_N^2}\right)^2 \left(\frac{n_B}{n_0}\right) x_n \frac{S_{np2}}{\text{mb}}. \tag{B.31}$$

Table 3 Fit parameters for the Eq. (B.32)

Cross-sec.	a	p	b	q	c	rrms (%)	Max error (%)
S_{nn2}	0.912	1.23	0.00631	2.248	4.045	0.05	0.1
S_{pp2}	25.6	1.23	0.404	0.932	0.000	0.7	3.1
S_{nn4}	0.0151	2.42	-0.00334	1.26	0.409	0.2	0.5
S_{pp4}	3.04	1.12	-2.00	-0.336	1.10	1.1	2.2
S_{np1}	7.03	0.518	0.0789	1.43	0.000	0.3	0.8
S_{np2}	2.879	0.03806	0.02942	1.115	-2.674	1.0	2.4
S_{np4}	0.03562	0.0514	0.001068	1.802	-0.02000	1.8	3.9
S'_{np2}	-0.1833	0.5109	0.001413	2.139	-0.4024	0.2	0.4
S'_{np4}	-0.4658	-0.03099	0.06761	0.2137	0.3855	1.3	4.0

If the effective masses of nucleons are not known, we suggest to use some typical effective mass, e.g., $m_n^* = m_p^* = 0.8m_N$.

We provide two types of fits for the transport cross-sections S_α in expressions above. First ones are for the toy model where particle fractions are given in Eq. (233). These fits give $S_\alpha(n_B)$. The second fits are valid for any particle fractions and give $S_\alpha(p_{Fn}, p_{Fp})$. Both fits are based on the in-vacuum interaction.

1. Fits for the toy model Eq. (233).

In this case all nine cross-sections S_α could be fitted by the formula

$$S_\alpha(n_B) = a \left(\frac{n_0}{n_B}\right)^p + b \left(\frac{n_B}{n_0}\right)^q + c, \tag{B.32}$$

where the appropriate values of fitting parameters $a, b, c, p,$ and q are listed in Table 3. The fitting domain is $n_B = 0.08 \dots 1 \text{ fm}^{-3}$.

2. Fits for the general compositions.

In expressions below p_{Fn} and p_{Fp} are measured in fm^{-1} and $P_{\min} = |p_{Fn} - p_{Fp}|, P_{\max} = p_{Fn} + p_{Fp}$. All functions are fitted on a grid $0.1 < p_{Fn,p} < 3.5 \text{ fm}^{-3}$.

$$S_{aa2} = 7.82 \frac{1 + 0.576|p_{Fa} - 1.05|^{1.47}}{(1 - 0.198p_{Fa})(0.0349 + p_{Fa}^{2.14})} \text{mb}, \tag{B.33}$$

rrms¹¹ = 1.2%, max error = 2.9% at $p_{Fa} = 0.2 \text{ fm}^{-1}$.

$$p_{Fn} S_{np1} = 79.5(P_{\max} - P_{\min}) \times \frac{1 - 0.164P_{\max} + 0.0258P_{\max}^2}{P_{\max}^{1.52}} \times \frac{\sqrt{1 + 0.637P_{\min}^4}}{1 + 1.35P_{\min}^2} \text{mb}, \tag{B.34}$$

where rrms = 4.2%, max error = 12% at $p_{Fn} \approx 0.7 \text{ fm}^{-1}, p_{Fp} = 0.7 \text{ fm}^{-1}$.

$$p_{Fn}^3 S_{np2} = 5.158 \frac{(P_{\max} - P_{\min})^{3.342}}{P_{\max}^{1.618} (1 + 0.3691P_{\max}^{1.985})} \times (1 + 0.2072(P_{\max} - P_{\min} - 1.505)^2) \times (1 + 0.2279P_{\min} - 0.6076P_{\min}^2 + 0.4962P_{\min}^3 - 0.07539P_{\min}^4) \text{mb}, \tag{B.35}$$

rrms = 2.6%, max error = 14% at $p_{Fn} \approx 0.1 \text{ fm}^{-1}, p_{Fp} = 0.1 \text{ fm}^{-1}$.

$$S_{aa4} = 2.84 \frac{1 + 1.65(p_{Fa} - 0.903)^2}{(1 + 1.70p_{Fa})(p_{Fa} + 0.165)^2 + 0.103} \text{mb}, \tag{B.36}$$

rrms = 0.95%, max error = 2.1% at $p_{Fa} = 0.6 \text{ fm}^{-1}$.

$$p_{Fn}^5 S_{np4} = 0.621 \frac{(P_{\max} - P_{\min})^{5.33}}{P_{\max}^{1.64}} \times \frac{1 + 0.274(P_{\max} - P_{\min} - 1.62)^2}{(1 + 0.262P_{\max}^{2.12})} \times (1 + 0.122P_{\min} - 0.616P_{\min}^2 + 0.538P_{\min}^3 - 0.0860P_{\min}^4) \text{mb}, \tag{B.37}$$

rrms = 4.0%, max error = 19% at $p_{Fn} \approx 0.1 \text{ fm}^{-1}, p_{Fp} = 0.1 \text{ fm}^{-1}$.

$$-p_{Fn}^3 S'_{np2} = 1.858 \frac{(P_{\max} - P_{\min})^{3.250}}{P_{\max}^{2.415}} \times (-1 + 7.383P_{\max} - 1.695P_{\max}^2 + 0.2441P_{\max}^3 - 0.01657P_{\max}^4 + 9.700P_{\min} - 7.698P_{\max}P_{\min} + 0.9015P_{\max}^2P_{\min})$$

¹¹ rrms = root mean square relative error.

$$\begin{aligned}
 & -0.04207 P_{\max}^3 P_{\min} \\
 & -9.511 P_{\min}^2 + 3.939 P_{\max} P_{\min}^2 \\
 & -0.3213 P_{\max}^2 P_{\min}^2 \\
 & +2.822 P_{\min}^3 - 0.4262 P_{\max} P_{\min}^3 \\
 & - 0.2448 P_{\min}^4) \text{ mb}, \tag{B.38}
 \end{aligned}$$

rrms = 2.7%, max error = 18% at $k_n \approx 1.5 \text{ fm}^{-1}$, $k_p = 0.2 \text{ fm}^{-1}$.

$$- p_{\text{Fn}}^5 S'_{np4} = p_{\text{Fn}}^5 S_{np4} - \frac{P_{\text{Fn}}^2 + P_{\text{Fn}}^2}{2} p_{\text{Fn}}^3 S_{np2} + U'_{np4}, \tag{B.39a}$$

where

$$\begin{aligned}
 U'_{np4} = 0.0451 \frac{(P_{\max} - P_{\min})^{3.27}}{P_{\max}^{0.448}} & \left(0.403 P_{\max}^4 P_{\min} \right. \\
 & -0.918 P_{\max}^3 P_{\min}^2 - 5.54 P_{\max}^3 P_{\min} + 1.78 P_{\max}^2 P_{\min}^3 \\
 & +8.28 P_{\max}^2 P_{\min}^2 + 28.7 P_{\max}^2 P_{\min} - 0.331 P_{\max} P_{\min}^4 \\
 & -16.2 P_{\max} P_{\min}^3 - 15.7 P_{\max} P_{\min}^2 - 74.6 P_{\max} P_{\min} \\
 & -0.00111 P_{\max}^5 - 0.118 P_{\max}^4 + 1.77 P_{\max}^3 \\
 & -8.17 P_{\max}^2 + 17.2 P_{\max} - 0.118 P_{\min}^5 + 1.77 P_{\min}^4 \\
 & \left. + 41.1 P_{\min}^3 - 21.0 P_{\min}^2 + 94.6 P_{\min} + 1 \right) \text{ mb}. \tag{B.39b}
 \end{aligned}$$

For U'_{np4} , rrms=0.5% and max error = 1.9%. Notice that in the region where S'_{np4} changes sign and is therefore small, this fit can give large relative error for S'_{np4} . In this case, however, precise calculation of S'_{np4} is not necessary as being small it drops out of the equations.

Appendix C: Electrical conductivity of the NS core matter

Electrical conductivity in a multicomponent plasma is an aspect of the general diffusion process. In this appendix we discuss the relation between the electrical conductivity and momentum transfer rates J_{ab} and give practical expressions for the $npe\mu$ matter composition. Below we do not consider thermal diffusion.

In the discussion in the main part of the manuscript, the diffusion in NS cores was described via the generalized Ohm law (164) which we repeat here for convenience

$$\begin{aligned}
 n_a \left(\mathbf{d}_{(a)} + \frac{h_a}{\hbar n} [\mathbf{J} \times \mathbf{B}] \right) &= \sum_b J_{ab} (\mathbf{w}_b - \mathbf{w}_a) \\
 &+ n_a q_a [\mathbf{w}_a \times \mathbf{B}]. \tag{C.40}
 \end{aligned}$$

According to Eqs. (95), (162), and (164), the entropy production rate in the diffusion process is given by multiplication

of Eq. (C.40) by \mathbf{w}_a and summing over species

$$\begin{aligned}
 T\zeta &= - \sum_a n_a \mathbf{w}_a \left(\mathbf{d}_{(a)} + \frac{h_a}{\hbar n} [\mathbf{J} \times \mathbf{B}] \right) \\
 &= \frac{1}{2} \sum_{ab} J_{ab} (\mathbf{w}_b - \mathbf{w}_a)^2. \tag{C.41}
 \end{aligned}$$

Notice that the Eq. (C.40) is valid in general frame (without imposing conditions of fit) and the second line in Eq. (C.41) shows that the entropy generation rate is frame-independent. Assume now that the only source for diffusion is the electric field, so that Eq. (87) becomes

$$\mathbf{d}_{(a)} = -q_a \mathbf{E}. \tag{C.42}$$

Then the first line of Eq. (C.41) reduces to

$$T\zeta = \mathbf{J} \mathbf{E} - \mathbf{u}_g [\mathbf{J} \times \mathbf{B}] \equiv \mathbf{J} \mathbf{E}', \tag{C.43}$$

where

$$\mathbf{u}_g = \sum_a \mathfrak{X}_a \mathbf{w}_a, \quad \mathfrak{X}_a = \frac{n_a h_a}{\hbar n}, \tag{C.44}$$

may be called the relativistic ‘center of mass’ velocity of a liquid, and

$$\mathbf{E}' = \mathbf{E} + [\mathbf{u}_g \times \mathbf{B}] \tag{C.45}$$

is the electric field in the center of mass frame, in which $\mathbf{u}_g = 0$. The terms \mathfrak{X}_a in Eq. (C.44) are the ‘mass’ fractions which in strongly degenerate matter ($h_a \approx \mu_a$) are

$$\mathfrak{X}_a \approx \frac{\mu_a n_a}{\sum_b \mu_b n_b}. \tag{C.46}$$

The center-of-mass frame is defined by the condition

$$\mathbf{u}_g = \sum_a \mathfrak{X}_a \mathbf{w}_a = 0. \tag{C.47}$$

Since the center-of-mass frame and hence \mathbf{E}' is unique, the Eq. (C.43) is frame-independent in accordance with Eq. (C.41). Notice that only¹² in the center-of-mass frame, the heat release is given by the standard $\mathbf{J} \mathbf{E}$ expression.

When the diffusion driving forces are given by Eq. (C.42), all diffusion velocities and any their linear combination (i.e. \mathbf{J} and \mathbf{u}_g) will be linear in components of \mathbf{E} . Namely,

$$\mathbf{J} = \hat{\sigma} \mathbf{E}, \tag{C.48}$$

where $\hat{\sigma}$ is the electrical conductivity tensor. This tensor, however, is not frame-independent since the electric field (at $\mathbf{B} \neq 0$) depends on the frame. Indeed, let us denote the electrical conductivity in the center-of-mass frame as $\hat{\sigma}'$ and let

$$\mathbf{u}_g = \hat{\mathcal{U}} \mathbf{E}. \tag{C.49}$$

¹² Of course, this is strictly true only if $\mathbf{d}_{(a)} = -q_a \mathbf{E}$. More general case is considered, e.g., in [96], where $\mathbf{d}_{(a)}$ includes additional diffusion terms $\propto \nabla \mu_a$.

Then

$$\mathbf{J} = \hat{\sigma}' \mathbf{E}' = \hat{\sigma}' (\mathbf{E} + [\hat{\boldsymbol{\mu}} \times \mathbf{B}]) = \hat{\sigma} \mathbf{E}, \tag{C.50}$$

where

$$\sigma_{ij} = \sigma'_{im} (\delta_{mj} + \epsilon_{mkl} B_k \mu_{lj}). \tag{C.51}$$

The electrical conductivity tensor can be found by inversion of the Eq. (C.40) in any frame, however according to Eq. (C.43) it is physically motivated to do this in the center-of-mass frame characterized by Eq. (C.47).

Let us, however, start from the case $B = 0$ in general frame, characterized by

$$\sum_a \mathfrak{z}_a \mathbf{w}_a = 0, \quad \sum_a \mathfrak{z}_a = 1, \tag{C.52}$$

where $\{\mathfrak{z}_a\}$ is a constant set. The general Ohm law Eq. (C.40) takes the Stephan–Maxwell form

$$n_a \mathbf{d}_{(a)} = \sum_b J_{ab} (\mathbf{w}_b - \mathbf{w}_a). \tag{C.53}$$

Remind that the vectors in right hand side, given by Eq. (87) [not necessary by Eq. (C.42)], obey

$$\sum_a n_a \mathbf{d}_{(a)} = 0. \tag{C.54}$$

The system (C.53) is singular and can not be inverted directly. Assume that the inverse relationship has the form

$$\mathbf{w}_a = - \sum_b \mathcal{D}_{ab} n_b \mathbf{d}_{(b)} \tag{C.55}$$

with \mathcal{D}_{ab} being the matrix of diffusion coefficients. Due to singularity of this equation, diffusion coefficients \mathcal{D}_{ab} are not uniquely defined. From a general point of view it is convenient to require this matrix to be symmetric [159, 160] that satisfy the Onsager relations manifestly. Since Eq. (C.52) should hold for any set $\mathbf{d}_{(a)}$, the symmetric diffusion matrix must obey [161]

$$\sum_a \mathfrak{z}_a \mathcal{D}_{ab} = \sum_b \mathcal{D}_{ab} \mathfrak{z}_b = 0. \tag{C.56}$$

It was shown in [161] that the following linear system relates symmetric matrix \mathcal{D}_{ab} and the symmetric matrix J_{ab}

$$\sum_c \left(J_{ac} - \frac{\mathfrak{z}_c}{\mathfrak{z}_a} J_{ca} \right) \mathcal{D}_{cb} = -\delta_{ab} + \mathfrak{z}_a, \tag{C.57}$$

where the diagonal elements J_{aa} are defined in such a way to satisfy

$$\sum_a J_{ab} = 0. \tag{C.58}$$

The advantage of Eq. (C.57) is that it automatically leads to the symmetric diffusion coefficient matrix \mathcal{D}_{ab} , as proved in [161]. However, no simple method of the analytical solution of this equation is known. The explicit expressions \mathcal{D}_{ab} in

terms of J_{ab} are given in [161] for two- three- and four-component system.

Notice that if \mathcal{D}_{ab} is found in some frame, then the matrix $\overline{\mathcal{D}}_{ab}$ in a different frame, described by a different set of coefficients $\{\overline{\mathfrak{z}}_a\}$, is given by

$$\overline{\mathcal{D}}_{ab} = \mathcal{D}_{ab} - \sum_c \overline{\mathfrak{z}}_c \mathcal{D}_{cb} - \sum_c \overline{\mathfrak{z}}_c \mathcal{D}_{ac} + \sum_{cd} \overline{\mathfrak{z}}_c \overline{\mathfrak{z}}_d \mathcal{D}_{cd}. \tag{C.59}$$

For the electric current from Eq. (C.55) using Eq. (C.42) one obtains

$$\mathbf{J} = \sigma \mathbf{E}, \tag{C.60}$$

where

$$\sigma = \sum_{ab} q_a q_b n_a n_b \mathcal{D}_{ab}. \tag{C.61}$$

In the absence of magnetic field, σ is a scalar quantity, moreover from (C.61) and (C.59) it is clear that it does not depend on the choice of frame.

Now let us turn to the case of non-zero magnetic field. Following the formalism of Sect. 3.3 we direct the Z axis along the direction of \mathbf{B} and introduce cyclic components of vector. We define in this section $\tilde{w}_a = w_{ax} + i w_{ay}$ and similarly for \mathbf{J} , $\mathbf{d}_{(a)}$, and \mathbf{E} vectors (in this definition we omit normalization constants for brevity). Equation (C.40) takes the form [8]

$$n_a \tilde{\mathbf{d}}_{(a)} - i \mathfrak{X}_a \tilde{\mathbf{J}} B = \sum_b J_{ab} (\tilde{\mathbf{w}}_b - \tilde{\mathbf{w}}_a) - i q_a n_a \tilde{\mathbf{w}}_a B. \tag{C.62}$$

Formally, if \mathcal{D}_{ab} is known from the non-magnetized problem, one can first transform Eq. (C.62) as

$$\tilde{\mathbf{w}}_a = - \sum_b \mathcal{D}_{ab} (n_b \tilde{\mathbf{d}}_{(b)} + i q_b n_b \tilde{\mathbf{w}}_b B - i \mathfrak{X}_b B \tilde{\mathbf{J}}) \tag{C.63}$$

Exclusion of $\tilde{\mathbf{w}}_a$ from Eq. (C.63) requires another linear system solution which can be written as

$$\tilde{\mathbf{w}}_a = - \sum_{bc} \mathfrak{R}_{ac} \mathcal{D}_{cb} (n_b \tilde{\mathbf{d}}_{(b)} - i \mathfrak{X}_b B \tilde{\mathbf{J}}), \tag{C.64}$$

where \mathfrak{R}_{ab} is the following matrix inverse

$$\mathfrak{R}_{ab} = (\delta_{ab} - i \mathcal{D}_{ab} q_b B)^{-1}. \tag{C.65}$$

Electric current can be now calculated as $\tilde{\mathbf{J}} = \sum_a n_a q_a \tilde{\mathbf{w}}_a = \tilde{\sigma} \tilde{\mathbf{E}}$, where $\tilde{\mathbf{d}}_{(a)} = -q_a \tilde{\mathbf{E}}$, cf. Eq. (C.42). Then the complex electrical conductivity is

$$\tilde{\sigma} = \frac{\sum_{abc} q_a n_a \mathfrak{R}_{ac} \mathcal{D}_{cb} n_b q_b}{1 - i B \sum_{abc} q_a n_a \mathfrak{R}_{ac} \mathcal{D}_{cb} \mathfrak{X}_b}. \tag{C.66}$$

If the calculations are performed in the center-of-mass frame, i.e. $\mathfrak{z}_a = \mathfrak{X}_a$ and $\tilde{\mathbf{J}} = \tilde{\sigma}' \tilde{\mathbf{E}}$, the sum in the denominator in Eq. (C.66) vanishes and one obtains

$$\tilde{\sigma}' = \sum_{abc} q_a q_b n_a n_b \mathfrak{R}_{ac} \mathcal{D}_{cb}. \tag{C.67}$$

The complex electrical conductivity $\tilde{\sigma}'$ in Eq. (C.67) is related to the Cartesian components of the electrical conductivity tensor as [cf. Eq. (119)] $\tilde{\sigma}' = \sigma_{\perp} - i\sigma_{\wedge}$.

The analytical calculations along these lines are cumbersome and not easily tractable since they require additional matrix inversion/linear system solution in order to find \mathfrak{R}_{ab} . Therefore, one usually directly inverts Eq. (C.62) replacing one of the equations (i.e. for $a = 1$) with Eq. (C.47) (see, e.g., [74]). In any case, tractable analytical expressions can be obtained only for small number of species r . For two- three- and four-component matter, the resulting general expressions for $\tilde{\sigma}'$ can be found in [8].

Finally we show below the solution of Ref. [8] adapted for the $npe\mu$ NS core composition. We take into account that $q_n = 0$ and neglect lepton-neutron interactions. The resulting expression reads [8, 105]

$$\begin{aligned} \tilde{\sigma}'^{-1} &= \frac{d_0 + iBd_1 - B^2d_2}{a_0 + iBa_1} + \frac{\mathfrak{X}_n^2}{J_{pn}} B^2, \\ a_0 &= e^2(J_{ep}n_{\mu}^2 + J_{\mu p}n_e^2 + J_{e\mu}n_p^2), \\ a_1 &= -e^3n_en_{\mu}n_p, \\ d_0 &= J_{ep}J_{\mu p} + J_{e\mu}J_{\mu p} + J_{e\mu}J_{ep}, \\ d_1 &= -en_e(1 - 2\mathfrak{X}_e)J_{\mu p} - en_{\mu}(1 - 2\mathfrak{X}_{\mu})J_{ep} \\ &\quad - en_p(1 - 2\mathfrak{X}_e - 2\mathfrak{X}_{\mu})J_{e\mu}, \\ d_2 &= e^2 \left[n_en_{\mu}(1 - \mathfrak{X}_e - \mathfrak{X}_{\mu})^2 - n_p(\mathfrak{X}_e^2n_{\mu} + \mathfrak{X}_{\mu}^2n_e) \right], \end{aligned} \quad (\text{C.68})$$

where $e = |e|$ is an elementary charge.

The last term in Eq. (C.68) which contains J_{pn} is responsible for increase of the resistivity at large B [105, 162] observed in plasma containing neutral species [163].

References

- A. Schmitt, P. Shternin, in *The Physics and Astrophysics of Neutron Stars*, ed. by L. Rezzolla, P. Pizzochero, D.I. Jones, N. Rea, I. Vidaña (Springer International Publishing, Cham, 2018), pp. 455–574
- V.M. Kaspi, A.M. Beloborodov, *Ann. Rev. Astron. Astrophys.* **55**(1), 261 (2017). <https://doi.org/10.1146/annurev-astro-081915-023329>
- A.Y. Potekhin, *Astron. Astrophys.* **351**, 787 (1999)
- A.Y. Potekhin, J.A. Pons, D. Page, *Space Sci. Rev.* **191**, 239 (2015). <https://doi.org/10.1007/s11214-015-0180-9>
- D.D. Ofengeim, D.G. Yakovlev, *EPL (Europhys. Lett.)* **112**, 59001 (2015). <https://doi.org/10.1209/0295-5075/112/59001>
- D.A. Baiko, *Mon. Not. R. Astron. Soc.* **458**, 2840 (2016). <https://doi.org/10.1093/mnras/stw504>
- A. Harutyunyan, A. Sedrakian, *Phys. Rev. C* **94**(2), 025805 (2016). <https://doi.org/10.1103/PhysRevC.94.025805>
- D.G. Iakovlev, D.A. Shalybkov, *Astrophys. Space Sci.* **176**(2), 171 (1991). <https://doi.org/10.1007/BF00646697>
- D.G. Yakovlev, D.A. Shalybkov, *Astrophys. Space Sci.* **176**, 171 (1991). <https://doi.org/10.1007/BF00646697>
- L. Rezzolla, O. Zanotti, *Relativistic Hydrodynamics* (Oxford University Press, Oxford, 2013)
- P. Romatschke, U. Romatschke, in *Relativistic Fluid Dynamics In and Out of Equilibrium: And Applications to Relativistic Nuclear Collisions*. *Cambridge Monographs on Mathematical Physics* (Cambridge University Press, Cambridge, 2019). <https://doi.org/10.1017/9781108651998>
- M.E. Gusakov, V.A. Dommès, *Phys. Rev. D* **94**(8), 083006 (2016). <https://doi.org/10.1103/PhysRevD.94.083006>
- P.B. Rau, I. Wasserman, *Phys. Rev. D* **102**(6), 063011 (2020). <https://doi.org/10.1103/PhysRevD.102.063011>
- N. Andersson, G.L. Comer, *Living Rev. Relativ.* **24**(1), 3 (2021). <https://doi.org/10.1007/s41114-021-00031-6>
- V.A. Dommès, M.E. Gusakov, *Phys. Rev. D* **104**(12), 123008 (2021). <https://doi.org/10.1103/PhysRevD.104.123008>
- X.G. Huang, A. Sedrakian, D.H. Rischke, *Ann. Phys.* **326**(12), 3075 (2011). <https://doi.org/10.1016/j.aop.2011.08.001>
- S.I. Finazzo, R. Critelli, R. Rougemont, J. Noronha, *Phys. Rev. D* **94**(5), 054020 (2016). <https://doi.org/10.1103/PhysRevD.94.054020>
- J. Hernandez, P. Kovtun, *J. High Energy Phys.* **2017**(5), 1 (2017). [https://doi.org/10.1007/JHEP05\(2017\)001](https://doi.org/10.1007/JHEP05(2017)001)
- L.D. Landau, E.M. Lifshitz, *Fluid Mechanics, Second Edition: Volume 6 (Course of Theoretical Physics)*, 2nd edn. (Butterworth-Heinemann, Oxford, 1987)
- P. Kovtun, *J. High Energy Phys.* **2019**(10), 34 (2019). [https://doi.org/10.1007/JHEP10\(2019\)034](https://doi.org/10.1007/JHEP10(2019)034)
- C. Eckart, *Phys. Rev.* **58**, 919 (1940). <https://doi.org/10.1103/PhysRev.58.919>
- W.A. Hiscock, L. Lindblom, *Phys. Rev. D* **31**, 725 (1985). <https://doi.org/10.1103/PhysRevD.31.725>
- I. Müller, *Z. Angew. Phys.* **198**(4), 329 (1967). <https://doi.org/10.1007/BF01326412>
- W. Israel, *Ann. Phys.* **100**(1), 310 (1976). [https://doi.org/10.1016/0003-4916\(76\)90064-6](https://doi.org/10.1016/0003-4916(76)90064-6)
- W. Israel, J.M. Stewart, *Ann. Phys.* **118**(2), 341 (1979). [https://doi.org/10.1016/0003-4916\(79\)90130-1](https://doi.org/10.1016/0003-4916(79)90130-1)
- L. Gavassino, M. Antonelli, *Front. Astron. Space Sci.* **8**, 92 (2021). <https://doi.org/10.3389/fspas.2021.686344>
- T. Tsumura, T. Kunihiro, K. Ohnishi, *Phys. Lett. B* **646**(2–3), 134 (2007). <https://doi.org/10.1016/j.physletb.2006.12.074>
- K. Tsumura, T. Kunihiro, *Phys. Lett. B* **668**(5), 425 (2008). <https://doi.org/10.1016/j.physletb.2008.07.109>
- P. Ván, T.S. Biró, *Phys. Lett. B* **709**(1–2), 106 (2012). <https://doi.org/10.1016/j.physletb.2012.02.006>
- H. Freistühler, B. Temple, *Proc. R. Soc. Lond. Ser. A* **470**(2166), 20140055 (2014). <https://doi.org/10.1098/rspa.2014.0055>
- H. Freistühler, B. Temple, *Proc. R. Soc. Lond. Ser. A* **473**(2201), 20160729 (2017). <https://doi.org/10.1098/rspa.2016.0729>
- H. Freistühler, B. Temple, *J. Math. Phys.* **59**(6), 063101 (2018). <https://doi.org/10.1063/1.5007831>
- F.S. Bemfica, M.M. Disconzi, J. Noronha, *Phys. Rev. D* **98**(10), 104064 (2018). <https://doi.org/10.1103/PhysRevD.98.104064>
- F.S. Bemfica, M.M. Disconzi, C. Rodriguez, Y. Shao, *arXiv e-prints* (2019). [arXiv:1911.02504](https://arxiv.org/abs/1911.02504)
- F.S. Bemfica, M.M. Disconzi, J. Noronha, *Phys. Rev. D* **100**(10), 104020 (2019). <https://doi.org/10.1103/PhysRevD.100.104020>
- F.S. Bemfica, M.M. Disconzi, J. Noronha, *arXiv e-prints* (2020). [arXiv:2009.11388](https://arxiv.org/abs/2009.11388)
- R.E. Hout, P. Kovtun, *J. High Energy Phys.* **2020**(6), 67 (2020). [https://doi.org/10.1007/JHEP06\(2020\)067](https://doi.org/10.1007/JHEP06(2020)067)
- A. Pandya, F. Pretorius, *Phys. Rev. D* **104**(2), 023015 (2021). <https://doi.org/10.1103/PhysRevD.104.023015>

39. J. Noronha, M. Spaliński, E. Speranza, arXiv e-prints (2021). [arXiv:2105.01034](https://arxiv.org/abs/2105.01034)
40. F. Becattini, L. Bucciattini, E. Grossi, L. Tinti, Eur. Phys. J. C **75**, 191 (2015). <https://doi.org/10.1140/epjc/s10052-015-3384-y>
41. D.N. Zubarev, *Nonequilibrium Statistical Thermodynamics* (Consultants Bureau, New York, 1974)
42. L. Gavassino, M. Antonelli, B. Haskell, Phys. Rev. D **102**(4), 043018 (2020). <https://doi.org/10.1103/PhysRevD.102.043018>
43. S.R. De Groot, *Relativistic Kinetic Theory, Principles and Applications* (North-Holland, Amsterdam, 1980)
44. S. Bhattacharyya, J. High Energy Phys. **2014**, 165 (2014). [https://doi.org/10.1007/JHEP08\(2014\)165](https://doi.org/10.1007/JHEP08(2014)165)
45. S. Bhattacharyya, J. High Energy Phys. **2014**, 139 (2014). [https://doi.org/10.1007/JHEP07\(2014\)139](https://doi.org/10.1007/JHEP07(2014)139)
46. F. Becattini, D. Rindori, Phys. Rev. D **99**(12), 125011 (2019). <https://doi.org/10.1103/PhysRevD.99.125011>
47. N. Dowling, S. Floerchinger, T. Haas, Phys. Rev. D **102**(10), 105002 (2020). <https://doi.org/10.1103/PhysRevD.102.105002>
48. T. Metens, R. Balescu, Phys. Fluids B **2**(9), 2076 (1990). <https://doi.org/10.1063/1.859428>
49. H. van Erkelens, W.A. van Leeuwen, Phys. A **89**(2), 225 (1977). [https://doi.org/10.1016/0378-4371\(77\)90103-0](https://doi.org/10.1016/0378-4371(77)90103-0)
50. L.D. Landau, E.M. Lifshitz, *Statistical Physics, Part 1, Course of Theoretical Physics*, vol. 5, 3rd edn. (Elsevier, Oxford, 1980)
51. S.R. de Groot, P. Mazur, *Non-equilibrium Thermodynamics* (Dover Publications, New York, 1984)
52. L. Pitaevskii, E. Lifshitz, Physical kinetics, in *Course of Theoretical Physics*, vol. 10, ed. by L.D. Landau, E.M. Lifshitz (Butterworth-Heinemann, Oxford, 2008)
53. V. Zhdanov, *Transport Processes in Multicomponent Plasma* (Taylor & Francis, London, 2002)
54. G.D. Mahan, *Many-Particle Physics* (Plenum Press, New York, 1993)
55. A. Harutyunyan, A. Sedrakian, D.H. Rischke, Particles **1**(1), 155 (2018). <https://doi.org/10.3390/particles1010011>. <https://www.mdpi.com/2571-712X/1/1/11>
56. G. Baym, C. Pethick, *Landau Fermi-Liquid Theory: Concepts and Applications* (Wiley, New York, 1991). <https://doi.org/10.1002/9783527617159>
57. G. Baym, S.A. Chin, Nucl. Phys. A **262**(3), 527 (1976). [https://doi.org/10.1016/0375-9474\(76\)90513-3](https://doi.org/10.1016/0375-9474(76)90513-3)
58. M.E. Gusakov, E.M. Kantor, P. Haensel, Phys. Rev. C **79**(5), 055806 (2009). <https://doi.org/10.1103/PhysRevC.79.055806>
59. C.G. van Weert, M.C.J. Leermakers, Phys. Lett. A **101**(4), 195 (1984). [https://doi.org/10.1016/0375-9601\(84\)90377-3](https://doi.org/10.1016/0375-9601(84)90377-3)
60. C.G. Van Weert, M.C.J. Leermakers, Phys. A **131**(3), 465 (1985). [https://doi.org/10.1016/0378-4371\(85\)90126-8](https://doi.org/10.1016/0378-4371(85)90126-8)
61. C.G. van Weert, M.C.J. Leermakers, A.M.J. Schakel, Phys. A **138**(3), 404 (1986). [https://doi.org/10.1016/0378-4371\(86\)90024-5](https://doi.org/10.1016/0378-4371(86)90024-5)
62. T. Hayata, Y. Hidaka, T. Noumi, M. Hongo, Phys. Rev. D **92**(6), 065008 (2015). <https://doi.org/10.1103/PhysRevD.92.065008>
63. C. Cercignani, G.M. Kremer, *The Relativistic Boltzmann Equation: Theory and Applications* (Birkhäuser, Boston, 2002)
64. H. Grad, Commun. Pure Appl. Math. **2**(4), 331 (1949). <https://doi.org/10.1002/cpa.3160020403>
65. S. Chapman, T.G. Cowling, D. Burnett, *The Mathematical Theory of Non-uniform Gases: An Account of the Kinetic Theory of Viscosity, Thermal Conduction and Diffusion in Gases*, 3rd edn. (Cambridge University Press, Cambridge, 1999)
66. G.S. Denicol, J. Phys. G Nucl. Phys. **41**(12), 124004 (2014). <https://doi.org/10.1088/0954-3889/41/12/124004>
67. A. Gabbana, D. Simeoni, S. Succi, R. Tripiccone, Phys. Rep. **863**, 1 (2020). <https://doi.org/10.1016/j.physrep.2020.03.004>
68. A.L. García-Perciante, M.E. Rubio, O.A. Reula, J. Stat. Phys. **181**(1), 246 (2020). <https://doi.org/10.1007/s10955-020-02578-0>
69. G.S. Denicol, J. Noronha, arXiv e-prints (2016). [arXiv:1608.07869](https://arxiv.org/abs/1608.07869)
70. D.A. Varshalovich, A.N. Moskalev, V.K. Khersonskii, *Quantum Theory of Angular Momentum* (World Scientific Publishing Co, Singapore, 1988). <https://doi.org/10.1142/0270>
71. R.H. Anderson, C.J. Pethick, K.F. Quader, Phys. Rev. B **35**, 1620 (1987). <https://doi.org/10.1103/PhysRevB.35.1620>
72. L.A. Viehland, C.F. Curtiss, J. Chem. Phys. **60**(2), 492 (1974). <https://doi.org/10.1063/1.1681066>
73. H. van Erkelens, W.A. van Leeuwen, Phys. A **91**(1), 88 (1978). [https://doi.org/10.1016/0378-4371\(78\)90059-6](https://doi.org/10.1016/0378-4371(78)90059-6)
74. V.A. Dommès, M.E. Gusakov, P.S. Shternin, Phys. Rev. D **101**(10), 103020 (2020). <https://doi.org/10.1103/PhysRevD.101.103020>
75. J.L. Anderson, H.R. Witting, Physica **74**(3), 466 (1974). [https://doi.org/10.1016/0031-8914\(74\)90355-3](https://doi.org/10.1016/0031-8914(74)90355-3)
76. P.L. Bhatnagar, E.P. Gross, M. Krook, Phys. Rev. **94**(3), 511 (1954). <https://doi.org/10.1103/PhysRev.94.511>
77. M. Formanek, C. Grayson, J. Rafelski, B. Müller, Ann. Phys. **434**, 168605 (2021). <https://doi.org/10.1016/j.aop.2021.168605>
78. G.S. Rocha, G.S. Denicol, J. Noronha, Phys. Rev. Lett. **127**(4), 042301 (2021). <https://doi.org/10.1103/PhysRevLett.127.042301>
79. J.M. Ziman, *Electrons and Phonons. Oxford Classical Texts in the Physical Sciences* (Clarendon Press/Oxford University Press, Oxford, 2001)
80. H. Højgård Jensen, H. Smith, J.W. Wilkins, Phys. Lett. A **27**, 532 (1968). [https://doi.org/10.1016/0375-9601\(68\)90904-3](https://doi.org/10.1016/0375-9601(68)90904-3)
81. G.A. Brooker, J. Sykes, Phys. Rev. Lett. **21**, 279 (1968). <https://doi.org/10.1103/PhysRevLett.21.279>
82. J. Sykes, G.A. Brooker, Ann. Phys. **56**, 1 (1970). [https://doi.org/10.1016/0003-4916\(70\)90002-3](https://doi.org/10.1016/0003-4916(70)90002-3)
83. E. Flowers, N. Itoh, Astrophys. J. **230**, 847 (1979). <https://doi.org/10.1086/157145>
84. C.J. Pethick, A. Schwenk, Phys. Rev. C **80**(5), 055805 (2009). <https://doi.org/10.1103/PhysRevC.80.055805>
85. A.D. Polyaniin, A.V. Manzhirrov, *Handbook of Integral Equations*, 2nd edn. (Chapman & Hall/CRC, Boca Raton, 2008)
86. M. Ichiyangi, Phys. Rep. **243**(3), 125 (1994). [https://doi.org/10.1016/0370-1573\(94\)90052-3](https://doi.org/10.1016/0370-1573(94)90052-3)
87. A.A. Abrikosov, I.M. Khalatnikov, Rep. Prog. Phys. **22**(1), 329 (1959). <https://doi.org/10.1088/0034-4885/22/1/310>
88. H. Heiselberg, G. Baym, C.J. Pethick, J. Popp, Nucl. Phys. A **544**, 569 (1992). [https://doi.org/10.1016/0375-9474\(92\)90620-Y](https://doi.org/10.1016/0375-9474(92)90620-Y)
89. P.S. Shternin, M. Baldo, Phys. Rev. D **102**(6), 063010 (2020). <https://doi.org/10.1103/PhysRevD.102.063010>
90. J.P. Blaizot, Nucl. Phys. A **606**(1), 347 (1996). [https://doi.org/10.1016/0375-9474\(96\)00209-6](https://doi.org/10.1016/0375-9474(96)00209-6)
91. J.H. Ferziger, H.G. Kaper, *Mathematical Theory of Transport Processes in Gases* (North-Holland, Amsterdam, 1972)
92. P. Goldreich, A. Reisenegger, Astrophys. J. **395**, 250 (1992). <https://doi.org/10.1086/171646>
93. D.A. Shalybkov, V.A. Urpin, Mon. Not. R. Astron. Soc. **273**(3), 643 (1995). <https://doi.org/10.1093/mnras/273.3.643>
94. A.M. Beloborodov, X. Li, Astrophys. J. **833**(2), 261 (2016). <https://doi.org/10.3847/1538-4357/833/2/261>
95. A. Passamonti, T. Akgün, J.A. Pons, J.A. Miralles, Mon. Not. R. Astron. Soc. **465**(3), 3416 (2017). <https://doi.org/10.1093/mnras/stw2936>
96. M.E. Gusakov, E.M. Kantor, D.D. Ofengeim, Phys. Rev. D **96**(10), 103012 (2017). <https://doi.org/10.1103/PhysRevD.96.103012>

97. F. Castillo, A. Reisenegger, J.A. Valdivia, *Mon. Not. R. Astron. Soc.* **498**(2), 3000 (2020). <https://doi.org/10.1093/mnras/staa2543>
98. R. Machleidt, D.R. Entem, *Phys. Rep.* **503**(1), 1 (2011). <https://doi.org/10.1016/j.physrep.2011.02.001>
99. P.S. Shternin, M. Baldo, P. Haensel, *Phys. Rev. C* **88**(6), 065803 (2013). <https://doi.org/10.1103/PhysRevC.88.065803>
100. P. Shternin, I. Vidaña, *Universe* **7**(6), 203 (2021). <https://doi.org/10.3390/universe7060203>
101. G. Baym, H. Monien, C.J. Pethick, D.G. Ravenhall, *Phys. Rev. Lett.* **64**(16), 1867 (1990). <https://doi.org/10.1103/PhysRevLett.64.1867>
102. H. Heiselberg, C.J. Pethick, *Phys. Rev. D* **48**, 2916 (1993). <https://doi.org/10.1103/PhysRevD.48.2916>
103. P.S. Shternin, D.G. Yakovlev, *Phys. Rev. D* **75**(10), 103004 (2007). <https://doi.org/10.1103/PhysRevD.75.103004>
104. P.S. Shternin, D.G. Yakovlev, *Phys. Rev. D* **78**(6), 063006 (2008). <https://doi.org/10.1103/PhysRevD.78.063006>
105. P.S. Shternin, *JETP* **107**, 212 (2008). <https://doi.org/10.1134/S1063776108080050>
106. S. Stetina, arXiv e-prints (2019). [arXiv:1902.10745](https://arxiv.org/abs/1902.10745)
107. S. Stetina, E. Rrapaj, S. Reddy, *Phys. Rev. C* **97**(4), 045801 (2018). <https://doi.org/10.1103/PhysRevC.97.045801>
108. D.A. Baiko, P. Haensel, D.G. Yakovlev, *Astron. Astrophys.* **374**, 151 (2001). <https://doi.org/10.1051/0004-6361/20010621>
109. A.D. Sedrakian, D. Blaschke, G. Röpke, H. Schulz, *Phys. Lett. B* **338**, 111 (1994). [https://doi.org/10.1016/0370-2693\(94\)91352-8](https://doi.org/10.1016/0370-2693(94)91352-8)
110. J. Wambach, T.L. Ainsworth, D. Pines, *Nucl. Phys. A* **555**, 128 (1993). [https://doi.org/10.1016/0375-9474\(93\)90317-Q](https://doi.org/10.1016/0375-9474(93)90317-Q)
111. O. Benhar, A. Polls, M. Valli, I. Vidaña, *Phys. Rev. C* **81**(2), 024305 (2010). <https://doi.org/10.1103/PhysRevC.81.024305>
112. O. Benhar, M. Valli, *Phys. Rev. Lett.* **99**(23), 232501 (2007). <https://doi.org/10.1103/PhysRevLett.99.232501>
113. A. Carbone, O. Benhar, *J. Phys. Conf. Ser.* **336**, 012015 (2011). <https://doi.org/10.1088/1742-6596/336/1/012015>
114. M. Baldo (ed.), *Nuclear Methods and the Nuclear Equation of State, International Review of Nuclear Physics*, vol. 8 (World Scientific, Singapore, 1999). <https://doi.org/10.1142/2657>
115. H.F. Zhang, U. Lombardo, W. Zuo, *Phys. Rev. C* **82**(1), 015805 (2010). <https://doi.org/10.1103/PhysRevC.82.015805>
116. P. Shternin, M. Baldo, H. Schulze, *J. Phys. Conf. Ser.* **932**, 012042 (2017)
117. A.B. Migdal, E.E. Saperstein, M.A. Troitsky, D.N. Voskresensky, *Phys. Rep.* **192**, 179 (1990). [https://doi.org/10.1016/0370-1573\(90\)90132-L](https://doi.org/10.1016/0370-1573(90)90132-L)
118. D. Blaschke, H. Grigorian, D.N. Voskresensky, *Phys. Rev. C* **88**(6), 065805 (2013). <https://doi.org/10.1103/PhysRevC.88.065805>
119. E.E. Kolomeitsev, D.N. Voskresensky, *Phys. Rev. C* **91**(2), 025805 (2015). <https://doi.org/10.1103/PhysRevC.91.025805>
120. G.Q. Li, R. Machleidt, *Phys. Rev. C* **48**(4), 1702 (1993). <https://doi.org/10.1103/PhysRevC.48.1702>
121. G.Q. Li, R. Machleidt, *Phys. Rev. C* **49**(1), 566 (1994). <https://doi.org/10.1103/PhysRevC.49.566>
122. R. Machleidt, K. Holinde, C. Elster, *Phys. Rep.* **149**(1), 1 (1987). [https://doi.org/10.1016/S0370-1573\(87\)80002-9](https://doi.org/10.1016/S0370-1573(87)80002-9)
123. R.B. Wiringa, V.G.J. Stoks, R. Schiavilla, *Phys. Rev. C* **51**, 38 (1995). <https://doi.org/10.1103/PhysRevC.51.38>
124. A.Y. Potekhin, A.F. Fantina, N. Chamel, J.M. Pearson, S. Goriely, *Astron. Astrophys.* **560**, A48 (2013). <https://doi.org/10.1051/0004-6361/201321697>
125. R. Machleidt, *Phys. Rev. C* **63**(2), 024001 (2001). <https://doi.org/10.1103/PhysRevC.63.024001>
126. J. Carlson, V.R. Pandharipande, R.B. Wiringa, *Nucl. Phys. A* **401**, 59 (1983). [https://doi.org/10.1016/0375-9474\(83\)90336-6](https://doi.org/10.1016/0375-9474(83)90336-6)
127. Z.H. Li, U. Lombardo, H.J. Schulze, W. Zuo, *Phys. Rev. C* **77**(3), 034316 (2008). <https://doi.org/10.1103/PhysRevC.77.034316>
128. Z.H. Li, H.J. Schulze, *Phys. Rev. C* **85**(6), 064002 (2012). <https://doi.org/10.1103/PhysRevC.85.064002>
129. M. Baldo, G.F. Burgio, H.J. Schulze, G. Taranto, *Phys. Rev. C* **89**(4), 048801 (2014). <https://doi.org/10.1103/PhysRevC.89.048801>
130. F. Gulminelli, A.R. Raduta, *Phys. Rev. C* **92**(5), 055803 (2015). <https://doi.org/10.1103/PhysRevC.92.055803>
131. V. Dexheimer, S. Schramm, *Astrophys. J.* **683**(2), 943 (2008). <https://doi.org/10.1086/589735>
132. V. Dexheimer, *Publ. Astron. Soc. Austral.* **34**, e066 (2017). <https://doi.org/10.1017/pasa.2017.61>
133. I. Bombaci, D. Logoteta, *Astron. Astrophys.* **609**, A128 (2018). <https://doi.org/10.1051/0004-6361/201731604>
134. M. Fortin, C. Providência, A.R. Raduta, F. Gulminelli, J.L. Zdunik, P. Haensel, M. Bejger, *Phys. Rev. C* **94**(3), 035804 (2016). <https://doi.org/10.1103/PhysRevC.94.035804>
135. F. Douchin, P. Haensel, *Astron. Astrophys.* **380**, 151 (2001). <https://doi.org/10.1051/0004-6361:20011402>
136. B.K. Sharma, M. Centelles, X. Viñas, M. Baldo, G.F. Burgio, *Astron. Astrophys.* **584**, A103 (2015). <https://doi.org/10.1051/0004-6361/201526642>
137. J.M. Pearson, N. Chamel, A.Y. Potekhin, A.F. Fantina, C. Ducoin, A.K. Dutta, S. Goriely, *Mon. Not. R. Astron. Soc.* **481**(3), 2994 (2018). <https://doi.org/10.1093/mnras/sty2413>
138. A. Akmal, V.R. Pandharipande, D.G. Ravenhall, *Phys. Rev. C* **58**(3), 1804 (1998). <https://doi.org/10.1103/PhysRevC.58.1804>
139. H. Heiselberg, M. Hjorth-Jensen, *Astrophys. J. Lett.* **525**(1), L45 (1999). <https://doi.org/10.1086/312321>
140. H. Heiselberg, M. Hjorth-Jensen, *Phys. Rep.* **328**(5–6), 237 (2000). [https://doi.org/10.1016/S0370-1573\(99\)00110-6](https://doi.org/10.1016/S0370-1573(99)00110-6)
141. M.E. Gusakov, A.D. Kaminker, D.G. Yakovlev, O.Y. Gnedin, *Mon. Not. R. Astron. Soc.* **363**(2), 555 (2005). <https://doi.org/10.1111/j.1365-2966.2005.09459.x>
142. M. Prakash, T.L. Ainsworth, J.M. Lattimer, *Phys. Rev. Lett.* **61**(22), 2518 (1988). <https://doi.org/10.1103/PhysRevLett.61.2518>
143. D. Page, J.H. Applegate, *Astrophys. J. Lett.* **394**, L17 (1992). <https://doi.org/10.1086/186462>
144. P. Haensel, A.Y. Potekhin, D.G. Yakovlev, *Neutron Stars 1: Equation of State and Structure* (Springer Science+Buisness Media, Berlin, 2007)
145. B.K. Agrawal, S. Shlomo, V.K. Au, *Phys. Rev. C* **72**(1), 014310 (2005). <https://doi.org/10.1103/PhysRevC.72.014310>
146. J. Friedrich, P.G. Reinhard, *Phys. Rev. C* **33**(1), 335 (1986). <https://doi.org/10.1103/PhysRevC.33.335>
147. H.S. Köhler, *Nucl. Phys. A* **258**(2), 301 (1976). [https://doi.org/10.1016/0375-9474\(76\)90008-7](https://doi.org/10.1016/0375-9474(76)90008-7)
148. P.G. Reinhard, H. Flocard, *Nucl. Phys. A* **584**(3), 467 (1995). [https://doi.org/10.1016/0375-9474\(94\)00770-N](https://doi.org/10.1016/0375-9474(94)00770-N)
149. W. Nazarewicz, J. Dobaczewski, T.R. Werner, J.A. Maruhn, P.G. Reinhard, K. Rutz, C.R. Chinn, A.S. Umar, M.R. Strayer, *Phys. Rev. C* **53**(2), 740 (1996). <https://doi.org/10.1103/PhysRevC.53.740>
150. L. Bennour, P.H. Heenen, P. Bonche, J. Dobaczewski, H. Flocard, *Phys. Rev. C* **40**(6), 2834 (1989). <https://doi.org/10.1103/PhysRevC.40.2834>
151. P.G. Reinhard, D.J. Dean, W. Nazarewicz, J. Dobaczewski, J.A. Maruhn, M.R. Strayer, *Phys. Rev. C* **60**(1), 014316 (1999). <https://doi.org/10.1103/PhysRevC.60.014316>
152. E. Chabanat, *Interactions effectives pour des conditions extremes d'isospin*, Ph.D. thesis, University Claude Bernard Lyon-1, Lyon, France (1995)

153. D.D. Ofengeim, M. Fortin, P. Haensel, D.G. Yakovlev, J.L. Zdunik, *Phys. Rev. D* **96**(4), 043002 (2017). <https://doi.org/10.1103/PhysRevD.96.043002>
154. D. Logoteta, *Universe* **7**(11), 408 (2021). <https://doi.org/10.3390/universe7110408>
155. A. Sedrakian, J.W. Clark, *Eur. Phys. J. A* **55**(9), 167 (2019). <https://doi.org/10.1140/epja/i2019-12863-6>
156. N. Andersson, *Universe* **7**(1), 17 (2021). <https://doi.org/10.3390/universe7010017>
157. D. Vollhardt, P. Wölfle, *The Superfluid Phases of Helium 3* (Taylor & Francis, Bristol, 1990). <https://doi.org/10.1201/b12808>
158. C. Manuel, L. Tolos, *Universe* **7**(3), 59 (2021). <https://doi.org/10.3390/universe7030059>
159. C.F. Curtiss, *J. Chem. Phys.* **49**(7), 2917 (1968). <https://doi.org/10.1063/1.1670528>
160. D.W. Condiff, *J. Chem. Phys.* **51**(10), 4209 (1969). <https://doi.org/10.1063/1.1671780>
161. C.F. Curtiss, R.B. Bird, *Ind. Eng. Chem. Res.* **38**(7), 2515 (1999). <https://doi.org/10.1021/ie9901123>
162. P. Haensel, V.A. Urpin, D.G. Iakovlev, *Astron. Astrophys.* **229**(1), 133 (1990)
163. A.M. Bykov, I. Toptygin, *Phys. Usp.* **50**(2), 141 (2007). <https://doi.org/10.1070/PU2007v050n02ABEH006177>